Evapotranspiration From Selected Fallowed Agricultural Fields on the Tule Lake National Wildlife Refuge, California, During May to October 2000

Prepared in cooperation with the
U.S. FISH AND WILDLIFE SERVICE

U.S. GEOLOGICAL SURVEY
Water-Resources Investigations Report 02-4055

USGS
science for a changing world

Evapotranspiration From Selected Fallowed Agricultural Fields on the Tule Lake National Wildlife Refuge, California, During May to October 2000

By William R. Bidlake

U.S. GEOLOGICAL SURVEY

Water-Resources Investigations Report 02-4055

Prepared in cooperation with

U.S. FISH and WILDLIFE SERVICE

Tacoma, Washington
2002

U.S. DEPARTMENT OF THE INTERIOR
GALE A. NORTON, Secretary

U.S. GEOLOGICAL SURVEY
Charles G. Groat, Director

For additional information write to:

District Chief
U.S. Geological Survey
1201 Pacific Avenue – Suite 600
Tacoma, Washington 98402
http://wa.water.usgs.gov

Copies of this report can be purchased from:

U.S. Geological Survey
Information Services
Building 810
Box 25286, Federal Center
Denver, CO 80225-0286

CONVERSION FACTORS, VERTICAL DATUM, SYMBOLS, AND ABBREVIATIONS

Multiply	By	To obtain
Length		
millimeter (mm)	0.03937	inch
meter (m)	3.281	foot
kilometer (km)	0.6214	mile
Area		
square meter (m^2)	0.0002471	acre
hectare (ha)	2.471	acre
Volume		
cubic meter (m^3)	35.31	cubic foot
Mass		
gram (g)	0.03527	ounce, avoirdupois
kilogram (kg)	2.205	pound avoirdupois
Energy		
joule (J)	0.2388	calorie
	9.4787×10^{-4}	British thermal unit
Pressure		
kilopascal (kPa)	0.01	bar
	0.1450	pound-force per square inch
Power		
watt (W)	0.2388	calorie per second
	3.412	British thermal unit per hour
Velocity or Rate		
meter per second (m/s)	2.2370	miles per hour
millimeter per day (mm/d)	0.03937	inch per day

Temperature in degrees Celsius (°C) may be converted to degrees Fahrenheit (°F) as follows:

°F= (1.8 °C)+32

Temperature in degrees Fahrenheit (°F) may be converted to degrees Celsius (°C) as follows:

°C= (°F-32)/1.8

Sea level: In this report "sea level" refers to the National Geodetic Vertical Datum of 1929 (NGVD of 1929)--a geodetic datum derived from a general adjustment of the first-order level nets of both the United States and Canada, formerly called Sea Level Datum of 1929.

SYMBOLS

Symbol	Meaning	Dimensions
A_0 to A_6	Coefficients	Variable
A_m	Measured available energy for the surface of interest	W/m^2
c_p	Specific heat of air at constant pressure	(J/g)/°C
c_{pd}	Specific heat of dry air at constant pressure	(J/g)/°C
c_{pv}	Specific heat of water vapor at constant pressure	(J/g)/°C

Symbol	Meaning	Dimensions
c_s	Specific heat of dry soil	(J/kg)/°C
c_w	Specific heat of water	(J/kg)/°C
D	Atmospheric water-vapor pressure deficit	kPa
d	Day of the calendar year	days
d_0	Zero-plane displacement height	m
d_p	Diameter of soil heat flux plate	mm
d_r	Day of the summer solstice	days
d_y	Number of days per year	days
E	Evapotranspiration rate	$(g/m^2)/s$ or mm/d
E_0	Reference evapotranspiration rate	mm/d
e	Water-vapor pressure	kPa
e_s	Water-vapor pressure at atmospheric saturation	kPa
F	Fetch-to-instrument-height ratio for westerly winds	Dimensionless
G	Soil heat flux at the soil surface	W/m^2
G_z	Soil heat flux at soil depth z	W/m^2
G'_z	Uncorrected measured G_z	W/m^2
H	Sensible heat flux	W/m^2
H_{BREB}	Sensible heat flux from the Bowen ratio energy balance technique	W/m^2
H_{EC}	Sensible heat flux from the eddy covariance technique	W/m^2
h_c	Height of crop canopy	m
k_c	Empirical crop coefficient	Dimensionless
h_r	Relative humidity	Dimensionless
k_m	Thermal conductivity of calibration medium for soil heat flux plate	(W/m)/°C
k_p	Thermal conductivity of soil heat flux plate	(W/m)/°C
k_s	Soil thermal conductivity	(W/m)/°C
L	Thickness of soil heat flux plate	mm
p	Atmospheric pressure	kPa
R	Ratio of available energy at the contaminating surface to that at the surface of interest	Dimensionless
R_d	Ideal gas constant for dry air	(J/g)/K
R_n	Net radiation	W/m^2
s	Slope of the relation between water-vapor pressure at atmospheric saturation and temperature	kPa/°C
T	Air temperature	°C
T'	Short-term fluctuation of air temperature from the time-averaged mean	°C
T_c	Temperature of cavity housing relative humidity sensor	°C
T_s	Soil temperature	°C
$\overline{T}_s$	Depth-averaged temperature of soil layer	°C

Symbol	Meaning	Dimensions
t	Time	s
t_{UTC}	Coordinated Universal Time	hours
w'	Short-term fluctuation of vertical wind speed from the time-averaged mean	m/s
x	Fetch	m
Z	Site altitude	m
z	Depth in soil	m
z_0	Roughness length	m
z_u	Height above land surface	m
α	Coefficient equal to the ratio of λE to λE_{EQ}	Dimensionless
β	Bowen ratio	Dimensionless
β_c	Bowen ratio for the contaminating surface	Dimensionless
β_i	Actual Bowen ratio for the surface of interest	Dimensionless
β_m	Measured Bowen ratio for the surface of interest	Dimensionless
Γ	Longitude	radians
γ	Psychrometer constant	kPa/°C
Δ	Difference over a vertical interval or vertical displacement	Variable
δ	Solar declination angle	radians
$\delta_{\lambda E}$	Error in λE_m due to the influence of the contaminating surface	W/m^2
ε	Ratio of the mass of a mole of water to the mass of a mole of dry air	Dimensionless
η	Prescribed minimum for the fetch-to-height ratio	Dimensionless
θ	Volumetric soil water content	Dimensionless
θ^*	Uncorrected volumetric soil water content	Dimensionless
λ	Latent heat of vaporization for water	J/g
λE	Latent heat flux	W/m^2
λE_c	Latent heat flux from the contaminating surface	W/m^2
λE_{EQ}	Equilibrium latent heat flux	W/m^2
λE_i	Latent heat flux from the surface of interest	W/m^2
λE_m	Measured latent heat flux from the surface of interest	W/m^2
ρ	Air density	g/m^3
ρ_d	Density of dry air	g/m^3
ρ_s	Soil bulk density	kg/m^3
ρ_v	Density of atmospheric water vapor	g/m^3
ρ_w	Density of water	kg/m^3
τ	Period of wave	ms
Φ	Latitude	radians

Symbol	Meaning	Dimensions
Φ_r	Latitude of the Tropic of Cancer	radians
Ψ	Solar elevation angle	radians
$\%Eq_{\lambda E}$	Percentage of equilibration of latent heat flux to the surface of interest	Dimensionless
$\%\delta_{\lambda E}$	Percentage error in λE_m due to the influence of the contaminating surface	Dimensionless
$\overline{}$	Overbar representing averaging over time or with distance	

Abbreviations	Meaning
n	Sample size
P	Piezometer
PDT	Pacific Daylight Time
PT	Priestley-Taylor
RMSD	Root-mean-square difference
RMSE	Root-mean-square error
r	Correlation coefficient
sd	Standard deviation
BREB	Bowen ratio energy balance
NWR	National Wildlife Refuge
USFWS	U.S. Fish and Wildlife Service
USGS	U.S. Geological Survey

CONTENTS

FIGURES

TABLES

Evapotranspiration From Selected Fallowed Agricultural Fields on the Tule Lake National Wildlife Refuge, California, During May to October 2000

By William R. Bidlake

ABSTRACT

An investigation of evapotranspiration, vegetation quantity and composition, and depth to the water table below the land surface was made at three sites in two fallowed agricultural lots on the 15,800-hectare Tule Lake National Wildlife Refuge in northern California during the 2000 growing season. All three sites had been farmed during 1999, but were not irrigated since the 1999 growing season. Vegetation at the lot C1B and lot 6 stubble sites included weedy species and small grain plants. The lot 6 cover crop site supported a crop of cereal rye that had been planted during the previous winter. Percentage of coverage by live vegetation ranged from 0 to 43.2 percent at the lot C1B site, from approximately 0 to 63.2 percent at the lot 6 stubble site, and it was estimated to range from 0 to greater than 90 percent at the lot 6 cover crop site. Evapotranspiration was measured using the Bowen ratio energy balance technique and it was estimated using a model that was based on the Priestley-Taylor equation and a model that was based on reference evapotranspiration with grass as the reference crop.

Total evapotranspiration during May to October varied little among the three evapotranspiration measurement sites, although the timing of evapotranspiration losses did vary among the sites. Total evapotranspiration from the lot C1B site was 426 millimeters, total evapotranspiration from the lot 6 stubble site was 444 millimeters, and total evapotranspiration from the lot 6 cover crop site was 435 millimeters. The months of May to July accounted for approximately 78 percent of the total evapotranspiration from the lot C1B site, approximately 63 percent of the evapotranspiration from the lot 6 stubble site, and approximately 86 percent of the total evapotranspiration from the lot 6 cover crop site. Estimated growing season precipitation accounted for 16 percent of the growing-season evapotranspiration at the lot C1B site and for 17 percent of the growing-season evapotranspiration at the lot 6 stubble and cover crop sites.

The ratio of evapotranspiration rate to the reference evapotranspiration rate was strongly correlated with percentage of site coverage by vegetation at the lot C1B and lot 6 stubble sites (correlation coefficient = 0.95, sample size = 6), where percentage of site coverage was determined from quantitative vegetation surveys. It is concluded that evapotranspiration was mediated by the vegetation at all three sites, and that the differences in seasonal timing of evapotranspiration losses were caused by differences in timing of vegetation growth and development and senescence among the sites. Depth to the water table below the land surface at lot C1B ranged from 0.67 meters in early July to greater than 1.39 meters in late August. Depth to the water table at lot 6 ranged from 0.77 meter in late May to greater than 1.40 meters in late August.

INTRODUCTION

Management of water resources for water supply or conservation typically involves manipulating hydrologic balances in space or time, or both. For example, a reservoir might be built to detain the waters of stream runoff so the waters can be distributed later to specified locations. The field of agricultural water management is replete with practices intended to alter local water balances to achieve conditions favorable to plant growth and development. Fallowing, the practice of allowing land ordinarily used for crops to lie idle during the growing season, can conserve water at a given place and time so the water can be used for other purposes. Fallowing can reduce evaporative water loss by reducing or eliminating water-consuming vegetation, thereby allowing some of the soil-moisture stores either to be retained for crop growth and development during future growing seasons or to drain from the soil to recharge an aquifer. Fallowing of agricultural lands that are normally irrigated also spares water normally diverted for irrigation to be conserved and used elsewhere.

Water conservation through selective fallowing of croplands may be an important tool for water management in the Upper Klamath River Basin of southern Oregon and northern California (fig. 1), where there are many demands for scarce water resources. The U.S. Fish and Wildlife Service (USFWS) administers six National Wildlife Refuges (NWR's) totaling approximately 80,000 hectares (ha) in the Klamath River Basin (U.S. Fish and Wildlife Service, 2001), and is a principal manager of land and water resources in the basin. Five of the six Klamath River Basin NWR's are shown in figure 1. The 15,800-ha Tule Lake NWR contains approximately 6,900 ha of croplands that have for many years been leased to farmers for agricultural production and to provide food and habitat for wildlife. Some of the water flowing into the Tule Lake NWR maintains water levels in its wetlands, some is diverted to irrigate croplands, and some is conveyed to the Lower Klamath NWR to help maintain wetland habitats in the latter refuge. The USFWS is investigating whether or not intermittent fallowing with the attendant cessation of irrigation on selected Tule Lake NWR croplands will conserve water that can then be used to maintain wildlife habitats in the basin.

Evapotranspiration often constitutes the greatest loss of water from terrestrial sites, and an understanding of evapotranspiration from fallowed croplands is important for evaluating the effectiveness of fallowing as a water conservation practice. Although many sources of information exist that can be used for estimating evapotranspiration from irrigated, actively farmed croplands in the Klamath River Basin (for example Doorenbos and Pruitt, 1977; Jensen and others, 1990; and Snyder and others, 1987), apparently little information is available for estimating evapotranspiration from fallowed croplands. Additionally, recently fallowed croplands are disturbed ecosystems consisting of plants sprouted from seeds of previous crops, weedy plants, bare soil, and crop residues. For this reason, a strong scientific justification probably does not exist for applying results of published case studies of evapotranspiration from rangelands (Harr and Price, 1972; Duell, 1990; Tomlinson, 1996) to estimate evapotranspiration from fallowed croplands.

An intensive study was made by the U.S. Geological Survey (USGS) with a primary objective of estimating evapotranspiration from three agricultural fields on the Tule Lake NWR during the 2000 growing season. The intent of this objective was to supply estimates of fallowed-field evapotranspiration that the USFWS can use in conjunction with estimates of evapotranspiration from selected crops to estimate water savings that would be realized if normally farmed fields were to be fallowed. The fields varied with respect to cropping histories and drainage structures and they were selected by the USFWS to be representative of future fallowed fields that might be anticipated on the Tule Lake NWR if cropland fallowing is applied as a water conservation strategy. The second objective of the study was to note and report on the field conditions during the growing season, including occurrence and relative abundance of crop residues and non-crop plants and depth to the water table below the soil surface.

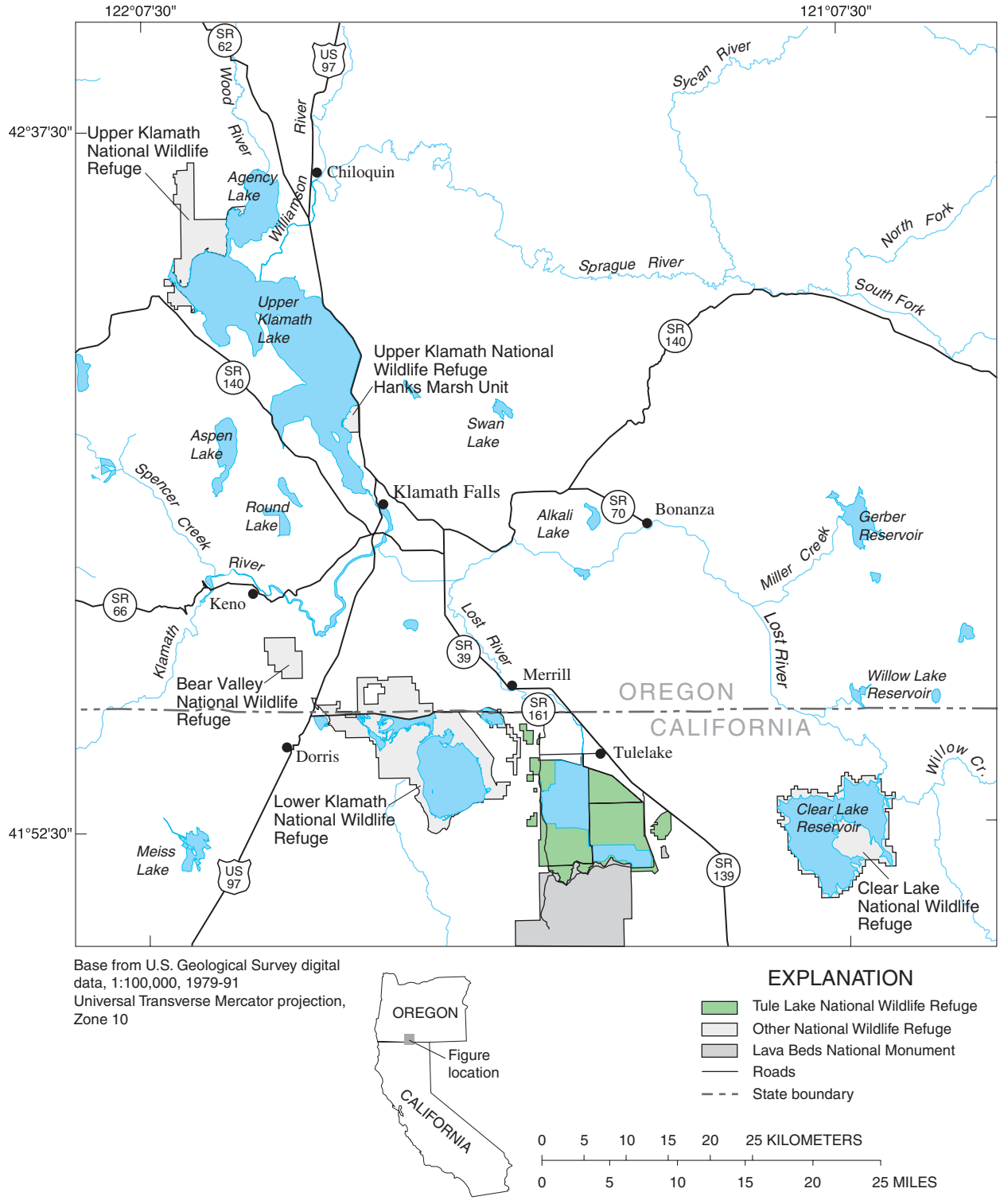

Figure 1. Part of the Upper Klamath Basin, northern California and southern Oregon, and the Tule Lake National Wildlife Refuge.

Acknowledgments

Funding for this work was provided by the U.S. Fish and Wildlife Service. Dave Stannard, U.S. Geological Survey, helped the author to implement the former's theory of airstream equilibration for the Bowen ratio energy balance technique. The loan of a critical sensor by Guy DeMeo, U.S. Geological Survey, to replace one that failed during the study is gratefully acknowledged. Tim Mayer and Sam Johnson, U.S. Fish and Wildlife Service, each provided technical suggestions for improving the report.

Purpose and Scope

This report describes the study area and the study sites and approaches, and it presents results relevant to the study's two objectives. The report describes the geographic setting and climate of the study area, and the size, soils, drainage structures, and vegetation of the study sites, and selected features in surrounding lands. Descriptions of study approaches include descriptions of the theory and application of the Bowen ratio energy balance (BREB) technique for estimating evapotranspiration and of the eddy covariance technique for estimating sensible heat flux, descriptions of data collection and estimation techniques, and descriptions of the development and application of simple models that were used to estimate evapotranspiration for periods when the BREB technique could not be used for that purpose. Techniques for measuring and tabulating relative abundance of crop residues and various plants are described, as are techniques for monitoring depth to the water table below the soil surface. The primary study results, the time series of measured and estimated daily evapotranspiration at each study site during May to October 2000, are presented with descriptions of the vegetation, depth to the water table, and other environmental variables that may have influenced evapotranspiration, as well as with discussions of evidence and observations pertaining to the reliability of the evapotranspiration estimates.

Climate of the Study Area

Although the Tule Lake NWR is less than 250 kilometers (km) inland from the Pacific Ocean, the influence of air masses from the Pacific Ocean on the local climate is reduced by the mountains to the west. At the nearby Tulelake meteorological station, which is near the town of Tulelake, Calif. (fig. 1), the 30-year monthly average precipitation, computed using data collected through 1999, averaged 12 millimeters (mm) among the three driest months July through September (Western Regional Climate Center, 2001). The 30-year monthly average precipitation averaged 34 mm for the three wettest months: November, January, and March. The 30-year calendar-year average precipitation, which was computed as the sum of the 12 monthly averages, was 288 mm, and approximately 36 percent of this precipitation occurred during the months of May to October. Annual precipitation reported by Western Regional Climate Center (2001) for Tulelake was 229 mm in 1999 and 306 mm in 2000. At the time the climate data from the Western Regional Climate Center were summarized for this report (October 2001), the data for year 2000 were provisional (Western Regional Climate Center, 2001). Minimum monthly average temperature averaged 0 degrees Celsius (°C) for the three coldest months, January, February, and December, during the 30 years prior to and including 1999. Maximum monthly average temperature averaged 17°C for the three warmest months of June through August.

Study Sites

The Tule Lake NWR, which is near the town of Tulelake, Calif. (fig. 1), consists of multiple distinct tracts with areas of open water, emergent vegetation, and croplands (fig. 2). Most of the largest tract of the Tule Lake NWR is on nearly flat terrain at an altitude of approximately 1,200 meters (m). Surface water flows into that tract from the Lost River and water-supply canals. Water on the largest Tule Lake NWR tract is regulated by a complex system of water-supply canals and ditches, drain canals and ditches, and pumps. Many of the water-supply canals deliver water to croplands by gravity, so they are elevated above the surface of those lands in a network of levees.

The drain canals and ditches accumulate water that drains from the croplands. Altitudes of water surfaces in the drain canals and ditches are generally maintained below the altitude of the land surface by pumps that remove the water to Tule Lake Sumps 1A and 1B, which are shallow water bodies (fig. 2). Several thousand hectares of irrigated croplands border the Tule Lake NWR to the north and east. Lava Beds National Monument lies to the south. Lands immediately to the west of the largest Tule Lake NWR tract are primarily mountainous rangelands.

Evapotranspiration and other measurements were made at three sites in two agricultural lots on the Tule Lake NWR. Lot C1B is approximately 41 ha in area (fig. 2, lot C1B). Drainage ditches along the northern and southern borders of lot C1B empty into a large drain canal that lies on the western border of the lot. Beyond the drain canal is an uncultivated buffer strip. West of the buffer strip is a levee upon which is a road. Immediately west of the levee is a waterway that connects Tule Lake Sumps 1A and 1B. A water-supply canal and a road are constructed in a levee that lies along the east side of lot C1B. The top of the levee is approximately 2 m higher than the surface of the lot. Irrigation checks, ridges of soil approximately 0.3 m in height, spanned almost the entire north-to-south width of the field and were spaced approximately 70 m apart. The irrigation checks had been constructed to control flow of water in the lot during flood-irrigation for the crop of the previous year. Lot C1B was not irrigated during 2000. Lot C1B was sown to the small grain crop barley during the 1999 growing season, and most of the eastern half was left unharvested; whereas, most of the western half was harvested, leaving stubble that was approximately 0.3 m or less in height. The unharvested grain was swept by a wildfire prior to late May 2000. When this study was begun during May 2000, surface coverage in lot C1B consisted of stubble and other crop residues, weedy plant species, and small grain plants that had sprouted from the seeds from the previous crop. During the 2000 growing season, a similarly sized lot immediately to the north was sown to a small grain crop, and a similarly sized lot immediately to the east was sown partly to a small grain crop and partly to onions. Land to the south of lot C1B was sown to a small grain crop for a estimated distance of several hundred meters. Lot C1B was selected for this study because it was farmed during 1999, and vegetation during 2000 at the lot was thought to be similar to what would appear under intermittent fallowing that may be practiced to conserve water in the future. An evapotranspiration measurement station designed for the BREB technique (hereafter, “BREB station”), was established in the western half of the lot (fig. 2, lot C1B).

Lot 6 is approximately 39 ha (fig. 2, lot 6). A drain ditch runs along the northern border of lot 6 and empties into a large drain canal that lies on the western border of the lot. Two east-west-trending, buried drains constructed from perforated pipe traverse most of the width of lot 6 and empty to the large drain canal (fig. 2, lot 6). Construction plans from 1974 specify a minimum depth below the soil surface of 1.2 m for the drain pipe. Beyond the drain canal lies a buffer strip. West of the buffer strip are the more northern sections of the same levee and road that were previously described as being to the west of lot C1B. Immediately west of the levee is an expanse of Tule Lake Sump 1A that is mostly occupied by emergent vegetation. A water-supply canal and a road are constructed in a levee that lies along the east side of lot 6. The top of the levee is approximately 2 m higher than the surface of the lot. Irrigation checks similar to those of lot C1B were present during this study. Lot 6 was last irrigated during 1999, when it was sown to a small grain crop of barley. Approximately 4 ha of the 1999 crop was left unharvested in parcels that were scattered throughout the lot. By early June 2000, the dead standing grain plants appeared to have been flattened by the weather. Cover crops are commonly sown after harvesting of some crops to protect soils from erosion, and part of lot 6 was tilled and sown to the small grain cereal rye as a cover crop during February 2000 to simulate a cover-crop that might exist during future fallowing (fig. 2, lot 6). Areas that were harvested in 1999 and that were not sown to the cover crop were occupied by stubble, weedy plants and small grain plants that had sprouted from the seeds from the crop of the previous year. A similarly sized lot immediately north of lot 6 was planted to potatoes during the 2000 growing season, and a similarly sized lot immediately to the south was sown partly to a small grain crop and partly to onions. A lot directly to the east of lot 6 was sown partly to onions and partly to a small grain crop during the 2000 growing season. Lot 6 was selected for this study because the presence of buried drains is representative of most of the farmed land of the refuge, and it was thought that those drains would result in a deeper water table than at lot C1B, which did not have the additional buried drains.

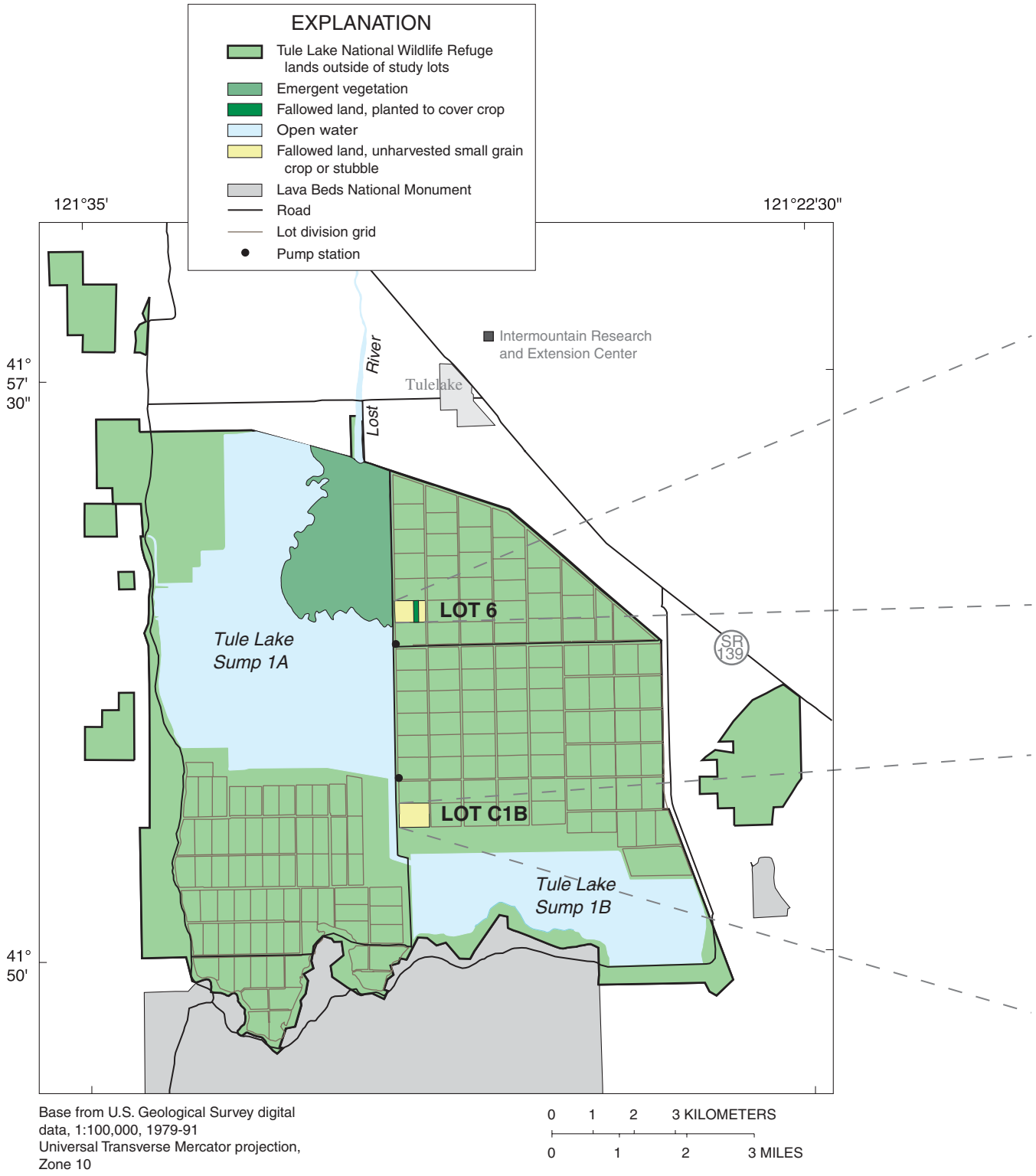

Figure 2. Tule Lake National Wildlife Refuge, lot C1B, and lot 6.

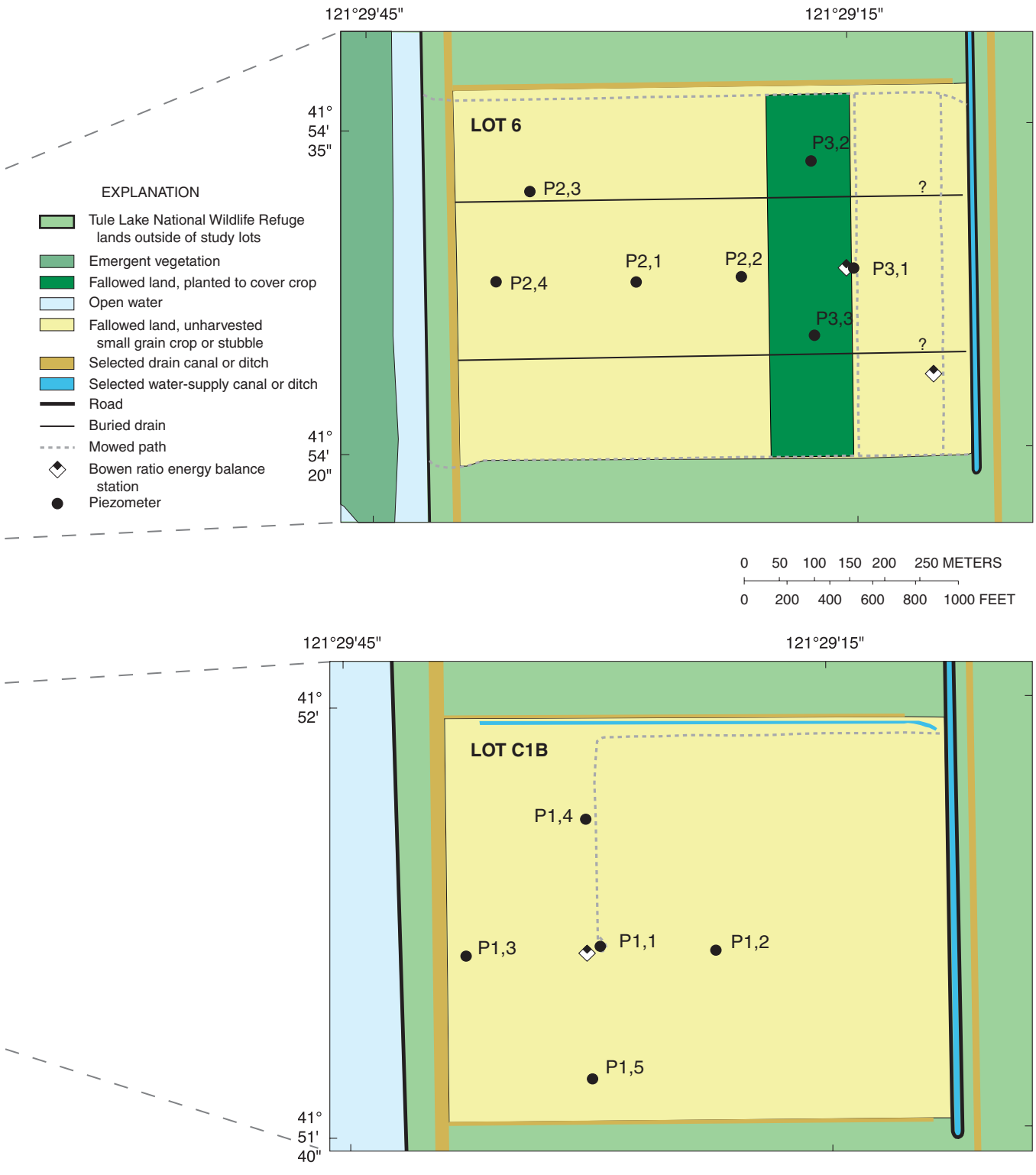

Figure 2. —*Continued*

The lot 6 stubble evapotranspiration measurement site was established in an area of the lot that had been left untreated after farming operations in 1999, and the lot 6 cover crop site was established in the cover crop. A BREB station was installed at each site (fig. 2, lot 6).

The soil mapped throughout lot 6 and lot C1B is Tulebasin mucky silty clay loam, a soil in the Tulebasin soil series with a land-surface slope gradient ranging between zero and one percent (Jahnke, 1994). Soils of the Tulebasin series are deep (approximately 1.5 m), artificially drained soils that formed in lake bed deposits of volcanic ash and diatomite, a material resembling chalk that is chiefly derived from skeletal remains of a type of algae called diatoms. Jahnke (1994) reports the depth to the water table below land surface generally ranges from about 0.5 m to about 0.9 m. Tulebasin-series soils are classified as fine, mixed, mesic Andaqueptic Haplaquolls under the United States Comprehensive Soil Classification System (Soil Survey Staff, 1975). These soils are extensively used for crop production. The uppermost 0.4 m contains between 10 and 15 percent organic matter by weight, and the entire soil profile has a shrink-swell potential ranking of moderate.

EVAPOTRANSPIRATION MEASUREMENT AND MODELING TECHNIQUES

Growing season evapotranspiration was evaluated using both measurement and modeling techniques. Evapotranspiration measurement techniques such as the BREB technique are generally technically demanding to apply; however, they can be applied at any suitable site without having to rely on the site-specific calibration coefficients that are needed to apply evapotranspiration modeling techniques. Empirically based evapotranspiration modeling techniques are advantageous from the standpoint that they are generally simpler to apply than are the measurement techniques. A weakness of modeling techniques is the uncertainty that is introduced into modeled evapotranspiration by uncertainty in the calibration coefficients where the coefficients have not been computed or verified for a particular site. Measurement and modeling approaches often can be used in a complementary manner to produce a more complete and reliable evapotranspiration record for a given site than can be obtained by either approach alone. An evapotranspiration measurement technique can yield a reliable estimate of evapotranspiration with which to reliably determine the model coefficients, and a model outfitted with those coefficients can then be applied to reliably estimate evapotranspiration for instances in which the more rigorous environmental or data requirements of the measurement technique cannot be met.

Bowen Ratio Energy Balance

Evaporation of water into the atmosphere constitutes one component of the energy balance of a land or water surface. The BREB technique (Tanner, 1960) is based on the premise that it is easier and more accurate to routinely evaluate all major components of the surface energy balance and compute evapotranspiration using the law of conservation of energy than it is to measure the evaporative vapor flux directly. An equation for the one-dimensional surface energy balance that is applicable for a terrestrial surface, such as a bare or vegetated field, can be written as

$$R_n - G = H + \lambda E \quad , \qquad (1)$$

where

R_n is net radiation, the energy difference between incoming and outgoing short- and long-wave radiation, in watts per square meter;

G is soil heat flux at the soil surface, in watts per square meter;

H is the predominantly turbulent sensible heat flux, in watts per square meter; and

λE is the predominantly turbulent latent heat flux, in watts per square meter,

where

λ is the latent heat of vaporization for water, in joules per gram; and

E is evapotranspiration rate, in grams per square meter per second.

The surface energy balance equation is an expression of the law of conservation of energy. In the sign conventions for equation 1, R_n is positive when the total energy of incoming radiation exceeds the total energy of outgoing radiation, G is positive when energy is flowing into the soil surface, and H and λE are positive when they are directed upward from the surface. Energy exchange from plant respiration and photosynthesis and rates of change of energy storage in the plant canopy or in the atmosphere below the height of measurements were assumed to be negligible in this study. The quantity $R_n - G$ is termed "available energy" because net radiant energy, less energy stored in soil, is usually the primary impetus for the turbulent fluxes H and λE.

The Bowen ratio (β) (Bowen, 1926), defined as $H/\lambda E$, permits equation 1 to be solved for λE without having to know H explicitly. The equation

$$\lambda E = \frac{R_n - G}{1 + \beta} \quad , \tag{2}$$

can then be rearranged to obtain

$$H = \frac{\beta(R_n - G)}{1 + \beta} \quad , \tag{3}$$

where all terms have been defined previously. For terrestrial surfaces, β is typically evaluated from measurements of temperature and water-vapor pressure that are made in the turbulent atmosphere above the surface. For instances in which measurements are confined to a height of a few meters above a surface, β can be computed using the equation (Monteith and Unsworth, 1990, eq. 14.26)

$$\beta = \gamma \frac{\Delta T}{\Delta e} \quad , \tag{4}$$

where

- γ is the psychrometer constant, in kilopascals per degree Celsius;
- T is air temperature, in degrees Celsius;
- e is water-vapor pressure, in kilopascals; and
- Δ signifies a difference over a vertical interval situated above the surface.

The psychrometer constant can be computed (Monteith and Unsworth, 1990, p. 181) as

$$\gamma = \frac{p c_p}{\lambda \varepsilon} \quad , \tag{5}$$

where

- p is atmospheric pressure, in kilopascals;
- c_p is specific heat of air at constant pressure, in joules per gram per degree Celsius;
- ε is a ratio (0.622) that is equal to the mass of a mole of water divided by the mass of a mole of dry air, dimensionless; and
- λ has been defined previously.

In computing λE and H by the BREB technique, R_n, G, ΔT, and Δe are measured and averaged for some specified period, typically 30 or 60 minutes. Measurements and supplementary computations needed to apply the BREB technique for this study are described in a subsequent section of this report.

The BREB technique described in this report relies on some hydrodynamic assumptions about the nature of the turbulent atmosphere near the surface where the measurements are made. An assumption that permits one-dimensional treatment of the turbulent fluxes is the equilibration of the surface with the airstream in which ΔT and Δe are determined. For a horizontal surface, equilibrium is a state in which the horizontal components of momentum, heat, and water-vapor fluxes are negligibly small in comparison to the respective vertical components. Equilibrium also implies the fluxes do not change with height and that profiles of wind speed, temperature, and water-vapor pressure are horizontally uniform.

When the wind passes between horizontal surfaces that differ with respect to aerodynamic roughness, temperature, or aridity, horizontal gradients potentially can develop as the air begins exchanging momentum, heat, and water vapor with the downwind surface. As the air travels downwind from the boundary between the surfaces, a locally equilibrated air layer develops in which horizontal gradients have substantially dissipated and in which fluxes of heat and water vapor are constant with height. The distance that the wind has traveled from the boundary is the fetch.

The locally equilibrated air layer grows from the downwind surface and increases in thickness with distance. Judging the thickness of the locally equilibrated air layer is important for determining where and at what heights to place the sensors used for determining ΔT and Δe. Maximum sensor height z_u is commonly computed using a relation similar to

$$\frac{x}{z_u - d_0} \geq \eta \quad , \tag{6}$$

where

x is fetch, in meters;

z_u is height above land surface, in meters;

d_0 is the zero-plane displacement height, in meters; and

η is a prescribed minimum for the fetch-to-instrument-height ratio, dimensionless.

Zero-plane displacement height is the effective height at which the surface exchanges momentum, heat, or water vapor with the atmosphere. For agricultural crops, where the vegetation is generally uniform and dense, Campbell (1985, p. 138) suggests $d_0 = 0.77h_c$, where h_c is height of the crop canopy, in meters. Although d_0 might be different for momentum, heat, and water vapor, d_0 for the latter two quantities are generally assumed to equal d_0 for momentum; empirical relations for heat and water vapor have not been formulated. For bare soil or sparse vegetation, d_0 can be assumed to be 0 (Brutsaert, 1982, p. 116). Values of d_0 for vegetation of intermediate densities can be expected to range between the values for sparse and dense vegetation. An acceptable minimum for the fetch-to-instrument-height ratio (η) has often been taken to be 100 (Weeks and others, 1987); however, results of some investigations with short vegetation have shown equilibration to be sufficient for successful application of the BREB technique with η as low as about 20 (Fritschen and others, 1983; Heilman and others, 1989). This lack of consensus in the literature regarding η contributes to uncertainty as to whether or not the BREB and related techniques are suitable for a particular site.

Stannard (1997) has presented a theory enabling one to estimate the degree of equilibration of the Bowen ratio and latent heat flux to the surface of interest where the airstream has been affected by an upwind surface, termed the "contaminating surface." For example, Stannard (1997, eq. 6) gives an equation for percentage of equilibration of latent heat flux to the surface of interest ($\%Eq_{\lambda E}$) as

$$\%Eq_{\lambda E} = 100\frac{1 + \beta_c - R(1 + \beta_m)(1 + \beta_i)}{1 + \beta_c - R(1 + \beta_i)(1 + \beta_m)} \quad , \tag{7}$$

where

β_c is the Bowen ratio for the contaminating surface, dimensionless;

R is the ratio of available energy at the contaminating surface to that at the surface of interest, dimensionless;

β_m is the measured Bowen ratio for the surface of interest, dimensionless; and

β_i is the actual Bowen ratio for the surface of interest, dimensionless.

Percentage of equilibration of λE indicates the completeness of the transition of λE from its value at the contaminating surface (λE_c) to its value at the surface of interest (λE_i). The percentage error in latent heat flux due to the influence of the contaminating surface ($\%\delta_{\lambda E}$) follows from equation 2 and is given by (D.I. Stannard, U.S. Geological Survey, oral commun., May 2001)

$$\%\delta_{\lambda E} = 100\frac{\beta_i - \beta_m}{1 + \beta_m} \quad , \tag{8}$$

where all terms have been defined previously.

In application of the BREB technique, the ideal situation is $\beta_i = \beta_m$, for which $\%\delta_{\lambda E}$ is 0. Divergence of β_i and β_m and error in measured latent heat flux is caused by lack of equilibration of the airstream to the surface of interest due to the influence of the contaminating surface. The airstream equilibration theory presented by Stannard (1997) can be used to iteratively compute β_i from measurements or estimates of β_m, β_c, R, x, d_0, heights of the sensors used for computing ΔT and Δe, and the roughness length z_0, in meters. The roughness length is a characteristic of the surface that influences turbulent exchange of momentum, heat, or water vapor with the atmosphere. Generally, the larger the z_0, the more intense is the turbulent exchange. Campbell (1985, p. 138) indicates z_0 for uniform crops can be computed using the equation $z_0 = 0.13h_c$, where h_c is as defined previously.

Another assumption underpinning the BREB technique, that the surface and atmosphere near the surface of interest are at steady state, is rarely met because of diurnal cycling and other variations of meteorological conditions. The transient state of the atmosphere can cause BREB-computed fluxes to be erroneous, particularly during rapidly changing conditions at dawn and dusk. For this study, R_n, G, ΔT, and Δe were initially computed for 15 minutes, and two 15-minute averages of each quantity were averaged to compute β and λE for 30-minute periods, which were brief enough that the assumption of steady-state conditions was thought to generally be valid. Thus, the dynamic, diurnally changing atmosphere was treated as though it evolved through a series of steady states. Daily and longer term averages or totals of energy balance components and other quantities were computed by summing or averaging 30-minute quantities.

Eddy Covariance

The eddy covariance technique is an alternative to the BREB technique for estimating turbulent fluxes of energy and mass from a surface. Unlike the BREB technique that relies on solution of the surface energy balance and measurements of the mean differences ΔT and Δe, the eddy covariance technique is based on analysis of individually sensed turbulent fluctuations. For example, in the equilibrated air above a level surface, H can be computed from a simplified, one-dimensional equation for turbulent transport (Brutsaert, 1982, eq. 3.75),

$$H = \rho c_p \overline{w'T'} \quad , \tag{9}$$

where

ρ is air density, in grams per cubic meter;

w' is short-term fluctuation of vertical wind speed from the time-averaged mean, in meters per second;

T' is short-term fluctuation of air temperature from the time-averaged mean, in degrees Celsius;

$\overline{}$ the overbar represents averaging for a specified period of time; and

other terms have been defined previously.

The quantity $\overline{w'T'}$ is the covariance between vertical wind speed and air temperature. In application of the eddy covariance technique, the fluctuations w' and T' are sampled using fast-response sensors. The fluctuations are tallied for a specified period of time to compute $\overline{w'T'}$. An equation similar to equation 9 can be applied to measure latent heat flux and evapotranspiration, although this was not done in this study. Although the BREB and eddy covariance techniques share many of the same hydrodynamic assumptions, measurement and sampling schemes for the two techniques are very different; therefore, the eddy covariance technique provides an independent means with which to check H computed by the BREB technique (equation 3). Because the BREB technique relies on specification of all components of the surface energy balance to compute H and λE, the independent check on H provided by the eddy covariance technique indirectly provides an indication of the reliability of the BREB estimates of λE. The eddy covariance technique was applied intermittently in this study to provide an overall check on turbulent fluxes that were computed by the BREB technique.

Priestley-Taylor

Models provide a means for estimating λE and E when and where data needed for more rigorous measurement techniques, such the BREB technique, are not available or are not sufficiently accurate, but where data for environmental variables that govern evapotranspiration are available or can be reliably estimated. The Priestley-Taylor (PT) equation (Priestley and Taylor, 1972) has been the basis for empirical models of evapotranspiration from many types of land surfaces, including croplands (Steiner and others, 1991), semiarid rangelands (Stannard, 1993), and forest clearcuts (Adams and others, 1991). The PT equation is a simplification of the physically based Penman-Monteith equation (Monteith, 1965), where the latter explicitly accounts for turbulent transfer with an aerodynamic component composed of variables that characterize fundamental properties of the surface, the atmosphere, and turbulent transfer mechanisms. By contrast, the simpler PT equation is

$$\lambda E = \alpha \lambda E_{EQ} \quad , \tag{10}$$

where

λE_{EQ} is equilibrium latent heat flux, in watts per square meter; and

α is a coefficient that is equal to the ratio of λE to λE_{EQ}, dimensionless.

Equilibrium latent heat flux, the latent heat flux that would prevail if the air in contact with the surface of interest is saturated with water vapor (Campbell, 1977, p. 140), is given by

$$\lambda E_{EQ} = \frac{s(R_n - G)}{s + \gamma} \quad , \tag{11}$$

where

s is slope of the relation between water-vapor pressure at atmospheric saturation and temperature, in kilopascals per degree Celsius; and

other terms have been defined previously.

A key to modeling evapotranspiration with the PT equation is the evaluation of α, which implicitly accounts for the contribution to λE from the aforementioned aerodynamic component of the Penman-Monteith equation. Priestley and Taylor (1972) examined data from several surfaces where availability of water was not limiting to evapotranspiration, and they concluded that daily average α for such surfaces is a constant of approximately 1.26 when the evapotranspiration rate is not affected by advected energy. Jury and Tanner (1975) modified Priestley and Taylor's (1972) approach for surfaces where water availability is not limiting by allowing α to vary with variations of atmospheric water-vapor pressure deficit, D, in kilopascals, where the latter is a composing variable of the aerodynamic component of the Penman-Monteith equation. Atmospheric water-vapor pressure deficit is computed from $D = e_s - e$, where e_s is water-vapor pressure at atmospheric saturation, in kilopascals, and e is as defined previously.

The PT equation has also been modified and applied to surfaces where evapotranspiration is water-limited, such as a drying soil (Barton, 1979) and water-stressed or senesced vegetation (Williams and others, 1978; Flint and Childs, 1991). Values reported for α for these water-limited situations typically are less than 1.26 and often are less than 1.0. In some work with water-limited surfaces, α as defined by Priestley and Taylor has been replaced by the modified variable, α'; however, no such distinction is made in this report. The PT equation was applied in this study to estimate evapotranspiration when estimates by the BREB technique were not available or were thought to be unreliable, but where the variables in equations 10 and 11 were measured or could be reliably estimated at a particular site.

Reference Evapotranspiration

An evapotranspiration modeling technique that is typically applied without measuring any environmental variables at the site of interest, which is hereafter referred to as the "reference evapotranspiration technique," can be summarized as (Jensen and others, 1990, p. 114)

$$E = k_c E_0 \quad , \tag{12}$$

where

E is evapotranspiration rate, in millimeters per day;

k_c is an empirical crop coefficient, dimensionless; and

E_0 is reference evapotranspiration rate, in millimeters per day.

Jensen and others (1990, p. 57) define E_0 as "... the rate at which water, if available, would be removed from the soil and plant surface of a specific crop, arbitrarily called a reference crop." The purpose of E_0 is to provide an evapotranspiration standard that controls for climate effects and with which to compute evapotranspiration from surfaces other than the reference crop in the same locale or region. A key to modeling evapotranspiration with equation 12 is the evaluation of k_c.

APPLICATIONS OF EVAPOTRANSPIRATION MEASUREMENT AND MODELING TECHNIQUES

Applications of the BREB, eddy covariance, and PT techniques to compute or model evapotranspiration require numerous field measurements that are made by a diverse set of instruments. This report section describes measurements, instruments, and supplementary computations that were used to evaluate terms in the previously presented technique-defining equations for the study sites. In addition, this section describes techniques and results of supporting work conducted to calibrate the type of a soil moisture sensor that was used in the field for the Tulebasin mucky silty clay loam that was present at the study sites, and to estimate bulk density, specific heat, and thermal conductivity of that soil.

Net Radiation

Net radiation (R_n) was measured directly at each site with a single net radiometer (model Q*7.1 or model Q*6.7.1, Radiation and Energy Balance Systems, Inc., Bellevue, Wash.) that was suspended at a height of approximately 3.5 m above the soil surface. Because the net radiometers are influenced by wind, they were equipped with ventilators that forced air over the hemispherical upper and lower windshields of the sensor at a constant speed. A wind correction that was based on the fixed speed of the forced ventilation and that was supplied by the manufacturer was applied to the sensed net radiation. The net radiometer was monitored by a data logger (model CR10X, Campbell Scientific, Inc., Logan, Utah) that also applied the wind correction and averaged R_n every 15 minutes.

Soil Heat Flux

The average of soil heat flux at the soil surface (G) sampled at three places was used to evaluate the energy balance at each evapotranspiration measurement site. At each sampling place, G was computed by summing soil heat flux that was measured at a fixed soil depth (z) and the rate of change of energy storage in soil above the fixed depth, where the latter rate was estimated calorically from the rate of change of depth-averaged soil temperature. An equation for G is

$$G = G_z + \Delta z \frac{d\bar{T}_s}{dt}(\rho_s c_s + \theta \rho_w c_w) \quad , \qquad (13)$$

where

G_z is soil heat flux, in watts per square meter, at soil depth z;

z is in meters;

Δz is thickness of the soil layer above depth z, in meters;

$\bar{T}_s$ is depth-averaged temperature of the soil layer, in degrees Celsius;

t is time, in seconds;

ρ_s is soil bulk density, in kilograms of dry soil per cubic meter;

c_s is specific heat of dry soil, in joules per kilogram per degree Celsius;

θ is volumetric soil water content, in volume of water per unit volume of soil, dimensionless;

ρ_w is density of water, in kilograms per cubic meter; and

c_w is specific heat of water, in joules per kilogram per degree Celsius.

Soil heat flux at depth z was measured with a heat flux plate (model HFT3.1, Radiation and Energy Balance Systems, Inc.); z was 0.1 m, except during May 19 to June 3 at lot C1B, when z was 0.05 m. The soil heat flux plates were monitored by a data logger (model CR10X) that averaged soil heat flux every 15 minutes. Measured soil heat flux was corrected to account for errors caused by the mismatch between the thermal conductivities of the heat flux plate and the soil. The correction equation provided by the manufacturer of the heat flux plate and based on Philip (1961) is

$$G_z = G'_z \frac{1 - 1.92L/d_p(1 - k_s/k_p)}{1 - 1.92L/d_p(1 - k_m/k_p)} \quad , \qquad (14)$$

where

G'_z is uncorrected, measured soil heat flux at soil depth z, in watts per square meter;

L is thickness of the soil heat flux plate, in millimeters;

d_p is diameter of the soil heat flux plate, in millimeters;

k_s is thermal conductivity of the soil, in watts per meter per degree Celsius;

k_p is thermal conductivity of the soil heat flux plate, in watts per meter per degree Celsius; and

k_m is thermal conductivity of the medium in which the soil heat flux plate was originally calibrated, in watts per meter per degree Celsius.

The manufacturer of the heat flux plate provided values for thickness of the soil heat flux plate (L, 3.91 mm), diameter of the plate (d_p, 38.2 mm), thermal conductivity of the plate (k_p, 1.22 watts per meter per degree Celsius, ((W/m)/ºC)), and thermal conductivity of the medium that was used to calibrate the plate (k_m, 0.906 (W/m)/ºC). Thermal conductivity of soil varies with water content (Campbell, 1985, p. 32), and laboratory experiments were conducted to describe the relation between k_s and volumetric soil water content for the soil at the study sites. A sample from the uppermost 0.1 m of soil at lot C1B was used to assemble a series of packed soil columns with different water contents. The sample was repeatedly packed into a 0.1-m-diameter, 0.32-m-long polyvinyl chloride cylinder to produce a series of soil columns of varying column-average θ. Soil thermal conductivity was measured by the line heat source technique (Jackson and Taylor, 1986), using a thermal conductivity sensor (model TC-18, Thermal Logic Co., Pullman, Wash.) that was coupled to a data logger (model 21X, Campbell Scientific, Inc.) and inserted into the exposed face of each soil column. Two or three replicate measurements of k_s were made at each water content, and measured k_s ranged between 0.08 and 0.41 (W/m)/ºC among the replicates and the columns.

Column-average ρ_s and θ were determined following the thermal conductivity measurements that were made in each column. Column-average ρ_s was computed by dividing the mass of the soil, oven-dried at 105ºC for a minimum of 37 hours, by the volume of the cylinder. Column-average θ was computed gravimetrically from the change in mass of the soil sample resulting from oven-drying and the volume of the cylinder. Column-average ρ_s ranged from 582 to 614 kilograms per cubic meter (kg/m^3) among six columns that were prepared, and column-average θ ranged from oven dry to 0.39. Soil that was oven-dried at 105ºC contained a small but unknown amount of water that was strongly adsorbed to the soil particles or was incorporated in the structures of those particles (Gardner, 1986). Nonetheless, the numerical value of θ for oven-dried samples was taken to be 0.

The data for θ and k_s that were obtained from the soil column experiments were fitted to equation 4.20 of Campbell (1985)

$$k_s = 0.2179 + 0.4055\theta - \frac{0.1510}{e^{(3.4054\theta)^4}} \quad , \qquad (15)$$

where each numerical coefficient, except the exponent 4, which is suggested by Campbell (1985, p. 34), was adjusted using the SOLVER tool of the Microsoft Excel program (Microsoft, Inc., Redmond, Wash.) to minimize the root-mean-square error (RMSE) of predicted k_s. The RMSE of k_s predicted by equation 15 was 0.01 (W/m)/ºC, and the sample size (n) was 17. Equation 15 was used to estimate k_s in the soil near the heat flux plates at the three evapotranspiration measurement sites for the purpose of correcting soil heat flux with equation 14.

Soil temperature T_s, in degrees Celsius, was sensed with a soil temperature sensor constructed with a 0.077-m-long platinum resistance temperature detector that spatially averaged temperature over its length (model STP1, Radiation and Energy Balance Systems, Inc.). A soil temperature sensor was inserted into the 0-to-z-m soil depth interval near each heat flux plate at a elevation angle of approximately 60 degrees (elevation angle was approximately 45 degrees when z was 0.05 m), such that the center of the detector was approximately $z/2$ m from the soil surface. The soil temperature sensors were monitored with a data logger (model CR10X) that averaged T_s and the quantity dT_s/dt every 15 minutes. Sensed soil temperature was assumed to be representative of the depth-averaged temperature $\overline{T}_s$ for the 0-to-z-m soil depth interval, and the quantity dT_s/dt was assumed to be representative of $d\overline{T}_s/dt$ in equation 13.

Soil bulk density (ρ_s) at the evapotranspiration measurement sites was computed from the oven-dried mass of soil samples taken from a known volume with a hammer-driven core sampler. Multiple samples were taken at each site. Bulk density of the uppermost 0.1 m of soil averaged 546 kg/m^3 at the lot C1B evapotranspiration measurement site (standard deviation (sd) = 24 kg/m^3, n = 12), 554 kg/m^3 at the lot 6 stubble evapotranspiration measurement site (sd = 48 kg/m^3, n = 12), and 494 kg/m^3 at the lot 6 cover crop evapotranspiration measurement site (sd = 45 kg/m^3, n = 11).

Specific heat of dry Tulebasin mucky silty clay loam soil was estimated using a sample collected from the uppermost 0.1 m of soil at lot C1B that was oven-dried at 105ºC. Specific heat was measured using the dual-probe heat-pulse technique of Campbell and others (1991). The sample was placed into a 0.054-m-diameter, 0.06-m-long cylinder. A specific-heat sensor (Thermal Logic Co.) that was coupled to a data logger (model 21X) was inserted in the center of the exposed soil face to measure volumetric specific heat of the sample, which is a close approximation of $\rho_s c_s$ for a dry soil. Specific heat of oven-dried soil in the sample (c_s) was computed by dividing volumetric specific heat by the bulk density of the sample (ρ_s, 561 kg/m^3). Two replicate c_s determinations that were made in the soil column were 1,150 and 1,180 joules per kilogram per degree Celsius ((J/kg)/ºC).

Volumetric soil water content was monitored near each heat flux plate using a soil water content reflectometer (model CS615, version 8221-07, Campbell Scientific, Inc.). The reflectometer senses the frequency of electromagnetic waves that are propagated along a twin-probe, 0.3-m-long wave guide that is inserted into the soil. The frequency of the waves, and therefore the period of the waves (τ, in milliseconds), vary with the dielectric constant of the soil. The dielectric constant of the soil is largely controlled by the soil volumetric water content. The signal from the reflectometer, τ that ranges from 0.7 to 1.6 milliseconds, can be applied to compute volumetric soil water content using a calibration function that relates τ directly to volumetric soil water content. For this study, the reflectometer probes were installed parallel to the plane of the soil surface and at a soil depth of $z/2$, which was 0.05 m, except during May 19 to June 3 at lot C1B, when $z/2$ was 0.025 m. The reflectometers were monitored with a data logger (model CR10X) that averaged τ every 15 minutes.

A single model CS615 reflectometer similar to the nine that were deployed at the evapotranspiration measurement sites was used to develop a soil-specific calibration model for the sensor in the Tulebasin mucky silty clay loam. A sample from the uppermost 0.1 m of soil at lot C1B was used to assemble a series of packed soil columns with different water contents. The sample was repeatedly packed into a 0.1-m-diameter, 0.32-m-long polyvinyl chloride cylinder to produce a series of soil columns. Column-average ρ_s and θ were determined as was discussed previously. Average ρ_s of the soil columns used for the calibration ranged from 582 to 614 kg/m^3, and column-average θ ranged from oven dry to 0.39. The reflectometer probes were inserted into the exposed face of each soil column and τ was read by a data logger (model 21X). The first three replicate measurements made at each water content were included in the calibration data set, and τ ranged from 0.79 to 1.54 milliseconds among the replicates and columns. Temperature of each column was sensed with a chromel-constantan thermocouple probe following each set of replicate measurements. Temperature of the columns ranged from 18ºC to 22ºC. A temperature-dependent calibration function was then developed for the reflectometer. The function is

$$\theta = \theta^* - (T_s - 20) * (-0.000346 + 0.019\theta^* - 0.045\theta^{*2}) \quad , (16)$$

where θ^* is given by

$$\theta^* = -3.1260 + 6.9708\tau - 4.6487\tau^2 + 1.04204\tau^3 \quad , \quad (17)$$

and other terms are as defined previously.

Equation 16 accounts for the temperature dependence of the reflectometer signal and is given by the manufacturer. The coefficients of equation 17 were computed using the SOLVER tool of the Microsoft Excel program to minimize the RMSE of predicted θ. The RMSE of θ predicted by the function was 0.01 (n = 20). The calibration function was applied with field measurements of τ and T_s to compute θ for use in equations 13 and 15. The use of θ measured at depth $z/2$ for correcting G'_z by equations 14 and 15, rather than θ at depth z where the soil heat flux plates were buried, introduced minimal error into G_z because the correction was small in magnitude and was fairly insensitive to θ.

The correction ranged from -9 to -14 percent of G'_z among the three evapotranspiration measurement sites; whereas, θ ranged from 0 to 0.38.

Reliability of the calibration function for the Tulebasin mucky silty clay loam for θ greater than was measured during development of the function (0.39) is not known. However, the range of θ in the calibrations was similar to the range measured at the evapotranspiration measurement sites. The maximum valid τ that was recorded at the evapotranspiration measurement sites was 1.3822 milliseconds (T_S= 13.7ºC), which corresponds to a value for θ of 0.38 according to equations 16 and 17. The minimum, valid field-recorded τ was 0.7867 milliseconds (T_S = 19.5ºC), for which θ computed by equations 16 and 17 is an implausible -0.01. This latter result likely was caused by variations of soil properties that influenced the response of the reflectometer and that are not (and likely cannot be) described using a single set of calibration coefficients. Negative computed values of θ were assigned a value of 0.0 for purposes of this study.

The dimensions of soil regions that influenced measurements made by the reflectometer were not known, and a simple experiment was conducted to examine possible effects of the finite volume of the soil columns on reflectometer measurements that were made to develop the calibration function. The 0.1-m-diameter soil columns were submerged in a water bath to approximately 0.02 m below the rim of the cylinder to determine whether or not τ was affected by the dielectric constant of material outside of the cylinder. Submerging a column of oven-dry soil and one with θ = 0.39 increased τ by 0.6 and 0.7 percent, respectively, indicating that the finite columns had only minimal effects on the reflectometer measurements.

Air Temperature and Vapor Pressure

The vertical differences ΔT and Δe were computed from T and e measured at an upper height minus T and e measured one m lower. T and e were measured at each height by an aspirated air sensor (model THP1, Radiation and Energy Balance Systems, Inc.). An aspiration fan drew air into a horizontally mounted radiation shield attached to each air sensor and past a platinum temperature resistance detector that sensed the temperature of the airstream. Relative humidity of the airstream was sensed with a capacitive-type humidity sensor that was housed in a cavity at the end of a shaft that was swept by the airstream. A filter across the cavity orifice that protected the humidity sensor from contaminants also slowed the movement of air in the cavity. The slower movement of air in the cavity at times caused the temperature of the cavity to differ from that of the airstream. Temperature of the cavity (T_c, in degrees Celsius) was sensed with an additional platinum temperature resistance detector for the sole purpose of obtaining accurate measurements of water-vapor pressure (e) of the airstream, which was computed from

$$e = h_r e_s \quad , \tag{18}$$

where

h_r is relative humidity, dimensionless; and

other terms are as defined previously.

The data logger (model CR10X) that monitored the air sensors computed e_s from T_c using the Lowe equation (Lowe, 1977; Campbell Scientific, Inc., 1997). The data logger also computed time-averaged ΔT and Δe every 15 minutes. The air sensors were mounted to a motor-driven exchange system (model AEM, Radiation and Energy Balance Systems, Inc.) that exchanged the sensors between the two heights every 15 minutes to reduce the effects of individual sensor bias on the computed differences ΔT and Δe.

Latent heat of vaporization of water (λ) varies weakly with temperature and was computed using (Jensen and others, 1990, eq. 7.1)

$$\lambda = 2,501 - 2.361T \quad , \tag{19}$$

where all terms have been defined previously. Atmospheric pressure (p), which is needed to compute the psychrometer constant (γ) and density of air (ρ), was estimated by the equation (Jensen and others, 1990, eq. 7.4)

$$p = 101.3 - 0.01055Z \quad , \tag{20}$$

where Z is site altitude, in meters.

Density of air (ρ) was computed as

$$\rho = \rho_d + \rho_v \quad , \tag{21}$$

where

ρ_d is density of dry air, in grams per cubic meter; and

ρ_v is density of atmospheric water vapor, in grams per cubic meter.

Density of dry air was computed from Brutsaert (1982, equation 3.4) as

$$\rho_d = \frac{1,000(p-e)}{R_d(T+273.15)} \quad , \tag{22}$$

where

R_d is the ideal gas constant for dry air, which equals 0.28704 joules per gram per kelvin (Brutsaert, 1982, p. 38);

273.15 was added to T, in degrees Celsius, to convert it to kelvins; and

other terms are as defined previously.

Density of atmospheric water vapor was computed using (Brutsaert, 1982, equation 3.5)

$$\rho_v = \frac{1,000\varepsilon e}{R_d(T+273.15)} \quad , \tag{23}$$

where all terms have been defined previously.

Specific heat of air at constant pressure (c_p) was computed from the specific heats of dry air and water vapor weighted by their mass fractions as

$$c_p = \frac{c_{pd}\rho_d + c_{pv}\rho_v}{\rho_d + \rho_v} \quad , \tag{24}$$

where

c_{pd} is specific heat of dry air at constant pressure, which is equal to 1.005 joules per gram per degree Celsius (Brutsaert, 1982, p. 38);

c_{pv} is specific heat of water vapor at constant pressure, which is equal to 1.846 joules per gram per degree Celsius (Brutsaert, 1982, p. 38); and

other terms are as defined previously.

The slope of the relation between saturation water-vapor pressure of air and temperature was computed using a form of the Clausius-Clapeyron equation (Brutsaert, 1982, equation 3.22)

$$s = \frac{\varepsilon\lambda e_s}{R_d(T+273.15)^2} \quad , \tag{25}$$

where all terms have been defined previously, and where e_s was computed using the previously noted Lowe equation (Lowe, 1977), which can be written as

$$e_s = (A_0 + T(A_1 + T(A_2 + T(A_3 + T(A_4 + T(A_5 + TA_6))))))/10 \quad , \tag{26}$$

where the coefficients are

A_0: 6.107799961
A_1: $4.436518521 \times 10^{-1}$
A_2: $1.428945805 \times 10^{-2}$
A_3: $2.650648471 \times 10^{-4}$
A_4: $3.031240396 \times 10^{-6}$
A_5: $2.034080948 \times 10^{-8}$
A_6: $6.136820929 \times 10^{-11}$

and other terms are as defined previously.

Data Screening and Segregation

Sensible and latent heat fluxes computed by the BREB technique were examined to detect and reject those computed fluxes that either were physically implausible or were suspected to be erroneous. Physically implausible fluxes are those for which the signs of λE and H computed by the BREB technique are not consistent with the signs of Δe and ΔT and the overall surface energy balance. Specifically, BREB-computed λE and H were rejected when (modified from Ohmura, 1982)

$$\left(\frac{\lambda\varepsilon\Delta e}{p} + c_p\Delta T\right) \bullet (R_n - G) > 0 \quad , \tag{27}$$

where all terms have been defined previously.

In addition, λE and H from equations 2 and 3 are undefined for $\beta = -1$, and even relatively small measurement or sampling errors in R_n and G can lead to large-magnitude errors in computed λE and H when β approaches –1. For this reason, λE and H computed by the BREB technique were rejected when β was in the range of -1.25 to -0.75.

Finally, λE and H computed by the BREB technique for some 30-minute periods were rejected that were not detected by the previous two objective criteria, but that clearly appeared to be unreasonable. One example of the latter flux estimates was a sudden spike of H near the time of sunrise or sunset that was accompanied by negative λE.

Nighttime and daytime summaries of surface energy balance components and related environmental variables were made by discriminating nighttime from daytime if the solar elevation angle (Ψ, in radians), was less than 0 or greater than 0, respectively. Solar elevation angle was computed using (Stull, 1988, eq. 7.3.1c)

$$\sin\Psi = \sin\Phi\sin\delta - \cos\Phi\cos\delta\cos\left(\frac{\pi t_{UTC}}{12} - \Gamma\right), \quad (28)$$

where

Φ is latitude (positive north), in radians;

Γ is longitude (positive west), in radians;

δ is solar declination angle, the angle of the sun above the equator, in radians; and

t_{UTC} is Coordinated Universal Time, computed as Pacific Daylight Time plus 7 hours, in hours.

Solar declination angle varies with time of year and was computed from (Stull, 1988, equation 7.3.1d)

$$\delta = \Phi_r \cos\left(\frac{2\pi[d - d_r]}{d_y}\right), \quad (29)$$

where

Φ_r is latitude of the Tropic of Cancer (0.4093 radians);

d is day of the calendar year (for example, February 15 is day 46);

d_r is day of the summer solstice (173); and

d_y is the number of days per year (365.25).

Summaries of surface-energy balance components and other environmental variables also were made by segregating those data according to a simple wind-direction classification scheme. For each 30-minute period, wind direction was classified as westerly if the average wind direction azimuth during both composing 15-minute periods was equal to or greater than 180 degrees and less than 360 degrees. Wind direction for a given 30-minute period was classified as easterly if the average wind direction azimuth during both composing 15-minute periods was equal to or greater than 0 degrees and less than 180 degrees. Wind direction was classified as mixed if the wind direction was westerly during one of the 15-minute periods and easterly during the other 15-minute period.

Eddy Covariance and Other Measurements

Short-term fluctuations of vertical wind speed (w') and air temperature (T') were sensed with a one-dimensional sonic anemometer equipped with an air temperature sensor (model CA27, Campbell Scientific, Inc.), and the anemometer signals were sampled at a nominal frequency of 10 Hz by a data logger (model 21X) that also computed the covariance $\overline{w'T'}$ every 15 minutes. Average H was computed using equation 9 for every 15-minute period, and 30-minute-average H was computed as the average of two 15-minute averages.

Precipitation at the lot C1B and lot 6 cover crop evapotranspiration measurement sites was sensed with tipping-bucket rain gages (model 525, Texas Electronics, Inc., Dallas, Texas). The rain gages were monitored by a data logger (model CR10X) that also totaled precipitation every 15 minutes. Horizontal wind speed and direction were sensed at each evapotranspiration measurement site using a vane-and-propeller-type wind sensor (model 05103-5 or 05305, R.M. Young Co., Traverse City, Mich.). The wind sensors were monitored with a data logger (model CR10X) that also averaged wind speed and direction every 15 minutes.

Estimating Depth to the Water Table

Personnel of the USFWS installed piezometers at selected locations in lot C1B and lot 6 (fig. 2, lot C1B and lot 6) and monitored water levels in those piezometers. The piezometers were constructed using a 0.025-m-diameter polyvinyl chloride casing fitted on the bottom with a 0.3-m-long slotted well screen (slot size 2.5×10^{-4} m).

The casing-and-screen assembly was placed into a hole that was made with an auger. Sand was poured into the hole around the assembly to imbed the screen. The uppermost 0.3 m of the hole was filled with bentonite clay. Maximum depth of the piezometers below land surface ranged from approximately 1.1 to 1.5 m (Tim Mayer, USFWS, written commun., November 2000). Water level was measured using a measuring tape with a water-contact sensor.

Instrumentation Deployments

Each BREB station consisted of numerous sensors and an enclosure holding the BREB system control devices and data logger. The net radiometer and the air sensors were mounted on a tripod that was approximately 7 m south of a tripod that supported the enclosure holding the BREB system control devices and data logger. The wind sensor was mounted to a metal fence post that was driven into the ground approximately 9 m north-northwest of the tripod that supported the enclosure. Heights above the land surface of the air and wind sensors for each BREB station are given in table 1. An ensemble of sensors for computing soil heat flux at the soil surface (G) consisting of a heat flux plate, a water content reflectometer, and a soil temperature sensor, was buried at each of three places that were within approximately 10 m of the data logger enclosure. Burial locations were selected to sample G under the range of different types of surface cover that existed within the reach of the sensor cables.

The BREB station at the lot C1B evapotranspiration measurement site was placed in the unburned western part of the lot, and where homogeneity of vegetation and stubble cover for 200 m in all directions appeared to be greatest. Nonetheless, the vegetation and stubble coverage was not fully uniform. Patches of stubble with few green plants were interspersed with patches of weedy and small grain plants within 200 m of the BREB station when it was established during mid-May. In addition, an approximately 3-m-wide path was mowed to the east of the station during late July or early August (fig. 2, lot C1B).

The heterogeneous nature and limited patch size of the vegetation and other surface coverage at lot 6 precluded placing the BREB stations where fetch would have been adequate regardless of wind direction. During mid-May, vegetation west of the cover crop consisted of patches of weedy plants and barley that were interspersed with patches and strips of stubble. The strips ran in north-south directions and were estimated to range from 5 to 20 m in width. Approximately 30 percent of lot 6 outside of the cover crop was occupied by these “stubble barrens” in mid-May. The BREB station at the lot 6 stubble site was placed in an area of relatively homogeneous stubble near the southeast corner of the lot. Minimum fetch over the stubble and the vegetation that later grew among and overtopped the stubble was approximately 120 m during westerly winds. Minimum fetch was approximately 50 m during easterly winds, although the fetch was broken by a 3-m-wide path that was mowed during late July or early August (fig. 2, lot 6). Evapotranspiration estimates made by the BREB technique for favorable (westerly) wind directions were used to calibrate a simple evapotranspiration model that was based on the PT equation. The PT model was then used to estimate evapotranspiration for periods when the wind direction was not westerly or the when estimates from the BREB technique were otherwise not available or not reliable, but for which R_n, G, and average air temperature data were available for the stubble site.

Similarly, the BREB station at the lot 6 cover crop evapotranspiration measurement site was placed near the east edge of the area of the lot that was sown to a cover crop of cereal rye during February 2000 (fig. 2, lot 6). Fetch over the reasonably uniform cover crop was a minimum of approximately 115 m when winds were westerly, and fetch was approximately 10 m when the wind was directly from the east. Evapotranspiration estimates made by the BREB technique for favorable (westerly) winds were used to calibrate a simple evapotranspiration model that was based on the PT equation. The model was then used to estimate evapotranspiration for periods when the wind direction was not westerly. A data logger programming error caused the wind sensor data to be erroneous during June 9 to 27, and wind direction during that period was estimated using wind direction from the nearby lot 6 stubble site BREB station.

Finally, a mobile eddy covariance station was operated to compute sensible heat flux during at least one diurnal cycle at each evapotranspiration measurement site.

Table 1. Approximate maximum heights of vegetation or vegetation residues, and heights of air and wind sensors

[Approximate maximum vegetation or vegetation residue height: Height above the land surface of vegetation or vegetation residues near the air sensors was estimated average maximum height within a distance of approximately 15 meters from the sensors; maximum height of vegetation or vegetation residues for the quadrants was the tallest height class that was tallied in each quadrant during a vegetation survey. Height of vegetation or vegetation residues that were on the irrigation checks was estimated as the height of those materials above the land surface adjacent to those checks. **Air sensor height**: Height of air sensors is height of the midpoint between the upper and lower air sensors above the land surface; –, not measured; <, less than; >, greater than]

Date	Approximate maximum vegetation or vegetation residue height (meters)					Sensor height (meters)	
	Near air sensors	Northeast quadrant	Southeast quadrant	Southwest quadrant	Northwest quadrant	Air	Wind
Lot C1B evapotranspiration measurement site							
05-20-00	<0.5	0.5 to 0.59	0.5 to 0.59	0.2 to 0.29	0.3 to 0.39	1.5	2
06-02-00	0.8	–	–	–	–	1.9	2
06-11-00	0.9	–	–	–	–	1.9	2
07-07-00	1.4	–	–	–	–	1.9	2
07-12-00	1.3	–	–	–	–	2.1	2
07-20-00	1.2	1.1 to 1.19	1.1 to 1.19	0.9 to 0.99	1.0 to 1.09	2.3	2
08-04-00	1.1	–	–	–	–	2.2	2
08-11-00	1.1	–	–	–	–	2.3	2
08-24-00	1.1	–	–	–	–	2.3	2
08-29-00	1.4	1.0 to 1.09	0.9 to 0.99	>1.0 to 1.09	>1.0 to 1.09	2.3	2
08-30-00	–	–	–	–	–	2.5	
09-08-00	1.2	–	–	–	–	2.5	2
09-15-00	1.2	–	–	–	–	2.5	2
09-22-00	1.2	–	–	–	–	2.5	2
09-29-00	1.2	–	–	–	–	2.5	2
10-18-00	1.4	–	–	–	–	2.5	2
Lot 6 stubble evapotranspiration measurement site							
06-10-00	–	–	–	–	–	1.4	1.5
06-11-00	0.2	0.3 to 0.39	0.4 to 0.49	0.3 to 0.39	0.5 to 0.59	1.4	1.5
06-28-00	0.3	–	–	–	–	1.4	1.5
07-07-00	0.8	–	–	–	–	1.3	1.5
07-12-00	0.9	–	–	–	–	1.9	1.5
07-18-00	–	0.8 to 0.89	0.8 to 0.89	0.9 to 0.99	0.9 to 0.99	1.9	1.5
07-19-00	1.1	–	–	–	–	2.2	2
07-21-00	–	–	–	–	–	2.4	2
08-04-00	1.1	–	–	–	–	2.4	2
08-11-00	1.2	–	–	–	–	2.4	2
08-16-00	--	–	–	–	–	2.3	2
08-24-00	1.2	–	–	–	–	2.3	2
08-27-00	--	1.0 to 1.09	>1.0 to 1.09	1.1 to 1.19	>1.1 to 1.19	2.3	2
08-28-00	1.3	–	–	–	–	2.5	2
09-08-00	1.3	–	–	–	–	2.5	2
09-15-00	1.3	–	–	–	–	2.5	2
09-22-00	1.2	–	–	–	–	2.5	2
09-29-00	1.2	–	–	–	–	2.5	2
10-18-00	1.3	–	–	–	–	2.5	2

Table 1. Approximate maximum heights of vegetation or vegetation residues, and heights of air and wind sensors—*Continued*

Date	Approximate maximum vegetation or vegetation residue height (meters)					Sensor height (meters)	
	Near air sensors	Northeast quadrant	Southeast quadrant	Southwest quadrant	Northwest quadrant	Air	Wind
Lot 6 cover crop evapotranspiration measurement site							
06-03-00	0.4	–	–	–	–	1.5	2
06-11-00	0.5	–	–	–	–	1.6	2
07-07-00	1.4	–	–	–	–	2.1	2
07-12-00	1.3	–	–	–	–	2.1	2
07-19-00	1.4	–	–	–	–	2.5	2
08-04-00	0.9	–	–	–	–	2.5	2
08-11-00	0.9	–	–	–	–	2.5	2
08-16-00	–	–	–	–	–	2.2	2
08-24-00	0.9	–	–	–	–	1.8	2
08-28-00	1.0	–	–	–	–	2	2
09-08-00	0.8	–	–	–	–	2	2
09-15-00	0.7	–	–	–	–	2	2
09-18-00	–	–	–	–	–	1.5	2
09-22-00	0.6	–	–	–	–	1.5	2
09-29-00	0.5	–	–	–	–	1.5	2
10-18-00	0.5	–	–	–	–	1.3	2

The sonic anemometer and data logger were mounted on a tripod that was approximately 12 to 15 m north or north-northeast of the BREB data logger enclosure at each site. The sonic anemometer was oriented to the west at each site and was at a height approximately equal to the current average height of the air sensors of the nearby BREB station.

VEGETATION

Vegetation was described by using observations of general vegetation condition, such as whether particular types of plants appeared to be vigorous or senesced, judged by color or by changes of color with time, by estimates of vegetation height, and systematically by an objective survey technique. The survey technique was modified from the step-point technique (Interagency Technical Team, 1996). A pole approximately 1.3 m long was fixed with a sight consisting of an approximately 0.002-m-diameter metal shaft. The pole was placed and held vertically at a point on a temporary survey transect, and the operator sighted down the length of the pole to find the first object that intercepted the line of sight established by the operator's eye and the end of the shaft. The object was tallied as one of the known plants, as an unknown plant, as vegetation residue, or as the bare soil surface. Vegetation residue is defined as any nonliving vegetative matter. The height of the tallied object above the soil surface was classified in 0.1-m increments by comparing its height against height increments marked on the pole. Specimens of particular plants that were not tallied but that were observed as being present were so noted.

Transects at lot C1B were run in northeast, southeast, southwest, and northwest directions for distances of approximately 200 m from the BREB station. At the lot 6 stubble site, the survey transects were run in northeast and southeast directions from the BREB station to the edge of the lot, in southwest and northwest directions to the edge of the cover crop or to the mowed path along the southern edge of the lot, westerly to the edge of the cover crop, and on a bearing of 300 degrees to the edge of the cover crop.

Transects were established anew for each survey by pacing distances between points. Percentage of land coverage by each type of object was computed as the number of points where the object type was identified divided by the total number of points in the survey. Each vegetation survey consisted of between 595 and 722 points. Percentage of site coverage by vegetation at the lot 6 cover crop site was estimated by cursory observations, rather than by the objective survey technique. The stand of cereal rye at the cover crop site was dense and essentially a monoculture, and the estimates were considered to be sufficiently accurate to meet the study objectives.

Lot C1B Site

Vegetation at the lot C1B evapotranspiration measurement site was in a state of early growing–season growth and development when the site was established during late May 2000. On May 20, 33 percent of the surface was covered by vegetation, chiefly small grain plants and mustard plants, that had recently emerged from the soil surface or from beneath residues of the previous crop (table 2). Approximately half of the surface was covered by vegetation residues, chiefly standing stubble and matted straw from the previous crop, and 15.9 percent of the soil surface was exposed.

Table 2. Percentage of ground coverage by vegetation and vegetation residues, and percentage of exposed soil at the lot C1B and lot 6 stubble evapotranspiration measurement sites, by sampling date

[n, number of sampling points; P, plant was noted as present but was not tallied; –, plant was not tallied or noted as present; Because of rounding, percentages in each column might not total 100]

Common plant name, vegetation residues, or exposed soil	Lot C1B site, 05-20-00, n = 603	Lot C1B site, 07-20-00, n = 595	Lot C1B site, 08-29-00, n = 683	Lot 6 stubble site, 06-11-00, n = 722	Lot 6 stubble site, 07-18-00, n = 649	Lot 6 stubble site, 08-27-00, n = 653
Tansymustard[1]	8.8	2.0	–	P	–	–
Brown mustard[1]	P	0.3	P	P	–	0.2
Common tumblemustard[1]	3.8	3.9	–	–	–	--
Prickly lettuce[1]	1.7	6.9	2.8	1.8	13.4	4.9
Common lambsquarters[1]	0.8	5.2	3.8	0.3	3.5	2.3
Wild oat[1]	–	4.2	–	–	23.1	5.2
Kochia[1]	0.2	0.7	2.6	0.6	1.7	17.5
Small grains[1]	17.7	19.7	--	6.9	15.3	0.3
Perennial pepperweed	–	P	–	–	–	–
Curly dock	–	P	P	–	–	P
Unknown broadleaf plant(s)	P	0.3	P	P	1.9	0.3
Unknown grass(es)	–	–	–	–	4.3	–
All vegetation	**33.0**	**43.2**	**9.2**	**9.6**	**63.2**	**30.7**
Vegetation residues	51.1	55.0	81.1	79.6	35.1	67.4
Exposed soil	15.9	1.8	9.7	10.8	1.7	2.0

[1]Annual or biennial.

The stubble was generally less than 0.3 m in height and the vegetation was generally were less than 0.5 m in height. Vegetation to a distance of 200 m in easterly directions from the BREB station appeared to be slightly more dense than was the vegetation in westerly directions from the station. By June 11, the vegetation had become dense and reasonably uniform in all directions from the BREB station, except for areas on the irrigation checks, which remained stubble-covered. Composition, density, and height of vegetation that grew in the burned eastern part of the lot was similar to that of vegetation in the remainder of the lot. Approximate maximum height of the vegetation canopy in the vicinity of the air sensors was 0.9 m (table 1). The tallest individual plants were mustards, some of which had begun to flower by June 11. By the time of the second survey at lot C1B, on July 20, the total percentage of coverage by vegetation was 43.2 percent (table 2). The total percentage of coverage by mustard plants had decreased since the previous survey, and percentage of coverage by prickly lettuce, common lambsquarters, wild oat, and small grain plants had increased. The percentage of coverage by vegetation residues (55 percent) was almost the same as it was on May 20 (51.1 percent); however, more of the residues at the later date consisted of stems and leaves of erect plants that had senesced and died since June 11. The vegetative canopy in the vicinity of the air sensors was of a maximum height of approximately 1.2 m. Many of the plants had turned yellowish-green in color, suggesting the period of peak vegetation growth and physiological activity or physiologically mediated activity, including transpiration and carbon uptake, almost certainly had been completed prior to July 20. By the time of the final vegetation survey at lot C1B, on August 29, percentage of coverage by live vegetation was only 9.2 percent, and the only living plants that were tallied during the survey were prickly lettuce, common lambsquarters, and kochia. The small grain plants and mustards had all gone to seed and died. Total percentage of coverage by vegetation residues was 81.1 percent. No live plants were noted during the final site visit of October 19, indicating the growing season had come to an end at the C1B evapotranspiration measurement site before that time. Almost all of the plants identified at lot C1B are annuals, meaning they complete their life cycle during a single year, or biennials, meaning they require 2 years to complete their life cycle.

Lot 6 Stubble Site

The lot 6 stubble evapotranspiration measurement site was almost completely devoid of vegetation when the BREB station was installed there during June 10 and 11, 2000. What little vegetation that was present consisted chiefly of juvenile small grain plants. Overall, percentage of coverage by vegetation was 9.6 percent (table 2). Percentage of coverage by residues was 79.6 percent, and the residues consisted mostly of stubble and matted straw from the small grain crop that was harvested during the previous year. Maximum heights of stubble and vegetation near the air sensors was 0.2 m (table 1). By July 18, the time of the second vegetation survey, the site had become occupied by dense, dark-green vegetation. Total percentage of site coverage by vegetation was 63.2 percent, and the most common plants were prickly lettuce, wild oat, and small grain plants. Although the vegetation at the lot C1B evapotranspiration measurement site had likely passed its peak of growth and physiological activity by mid- to late July, the vegetation at the lot 6 stubble site clearly was near its seasonal peak. Maximum height of vegetation near the air sensors was estimated to be 1.1 m on July 19. Most of the vegetation at the lot 6 stubble site had senesced or had begun to senesce by August 27. Total percentage of site coverage by vegetation was 30.7 percent, and kochia was the most common plant. Percentage of coverage by vegetation residues, which by August 27 included many dead standing plants, had almost doubled since July 18. Maximum height of vegetation near the air sensors was estimated to be 1.3 m on August 28. By October 18, the only living plants observed at the site were small, scattered grass plants that were probably small grain plants that had recently sprouted in the mowed paths. Desiccated residues of vegetation that grew during 2000 stood erect at the site, except for a few patches that formerly were small grain plants that had collapsed. Almost all of the plants identified at the lot 6 stubble site are annuals or biennials.

Causes of the differences between the lot C1B and lot 6 stubble sites with respect to vegetation composition and percent cover are not known; however, the causes could have been related to differences in farming practices at the two lots prior to 1999.

For example, differences in past uses of herbicides at the two lots, such as the types of herbicides used, the number of years herbicides were applied, and the seasonal timing of herbicide applications, might have suppressed particular weedy plant species at one of the lots by more than they were suppressed at the other lot. Part of the reason that vegetation cover developed more rapidly at the lot C1B site than at the lot 6 stubble site was that the lot C1B site supported many more mustard plants than did the lot 6 stubble site; the mustards tend to grow and develop earlier in the growing season than do most of the other species that grew at the two sites (Sam Johnson, USFWS, oral commun., August 2001). In addition, crop residues tend to cause spring soils to be cooler than they would be without such residues (Bidlake and others, 1992), and the cooler soils can delay germination, growth, and development of vegetation. Differences in the quantity (thickness and bulk density) of residues, although not measured in this study, could have been partly responsible for the observed temporal differences in vegetation growth and development at the lot C1B and lot 6 stubble sites.

Lot 6 Cover Crop Site

The cover crop of cereal rye was planted at lot 6 during February 2000. By June 3, 2000, the dark-green crop was fairly uniform, except for areas on the irrigation checks and a few areas a few meters in width where the crop was sparse. Overall, vegetation coverage at the site appeared to be greater than 80 percent. Maximum height of the crop near the air sensors was approximately 0.4 m (table 1). The extensive stubble barren of the lot 6 stubble site was immediately to the east of the cover crop (fig. 2, lot 6), and the mixture of growing vegetation and smaller stubble barrens described previously extended from the west edge of the cover crop to the west edge of the lot. On July 19, maximum crop height near the air sensors was approximately 1.4 m. Seed kernels had developed. The obviously senescing, light yellowish green cereal rye plants contrasted with the dark-green vegetation that had by that time occupied the former stubble barrens. Coverage by the crop appeared to be greater than 90 percent. By August 28, the plants had turned light brown in color and appeared to be dead above ground. The desiccated standing crop residues had begun to collapse, and the average height of the crop residue canopy was approximately 1.0 m. By October 18, the crop residue canopy had collapsed to a height of approximately 0.5 m.

METEOROLOGICAL CONDITIONS AND SURFACE ENERGY BALANCE

Fair weather dominated the period of field measurements for this study. Total precipitation measured at lot C1B during May 20 to October 18 was 42.8 mm, and 69 percent of the precipitation fell during the rainy period of September 1 to 4 (table 3). Precipitation was measured at lot 6 from June 4 to October 18, although data for June 28 to July 18 were lost due to a data retrieval anomaly. Total precipitation measured at lot 6 was 36.9 mm. If precipitation data for lot C1B are substituted for the missing data, total estimated precipitation at lot 6 for May 20 to October 18 is 43.0 mm. Precipitation at the Tulelake meteorological station near Tulelake during May through October totaled 97 mm (Western Regional Climate Center, 2001). Precipitation at lot C1B during May and October was estimated by multiplying precipitation at the Tulelake meteorological station for each of those months by the ratio of total precipitation at lot C1B during June through September to total precipitation at the Tulelake meteorological station during those same months. The ratio was 0.70, and estimated precipitation at lot C1B for the complete months of May and October was 14 and 17 mm, respectively. Estimated total growing-season precipitation at lot C1B, which was computed by summing measured precipitation at the lot for June through September with estimated precipitation for May and October, was 68 mm. Estimated total growing-season precipitation at lot 6, which was computed using the approach that was used for lot C1B, was 75 mm.

Analysis and interpretation of surface energy balance and related data were first conducted for the lot C1B evapotranspiration measurement site where vegetation was thought to be generally extensive and homogeneous enough to enable valid BREB measurements to be made regardless of wind direction. An exception to the vegetation homogeneity occurred during May 20 and June 11, before the developing vegetation had become dense and uniform.

Table 3. Daily precipitation measured at the lot C1B and lot 6 cover crop evapotranspiration measurement sites, shown for days precipitation was detected at least one site

[**Lot C1B**: Period of record is May 20 to October 18, 2000. **Lot 6 cover crop**: Period of record is June 4 to June 27 and July 19 to October 18, 2000. Precipitation is in millimeters; -- no data]

Date	Evapotranspiration measurement site	
	Lot C1B	Lot 6 cover crop
06-08-00	1.8	0
07-05-00	5.3	–
07-06-00	0.3	–
07-10-00	0.5	–
09-01-00	16.8	22.4
09-02-00	5.3	4.6
09-03-00	2.8	0.5
09-04-00	4.6	3.0
09-05-00	0	0.3
10-09-00	4.3	4.3
10-10-00	0.8	1.0
10-11-00	0.3	0.5
10-12-00	0	0.3

Selected environmental variables that influenced or were related to variations of evaporative loss from lot C1B are depicted for selected days in figures 3 and 4. During the fair weather of June 14 to 17, R_n was negative at night and became positive shortly after sunrise (fig. 3). Net radiation reached a maximum of approximately 700 W/m^2 during 1300 to 1400 Pacific Daylight Time (PDT), and it then decreased and became negative roughly half an hour before sunset. Under the time notation used in this report, a day begins at 0000 PDT and ends at 2400 PDT. Noon is 1200 PDT, and 3:30 p.m. is 1530 PDT. Net radiation at lot C1B followed a similar pattern of diurnal variation during the fair weather of August 25 to 28, when the vegetation was largely senesced, except that maximum R_n was approximately 550 W/m^2 (fig. 4).

Soil heat flux at the soil surface (G) was negative at night, indicating energy was being discharged to the atmosphere, and G became positive in the mornings at approximately the same time as or shortly after R_n became positive (figs. 3 and 4). During mid-June, daytime G increased to a maximum of approximately 100 W/m^2 during 1000 to 1100 PDT, roughly 2 hours before R_n reached its daily maximum. During late August, daytime G reached a maximum of approximately 90 W/m^2. Average daytime G was equivalent to 7 percent of average daytime R_n during June 14 to 17, and average daytime G was equivalent to 10 percent of average daytime R_n during August 25 to 28. Average G during sunrise to 1200 PDT was equivalent to 13 percent of average R_n during June 14 to 17, and average G during sunrise to 1200 PDT was equivalent to 14 percent of average R_n during August 25 to 28.

Latent and sensible heat fluxes computed by the BREB technique varied diurnally in a manner similar to diurnal variations of R_n (figs. 3 and 4). Latent heat flux was very nearly zero at night, became positive after sunrise, and reached its daily maximum at the same time as or shortly after the R_n maximum. Daily maximum λE was approximately 450 W/m^2 during June 14 to 17, and daily maximum λE was approximately 100 W/m^2 during August 25 to 28. Sensible heat flux generally was negative at night, became positive after sunrise, and reached its daily maximum within an hour of the maximum R_n. The gaps in the time series of λE and H in figures 3 and 4 resulted from those data being rejected during the screening procedure that was described previously.

The partitioning of available energy (R_n - G) between latent and sensible heat fluxes during mid-June differed markedly from the partitioning during late August. During mid-June, when the vegetation at lot C1B was likely near its seasonal peak of growth and physiological activity, available energy was partitioned strongly to λE at the expense of H. The roles were reversed by late August, when the vegetation was mostly dead or senesced, and available energy was partitioned strongly to H. Latent heat flux during late August was substantially diminished as compared to λE during mid-June.

The Bowen ratio (β) is strongly influenced by the aridity of the surface where energy and water are exchanged with the atmosphere. As a result, some tentative inferences about the aridity of a surface can be made by examining β (Campbell, 1977; Lafleur and Rouse, 1988). For terrestrial surfaces where water to meet evaporative demand is scarce, available energy is partitioned strongly to H at the expense of λE, and midday β for such sites tends to be greater than 1.0. On the other hand, where the soil surface is moist or where the land is occupied by actively transpiring vegetation, β tends to be smaller than 1.0. Campbell (1977, p. 136) indicates $\beta = 0.2$ is typical for well-watered short grass or wet soil.

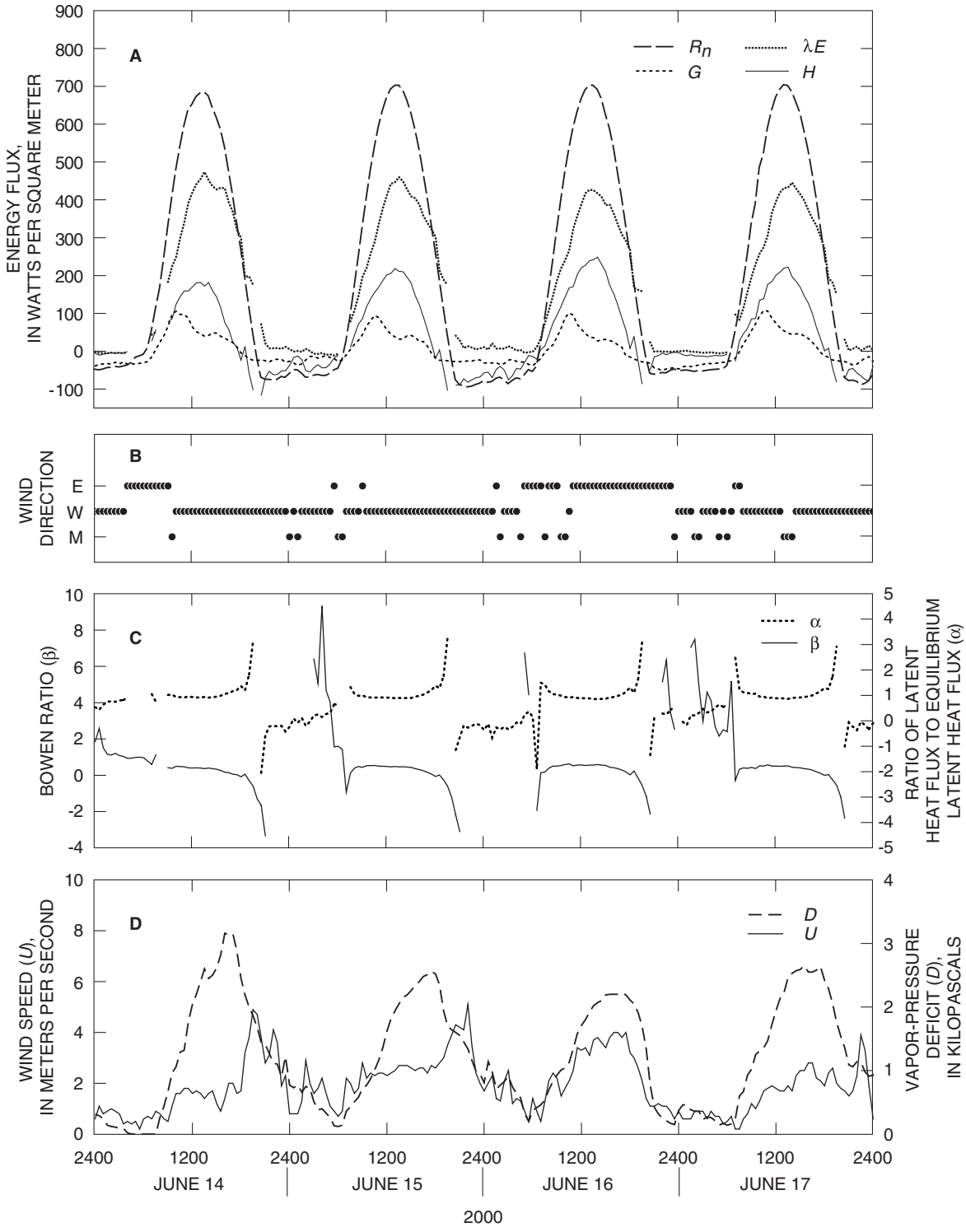

Figure 3. (A) Surface energy balance components net radiation (R_n), energy flux into the soil surface (G), and latent (λE) and sensible (H) heat fluxes; (B) wind direction, classified as easterly (E), westerly (W), or mixed easterly and westerly (M); (C) Bowen ratio (β) and ratio of latent heat flux to equilibrium latent heat flux (α); and (D) wind speed (U) and atmospheric water-vapor pressure deficit (D), all as they varied at the lot C1B evapotranspiration measurement site during June 14 to 17, 2000.

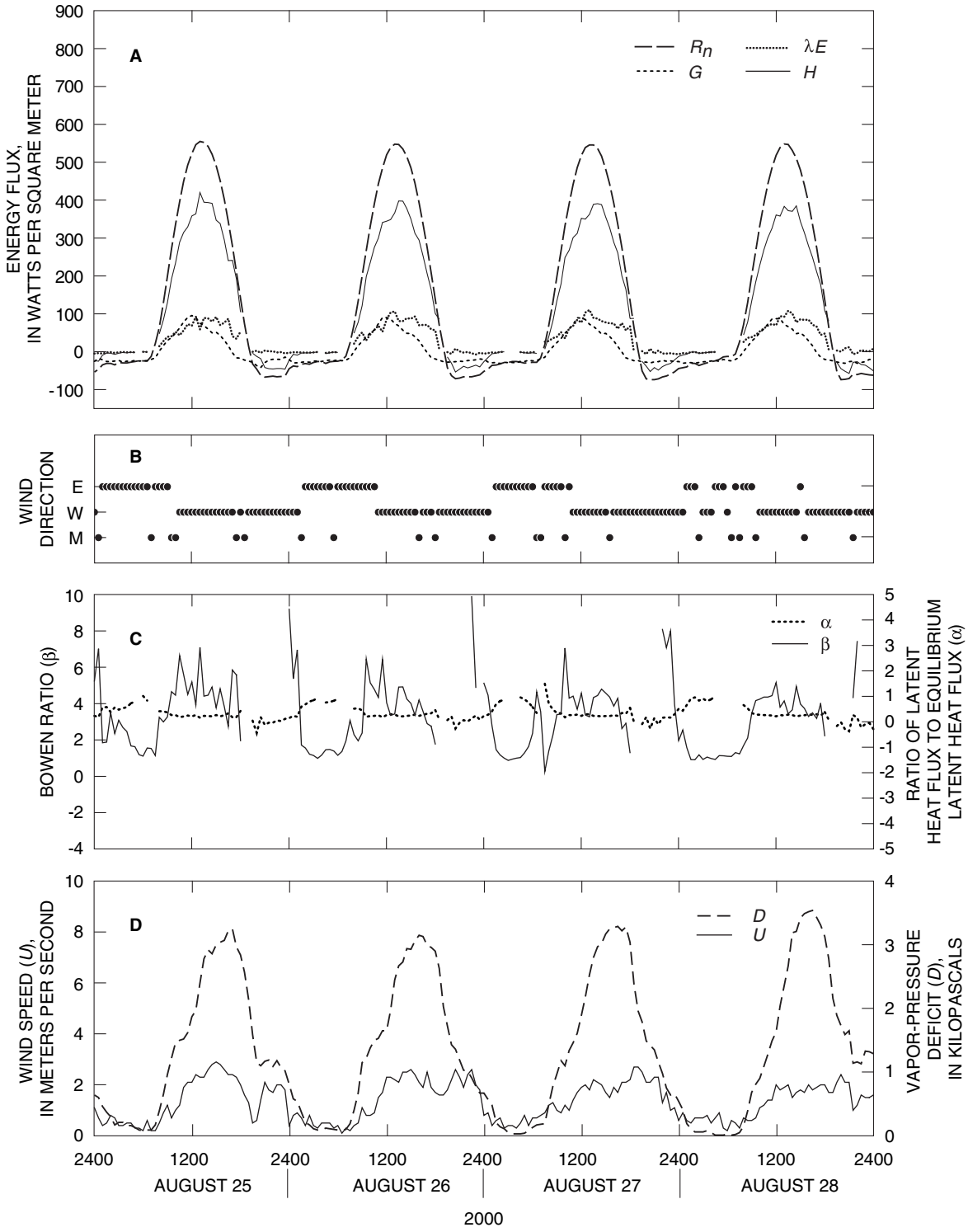

Figure 4. (A) Surface energy balance components net radiation (R_n), energy flux into the soil surface (G), and latent (λE) and sensible (H) heat fluxes; (B) wind direction, classified as easterly (E), westerly (W), or mixed easterly and westerly (M); (C) Bowen ratio (β) and ratio of latent heat flux to equilibrium latent heat flux (α); and (D) wind speed (U) and atmospheric water-vapor pressure deficit (D), all as they varied at the lot C1B evapotranspiration measurement site during August 25 to 28, 2000.

During June 14 to 17 at lot C1B, midday average β, computed using data from 1100 to 1500 PDT, ranged from 0.39 to 0.56 and averaged 0.48. During August 25 to 28, midday average β ranged from 4.08 to 4.66 and averaged 4.27.

The Bowen ratio also varied diurnally. Most typically, β increased from sunrise until about 1300 PDT, and it then decreased for the remainder of the daytime (fig. 3). The Bowen ratio often varied erratically during dusk, dawn, and at night, however, because the air-temperature and water-vapor pressure gradients were generally small in magnitude during those times, and even small measurement errors in ΔT and Δe could have caused large absolute errors in β. The BREB technique remains tenable for computing daily evapotranspiration because all of the surface energy balance components tended to be small in magnitude, and thus relatively unimportant for computing daily values, when the gradients ΔT and Δe were small.

The coefficient α is related to β through

$$\alpha = \frac{s + \gamma}{s} \bullet \frac{1}{1 + \beta} \quad , \qquad (30)$$

where all terms have been defined previously, and thus α is also strongly influenced by aridity of the surface of interest. Average midday (1100 to 1500 PDT) α at lot C1B during June 14 to 17 ranged from 0.87 to 0.93 and averaged 0.90 (fig. 3). During August 25 to 29, average midday α ranged from 0.23 to 0.26 and averaged 0.25 (fig. 4). The late August α values at lot C1B were similar to the minimum daily values reported by Williams and others (1978) for dry rangeland in British Columbia, Canada, and are indicative of evapotranspiration under strongly water-limited conditions.

The coefficient α also varied diurnally. During the daytime, α generally was largest in the morning, decreased to a minimum approximately at 1300 PDT, and increased late in the afternoon (figs. 3 and 4). De Bruin (1983) simulated a similar "U-shaped" daytime variation of α using a model of heat and moisture exchanges between the land surface and the lower atmosphere for a clear summer day in the Netherlands. At night at the lot C1B site, α could be negative or positive, depending on whether or not β was greater than -1, as is indicated by equation 30, because the quantity $(s + \gamma)/s$ is always positive. As was the case for β, the particular numerical values of α during nighttime were relatively unimportant for computing total daily evapotranspiration because all of the components of the surface energy balance tended to be small in magnitude at night.

Wind direction and speed and atmospheric water-vapor pressure deficit also exhibited characteristic diurnal variations (figs. 3 and 4). The most typical pattern of diurnal variation was for wind direction to be westerly from about midday until after midnight, when wind direction changed to easterly. Wind direction generally remained easterly until mid- to late morning, when it shifted back to westerly. The most common wind direction was westerly, followed by easterly, and then by mixed wind directions. Wind speed at night generally averaged less than 2 meters per second (m/s). Wind speed generally increased during mid-morning and it generally decreased to less than 2 m/s before midnight. Because of the previously described diurnal variations of wind direction and speed, wind speed tended to be largest when wind direction was westerly (figs. 3 and 4). An exception to this typical diurnal variation occurred at lot C1B on June 16, when wind direction was easterly or mixed during most of the day.

Diurnal cycling of the atmospheric water-vapor pressure deficit is chiefly due to cycling of air temperature, because water-vapor pressure at atmospheric saturation (e_s) varies strongly with temperature, as is predicted by equation 26. At lot C1B during mid-June and late August, daily maximum atmospheric water-vapor pressure deficits generally occurred during mid-afternoon, when wind direction was generally westerly (figs. 3 and 4). Daily maximum D ranged from 2.22 to 3.16 kilopascals (kPa) during June 14 to 17, and it ranged from 3.15 to 3.54 kPa during August 25 to 28. The daily minimum atmospheric water-vapor pressure deficit generally approached zero shortly before sunrise, indicating the atmosphere near the surface was saturated or almost saturated with water vapor at those times.

Variations of selected surface energy balance components, β, and α for the lot C1B evapotranspiration measurement site that are depicted in the long-term, tabular summary (table 6, at back of report) exhibited many of the same features that were previously described for the short-term, graphical summaries. The tabular summary was made from the complete data record for the lot C1B BREB station by averaging available energy, λE, β, and α for all 30-minute periods when λE and H computed by the BREB were valid.

This excluded all data from periods when λE and H were rejected as a result of the screening procedures that were described previously, and other periods for which λE and H were not available due to such factors as a shutdown of the BREB station or to known system malfunctions. Most notable among the malfunctions was the bird-wrought destruction of the net radiometer that occurred sometime between October 7 and October 18. The selected energy balance components, β, and α were averaged by wind direction, by selected intervals of time of day, and for periods that nominally were 7 days, but that ranged 2 to 7 days. Duration of multi-day averaging periods was varied to capture shorter-term variations of the components that were associated with precipitation or because of breaks in data continuity. Finally, multi-day average β and α were computed from multi-day-average available energy, λE and $\lambda E_{EQ,}$ rather than as the averages of β and α from each 30-minute period.

Among the similarities between the long- and short-term summaries are the overall predominance of westerly winds, the tendency for easterly winds to occur at night or in the morning, and the relative scarcity of periods of mixed easterly-and-westerly winds. Easterly winds during sunrise to 1100 PDT tended to occur earlier during that period than did westerly winds, as is evidenced by the generally smaller average available energy for easterly winds (table 6). Also, average nighttime available energy and λE were negligibly small during the entire period of the summarized data for the lot C1B evapotranspiration measurement site.

Long-term variations of β and α at the lot C1B evapotranspiration measurement site reflected variations of surface energy balance partitioning that likely were caused by variations of surface aridity. For westerly winds, average midday (1100 to 1500 PDT) β decreased from 0.90 during May 19 to May 25 to a minimum of 0.55 during June 9 to 15, when 65 percent of the available energy was partitioned to λE (table 6). After June 9 to 15, β began to increase until, by October 4 to 7, average midday β during westerly winds was 7.89. The trend of increasing β was interrupted by the rainy spells of early July and early September. For example, average midday β for westerly winds decreased from 1.32 during June 30 to July 4, immediately before the rain, to 0.39 during July 5 to July 7 (table 6). The rainfall during July 5 and 6 wetted the plants and the soil, and the decreased aridity of the surface caused a shift in available energy partitioning to favor λE at the expense of H. Long-term variations of α and the responses of α to precipitation substantially mirrored those of β.

The long-term summaries of selected energy balance components, β, and α for the lot 6 stubble and cover crop evapotranspiration measurement sites (tables 7 and 8, at back of report) exhibited features that were similar to those depicted in the summary for lot C1B. The similarities included the predominance of westerly winds, the tendency for any easterly winds to occur at night or during the morning, relatively infrequent periods of mixed-direction winds, and negligibly small nighttime λE. As was discussed previously, the fetch-to-instrument-height ratios at the lot 6 sites for all but westerly winds likely were too small to obtain reliable estimates of λE and H by the BREB technique. Summaries of λE, β, and α computed by the BREB technique for easterly and mixed-direction winds, although they are presented in tables 7 and 8 (at back of report), were not used to compute daily or growing-season evapotranspiration.

Surface energy balance partitioning at the lot 6 stubble evapotranspiration measurement site trended differently from the partitioning at the lot C1B site, suggesting that trends of surface aridity were dissimilar for the two sites. At the lot 6 stubble site, average midday β during westerly winds decreased from 2.97 during June 11 to 15 to a minimum of 0.19 during July 29 to August 4, when 84 percent of the available energy was partitioned to λE (table 7, at back of report). After July 29 to August 4, average midday β began an increasing trend, a trend that was interrupted by the rainy spell of early September, but that culminated with a value of 7.30 for westerly winds during October 4 to 7. Thus, excluding the rainy period of early July, the growing-season minimum of midday β during westerly winds at the lot 6 stubble site occurred approximately six weeks after the minimum occurred at the lot C1B evapotranspiration measurement site. Excluding the rainy period of early July, the maximum percentage of midday available energy partitioned to λE during westerly winds was 84 percent at the lot 6 stubble site and 65 percent at the lot C1B site. Peak availability of moisture to meet evaporative demand was greater at the lot 6 stubble site than at the lot C1B site.

Although part of the June and most of the July data from the BREB station at the lot 6 cover crop site were lost or were unreliable due to a data retrieval anomaly and to equipment malfunctions, the available data suggest energy balance partitioning trends at the lot 6 cover crop site differed from the trends at the lot C1B and lot 6 stubble sites. Average midday β during westerly winds at the cover crop site decreased slightly from 0.48 during June 3 to 8 to a minimum of 0.40 during June 23 to 27, when 71 percent of the available energy was partitioned to λE (table 8, at back of report). Following the data gap, average midday β during westerly winds increased from 1.29 during July 21 to 28 to a maximum of 9.69 during October 4 to 7, when 9 percent of available energy was partitioned to λE. The trend of increasing β was interrupted by the rain that fell during early September, as were the trends of increasing β at the lot C1B and lot 6 stubble sites. The growing-season minimum of β is not known for the lot 6 cover crop site because it could have occurred during the period for which the data were lost or unreliable.

AIRSTREAM EQUILIBRATION

The previously discussed airstream equilibration theory (Stannard, 1997) was used to explore possible effects of the limited fetch on λE measured by the BREB technique (λE_m) at the lot 6 stubble and cover crop evapotranspiration measurement sites during westerly winds. The theory was applied using fetch computed from wind direction and figure 2, using measured or estimated vegetation height, using d_0 and z_0 estimated as was described previously, and using measured heights of the air sensors for the BREB stations. Because many of the data needed to apply the theory were by necessity estimated, and because of a simplifying assumption in the theory, which is discussed later in this report, errors in λE_m computed using the theory are not considered to be accurate in an absolute sense. Instead, the computed errors are used to identify periods when accuracy of λE_m was most likely reduced by the limited fetch, and to provide rough estimates of the errors attributable to the limited fetch.

The cover crop was the contaminating surface for the stubble site during westerly winds (fig. 2, lot 6). The theory indicated that a lack of equilibrium of the airstream with the stubble site generally could have caused actual λE (λE_i) to be underestimated by less than 10 percent during midday (1100 to 1500 PST) (table 4). However, during the first two weeks of measurements at the stubble site, the theory indicated λE_i was overestimated by λE_m by as much as 60 percent. The cover crop was actively growing during June, and available energy was partitioned preferentially to λE at the expense of H, as was indicated by daytime β being less than 1.0 during that month (table 8). Vegetation at the stubble site probably remained sparse until late June and available energy at that site was strongly partitioned to H, as was indicated by a relatively large β (table 7). The airstream equilibration theory predicted that this sharp contrast in β between the two sites caused β_m to overestimate the actual Bowen ratio (β_i) at the lot 6 stubble BREB station due to the influence of heat and water vapor that arose from the cover crop and traveled in on the wind. Measured β for the two sites converged during late June, when vegetation at the stubble site likely grew rapidly. As a result of the reduced contrast of β that occurred by June 27, the theory predicted that airstream equilibration during westerly winds was almost complete by the time the air reached the stubble site BREB station, such that error in λE_m was less than 5 percent of λE_i (table 4).

The predicted error in midday λE_m for the stubble site was relatively small (-3.3 percent) on August 16, despite the fact that β_m for the stubble and cover crop sites differed by almost an order of magnitude (table 4). A key difference between the Bowen ratio contrast of August 16 compared to those of June 12 and 19 (when contrasting Bowen ratios yielded large theory-predicted percentage errors) was a larger β at the cover crop site on August 16 than at the stubble site. Thus, although the theory predicted that percentage errors in λE_m were relatively large under limited-fetch conditions when the wind transited from a moist to a dry surface, the same was not true for a dry-to-moist surface transit. In fact, the previously cited examples from the literature of successful applications of the BREB technique with fetch-to-instrument-height ratios as small as about 20 (Fritschen and others, 1983; Heilman and others, 1989) were applications of the technique that were made under dry-to-moist surface wind transitions.

Table 4. Fetch-to-instrument-height ratio for Bowen ratio energy balance measurements, measured and theory-predicted Bowen ratios and energy fluxes, and estimated percentage error and error in measured latent heat flux, all for westerly winds during midday (1100 to 1500 hours, Pacific Daylight Time) on selected days for the lot 6 stubble and the lot 6 cover crop evapotranspiration measurement sites during June to October, 2000

[F, fetch-to-instrument-height ratio for westerly winds; dimensionless; β_m, Measured Bowen ratio for surface of interest, dimensionless; β_c, Bowen ratio for the contaminating surface; dimensionless; β_i, Actual Bowen ratio for the surface of interest, dimensionless; A_m, measured available energy for the surface of interest, in watts per square meter; R, ratio of available energy at the contaminating surface to that at the surface of interest, dimensionless; λE_m, measured latent heat flux from the surface of interest, in watts per square meter; $\%\delta_{\lambda E}$, percentage error in λE_m due to the influence of the contaminating surface; $\delta_{\lambda E}$, error in λE_m due to the influence of the contaminating surface, in watts per square meter]

Date	F	β_m	β_c	β_i	A_m	R	λE_m	$\%\delta_{\lambda E}$	$\delta_{\lambda E}$
Surface of interest: Lot 6 stubble site Contaminating surface: Lot 6 cover crop site									
June 12	76	2.62	0.21	4.79	187	1.12	52	60	19
June 19	85	2.14	0.58	2.82	520	1.19	166	22	29
June 27	98	0.94	0.41	1.03	561	1.09	289	4.7	13
July 21	69	0.13	0.53	0.10	608	0.92	539	-2.4	-13
Aug. 4	68	0.23	1.92	0.17	572	0.85	464	-5.2	-25
Aug. 16	132	0.91	7.31	0.85	526	0.90	276	-3.3	-9
Aug. 28	151	2.18	10.36	2.08	457	0.98	144	-3.2	-5
Sept. 8	62	2.47	3.67	2.38	411	1.03	118	-2.7	-3
Sept. 21	89	3.07	5.96	2.90	413	1.17	101	-4.3	-5
Oct. 6	60	7.93	10.41	7.71	330	0.92	37	-2.4	-1
Surface of interest: Lot 6 cover crop site Contaminating surface: Lot 6 stubble site[1]									
June 12	70	0.21	4.79	0.12	209	0.89	172	-8.1	-15
June 19	98	0.58	2.82	0.53	619	0.84	392	-2.8	-11
June 27	111	0.41	1.03	0.40	610	0.92	432	-0.5	-2
July 21	92	0.53	0.10	0.58	559	1.09	366	3.5	12
Aug. 4	64	1.92	0.17	3.06	489	1.17	167	39	47
Aug. 16	94	7.31	0.85	14.25	472	1.11	57	84	26
Aug. 28	107	10.37	2.08	12.51	449	1.02	39	19	6
Sept. 8	64	3.68	2.38	3.91	422	0.97	90	5.1	4
Sept. 21	90	5.81	2.89	6.15	479	0.86	70	5.1	3
Oct. 6	87	10.42	7.71	10.70	305	1.08	27	2.5	1

[1]Lot 6 stubble site was used as a surrogate for the contaminating surface that was upwind of the cover crop site during westerly winds.

Depiction of airstream equilibration and potential errors in λE_m for the cover crop site required the additional assumption that β_c and R computed using measurements made at the stubble site, which actually was downwind of the cover crop site during westerly winds, accurately represented β_c and available energy for the contaminating surface for the cover crop during westerly winds. As was discussed previously, vegetation was less sparse west of the cover crop than east of the crop when measurements began at the stubble site during June, and use of the stubble site as a surrogate for the contaminating surface for the cover crop site is probably least tenable for theory predictions made for June. In addition, because β_m for the stubble site was influenced by the cover crop, theory-predicted β_i for the stubble site crop was used as β_c when the airstream equilibration theory was applied to predict potential errors in λE_m for the cover crop site. The theory indicated that the largest percentage errors in λE_m at the cover crop site during westerly winds occurred during moist-to-dry surface wind transitions during August. Measured β for the cover crop was consistent with the vegetation being either water stressed or in an advanced state of senescence (table 8). Conversely, β at the stubble site indicated that moisture availability was greater at the stubble site than at the cover crop site (table 7).

The airstream equilibration theory indicated that the greatest potential for fetch-related errors in λE computed by the BREB technique for westerly winds occurred in June for the lot 6 stubble site and in August for the lot 6 cover crop site. Errors computed using the theory are subject to numerous uncertainties, including errors in estimates of data that were supplied in implementing the theory, as well as a simplifying assumption in the theory. For example, degree of equilibration predicted by the theory is sensitive to the particular values used for the roughness parameters d_0 and z_0, and those parameters were computed for the theory computations using empirical relations intended for uniform crops. The lack of uniform vegetation height at the lot 6 stubble site imparts substantial uncertainty into the estimates of the roughness parameters for that site. Consequently, the accuracy of theory-predicted errors in λE_m for the lot 6 stubble site is uncertain.

Finally, the airstream equilibration theory does not account for variations of atmospheric stability (Stannard, 1997). Atmospheric turbulence is generated both by mechanical forces and vertically directed buoyant forces, and the state of atmospheric stability reflects the role buoyant forces play in enhancing or suppressing turbulence (Campbell, 1977, p. 40). Turbulent transport is enhanced in an unstable atmosphere, a state readily achieved when a relatively dry surface is heated by the sun. The enhanced turbulent transport of an unstable atmosphere would lead to more complete airstream equilibration than would occur in a neutral atmosphere, where buoyant forces sum to 0. The airstream equilibration theory assumes a neutral atmosphere. Moderately unstable conditions tended to prevail at the surface of interest when moist-to-dry wind transitions occurred; therefore, the airstream equilibration theory likely underestimated the degree of airstream equilibration and overestimated errors in λE_m during June 12 and 19 at the lot 6 stubble site and during August 4, 16, and 28 at the lot 6 cover crop site (table 4).

COMPARING SENSIBLE HEAT FLUX FROM THE BOWEN RATIO ENERGY BALANCE AND EDDY COVARIANCE TECHNIQUES

One technique for examining reliability of turbulent fluxes that are computed by the BREB technique is to measure one or more of those fluxes independently from the surface energy balance. In this study, sensible heat flux computed intermittently by the eddy covariance technique (H_{EC}) was compared with sensible heat flux computed by the BREB technique (H_{BREB}). The comparisons between H_{BREB} and H_{EC} did not provide direct evidence concerning reliability of λE that was computed by the BREB technique, but the comparisons did provide a sense of how well the surface energy balance was understood and characterized by measurements during selected days.

Sensible heat flux computed by eddy covariance at the lot C1B evapotranspiration measurement site during October 18 and 19 generally agreed closely with H_{BREB} (fig. 5). Overall, 30-minute-average H_{EC} averaged 3 W/m^2, or 5 percent, smaller than H_{BREB} (root-mean-squared difference (RMSD)= 15 W/m^2, n = 35). The close overall agreement is consistent with the notion that H computed by the two techniques approached the scientific true value of H. It is possible, but unlikely, that the agreement of H_{EC} and H_{BREB} was the result of compensating errors.

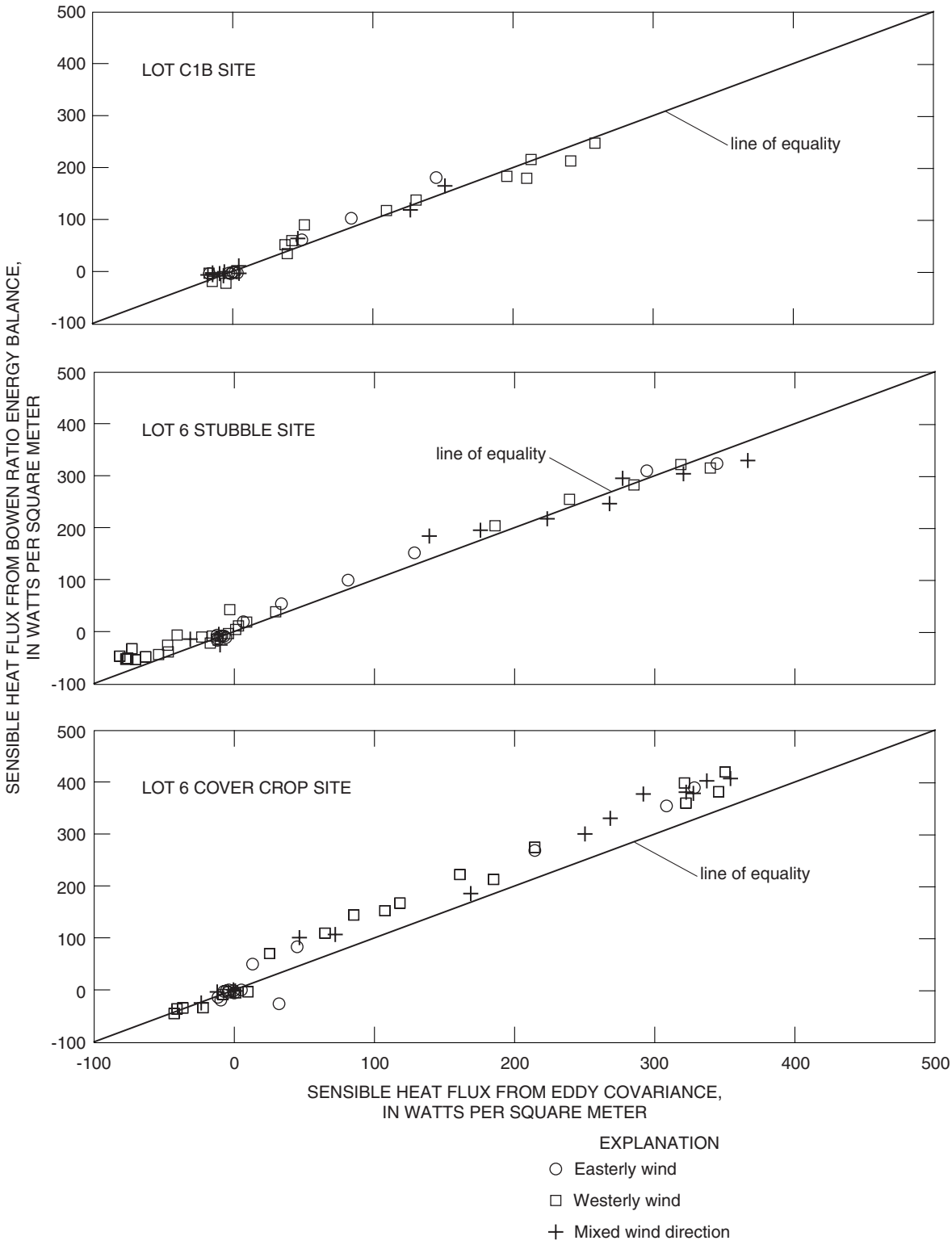

Figure 5. Comparisons between 30-minute-average sensible heat flux as computed by the Bowen ratio energy balance technique and by the eddy covariance technique at the lot C1B evapotranspiration measurement site during October 18 and 19, 2000, at the lot 6 stubble evapotranspiration measurement site during August 29 and 30, 2000, and at the lot 6 cover crop evapotranspiration measurement site during August 28 and 29, 2000.

The degree of agreement also did not appear to vary significantly with direction of the wind. An implication of this apparently negligible effect of wind direction is that available energy and partitioning of available energy to H and λE were probably spatially uniform and were accurately measured at the lot C1B site, at least during mid-October. Spatial uniformity of available energy and turbulent fluxes could have varied at lot C1B earlier during the growing season in response to vegetation heterogeneity; however, measurements of H_{EC} were not made at lot C1B to confirm this. Also, the comparisons between H_{BREB} and H_{EC} were made under the relatively dry surface conditions of mid-October, when the average midday β computed by the BREB technique was approximately 5.1, and agreement between H_{BREB} and H_{EC} might have not been as strong had the comparisons been made earlier in the growing season when, β was smaller.

Eddy covariance measurements of sensible heat flux were made at both lot 6 evapotranspiration measurement sites during August 28 to 30. Agreement between H_{EC} and H_{BREB} was generally close at the lot 6 stubble evapotranspiration measurement site during August 29 and 30 (fig. 5). Overall, 30-minute-average H_{EC} averaged 8 W/m^2, or 12 percent, less than H_{BREB} (RMSD = 19 W/m^2, n = 47). The degree of agreement also did not appear to vary significantly with direction of the wind, despite the relatively small fetch during easterly winds. As was the case for the lot C1B site, the close agreement of sensible heat flux computed by the BREB and eddy covariance techniques is consistent with the notion that available energy and the turbulent fluxes H and λE were spatially uniform and the surface energy balance was accurately characterized at the lot 6 stubble site during August 29 and 30. The agreement during periods when wind direction was thought to be unfavorable (easterly) also suggests (but does not prove) that the air stream at the heights of the BREB air sensors and the eddy correlation sensors was substantially in equilibrium with the stubble site surface. Average midday β at the lot 6 stubble site during westerly winds on August 29 and 30 was approximately 2.2.

Agreement between H_{BREB} and H_{EC} was generally poor at the lot 6 cover crop evapotranspiration measurement site during August 28 and 29 (fig. 5). Overall, 30-minute average H_{EC} averaged 26 W/m^2, or 23 percent, smaller than H_{BREB} (RMSD = 40 W/m^2, n = 49), and the degree of agreement did not appear to vary with wind direction. The causes of the disagreement between H_{BREB} and H_{EC} are not known. The previously discussed theory predictions of airstream equilibration for the cover crop site indicated the BREB technique would have overestimated λE during on August 28 (table 4). If λE had been overestimated by the BREB technique, H would have been underestimated; therefore, error in H_{BREB} due to the incomplete equilibration of the airstream to the cover crop does not help explain the observed differences between H_{BREB} and H_{EC} at that site. Average midday β at the lot 6 cover crop site during westerly winds was approximately 9.9 on August 28 and it was approximately 6.8 on August 29. Malfunction of the eddy covariance instrumentation or improper field procedures were unlikely to have caused the disagreement because H_{EC} at the cover crop site was computed using the same equipment and procedures that later agreed closely with H_{BREB} at the lot 6 stubble and C1B sites. Finally, a check of the eddy covariance instrumentation that was performed by the manufacturer following the field measurements revealed no significant deficiencies. Nonetheless, the generally poor agreement between H_{BREB} and H_{EC} at the cover crop site during August 28 and 29 indicates the surface energy balance was not well understood and characterized by measurements at that time.

EVAPOTRANSPIRATION MODELING

Both PT and reference-evapotranspiration modeling techniques were used to estimate λE and evapotranspiration during periods when it could not be reliably computed by the BREB technique. Site-specific PT models were developed and applied to augment the daily records of 30-minute λE for periods when λE computed by the BREB was not available or not reliable, but for which data were available to compute or estimate λE_{EQ}. Examples of periods when λE was estimated by a PT model include those when λE computed by the BREB technique was rejected as a result of the previously described screening procedures, and for the lot 6 sites, when wind direction was not westerly. Equilibrium latent heat flux for a given site, if it could not be computed using the data from the BREB station at the site, was estimated for 30-minute periods totaling up to two daytime hours during any day.

If gaps in 30-minute λE_{EQ} at a site totaled more than 2 hours during any given day, average λE for the entire day was computed using the reference evapotranspiration technique as is described subsequently in this report. Missing λE_{EQ} was estimated as the product of the ratio of λE_{EQ} for the station of interest to λE_{EQ} for another BREB station, computed using data from immediately before and after the data gap, and λE_{EQ} for the other BREB station. Daily average λE for each evapotranspiration measurement site was computed for each day that a complete record of measured or estimated 30-minute-average λE could be assembled by using the BREB technique and the site-specific PT model. Daily average λE, in W/m^2, was multiplied by the conversion factor 0.0351 to compute daily evapotranspiration rate, in millimeters per day (mm/d). The conversion factor was based on values of λ and ρ_w at a temperature of 15ºC, which are 2,466 J/g (Brutsaert, 1982; table 3. 4), and 998.98 kg/m^3 (Campbell, 1977; ρ_w was computed by interpolating between temperatures of 10ºC and 20ºC in table A2), respectively.

Differences among the PT models developed for the three sites were confined to the site-specific schemes for assigning α. The value assigned to α for a particular 30-minute period for each lot 6 evapotranspiration measurement site was taken directly from the "westerly winds" column for table 7 or 8, and for the appropriate multi-day period and time of day. For the lot C1B evapotranspiration measurement site, α was computed in a manner similar to that for the lot 6 sites, except α was averaged among all wind directions. This assignment scheme was intended to account for the previously discussed variations of α among the sites, during the growing season, and with the time of day.

Variations of α with wind direction can have implications for the reliability of evapotranspiration estimates that are made using PT models. Fluxes of heat and moisture that are directed into the atmosphere from distant surfaces upwind of the surface of interest can influence air temperature and water-vapor pressure to heights of several tens of meters or more above the locally equilibrated air layer that was described previously. This atmospheric conditioning can affect turbulent fluxes and parameters, such as β and α, that are properly determined from measurements made in a locally equilibrated air stream (Weeks and others, 1987; Lafleur and Rouse, 1988; and Souch and others, 1996). In general, development and application of a PT-type model where α is computed or assigned independently of wind direction, as was necessarily the case in this study (owing to insufficient fetch at the lot 6 sites), strictly should be supported by evidence that upwind conditioning is similar enough among all wind directions so that α does not vary with wind direction.

Analysis of the surface energy balance for lot C1B, the only site in this study where fetch was large enough to confidently compute λE, H, and α for all wind directions using the BREB technique, indicated that α generally did not vary substantially with wind direction. Excluding the data from before 1100 and after 1500 PDT, for which interactions between diurnal variations of α and wind direction make it impossible to isolate effects of wind direction alone, evidence for negligibly small daytime wind-direction effects in α can be seen in both the short- and long-term energy balance summaries for lot C1B. Firstly, on June 16, when the midday (1100 to 1500 PDT) wind direction was predominantly and uncharacteristically easterly, midday average α was 0.87 (fig. 3); whereas, midday average α during predominantly westerly winds on June 14, 15, and 17 averaged 0.91, a difference equal to 5 percent of the June 16 value. Secondly, midday α averaged for periods of several days generally did not vary significantly among easterly, westerly, and mixed wind directions (table 6). The most substantial exceptions to this uniformity of α were for periods that encompassed rainy spells (July 5 to 7 and September 1 to 5), and for periods when only 30 minutes of data were available for one or more wind directions (August 19 to 25, September 13 to 19, and September 27 to October 3). The wind direction-related variations of α that were associated with rainy spells were chiefly the result of the particular timing of precipitation and the unsteadiness of even midday conditions during the cloudy, rainy weather. Because of the general insensitivity of α to wind direction at lot C1B, and given that upwind surfaces at lot C1B and at lot 6 were generally similar in terms of moisture availability (irrigated agriculture, wetlands, or water), it was assumed that α was insensitive to wind direction at the lot 6 sites as well. Therefore, it was assumed that the PT models developed for the lot 6 sites with α computed during the favorable westerly winds could be used to reliably estimate λE at the lot 6 evapotranspiration measurement sites regardless of wind direction.

The reference-evapotranspiration modeling technique (eq. 12) was used to estimate daily evapotranspiration rate at an evapotranspiration measurement site for each day that a complete daily record of 30-minute λE could not be assembled by applying the BREB measurement and PT modeling techniques. Daily E_0 for a grass reference crop obtained from the nearby University of California Intermountain Research and Extension Center (University of California, 2000; fig. 2) was used to develop and apply the reference-evapotranspiration models for the three evapotranspiration measurement sites. Daily k_c for a given site was computed as the ratio of E_0 to daily evapotranspiration rate computed by the combined BREB and PT techniques. The value of k_c during May 1 to the first full day of successful operation of a given BREB station was assumed to equal the value on the first full day of operation. Similarly, the value of k_c from the last full day of successful station operation until the end of October was assumed to equal k_c on the last full day of successful station operation. The value of k_c during gaps in the record of daily evapotranspiration rate computed by the combined BREB and PT techniques was computed by assuming k_c changed linearly with time from the beginning to the end of the gap. Finally, for days precipitation fell and when evapotranspiration rate could not be reliably computed by the BREB and PT techniques, daily evapotranspiration rate was assumed to equal the greater of the evapotranspiration rate computed by equation 12 and a precipitation-modified rate. The precipitation-modified evapotranspiration rate was computed as the lesser of the daily precipitation rate and E_0.

EVAPOTRANSPIRATION AND DEPTH TO THE WATER TABLE

Total evapotranspiration during May to October did not differ significantly among the three evapotranspiration measurement sites; however, the seasonal distribution of evapotranspiration did vary among the sites. Total evapotranspiration for the 184 days was 426 mm for the lot C1B evapotranspiration measurement site, 444 mm for the lot 6 stubble site, and 435 mm for the lot 6 cover crop site. The maximum monthly average evapotranspiration rate occurred in June for the lot C1B and the lot 6 cover crop evapotranspiration measurement sites, and it occurred in July for the lot 6 stubble site (table 5). The months of May to July accounted for approximately 78 percent of the total evapotranspiration from the lot C1B site and approximately 86 percent of the total evapotranspiration from the lot 6 cover crop site (table 5). These same three months accounted for approximately 63 percent of the evapotranspiration from the lot 6 stubble site (table 5).

Table 5. Monthly average evapotranspiration rate and ratio of evapotranspiration rate to reference evapotranspiration rate for the lot C1B, lot 6 stubble, and lot 6 cover crop evapotranspiration measurement sites during May to October, 2000

[E, evapotranspiration rate, in millimeters per day (averaged for the month); E/E_0, ratio of evapotranspiration rate to reference evapotranspiration rate, dimensionless]

Month	Evapotranspiration measurement site					
	Lot C1B		Lot 6 stubble		Lot 6 cover crop	
	E	E/E_0	E	E/E_0	E	E/E_0
May	3.15	0.68	1.44	0.31	3.51	0.75
June	4.64	0.76	2.37	0.39	5.21	0.85
July	3.06	0.54	5.27	0.92	3.50	0.61
August	1.64	0.30	3.75	0.67	0.85	0.15
September	1.13	0.33	1.22	0.35	0.89	0.26
October	0.32	0.17	0.39	0.21	0.28	0.15
Overall average[1]	2.32	0.51	2.41	0.53	2.36	0.52

[1]Overall averages were computed by summing daily E and E/E_0 and thus do not necessarily equal the average of the monthly average rates or ratios.

Variations of evapotranspiration rate among the sites and with time at each site were linked to vegetation quantity and condition, indicating that evapotranspiration was mediated by the vegetation. As was indicated previously, the parameter α is of diagnostic value for describing the availability of water from a given surface to meet evaporative demand. Variations of α at each site can largely be explained by variations of vegetation quantity and condition. At the lot C1B evapotranspiration measurement site, the developing vegetation initially was sparse when measurements began during late May, and correspondingly, α was smaller than 1.0 (fig. 6), indicating that surface aridity was limiting evaporative loss from the site. Once the vegetation canopy at the lot C1B site had become dense during early June, α exceeded 1.0. Dense vegetation cover developed last at the lot 6 stubble evapotranspiration measurement site, and α did not exceed 1.0 there until early July (fig. 7). At the lot 6 cover crop site, the rapidly growing cereal rye plants had substantially occupied the site when energy balance measurements began there in early June, and correspondingly, α was greater than 1.1 (fig. 8). Furthermore, when the lot C1B and lot 6 cover crop sites were visited during late July, vegetation at both sites clearly had begun to senesce, and α was less than 0.8, indicating that aridity was limiting evaporative loss from both sites. Vegetation at the lot 6 stubble site was still green and probably physiologically active during late July, and α was greater than 1.2 during most of that month, indicating that evaporative loss was controlled principally by evaporative demand. Vegetation at the lot C1B and lot 6 cover crop sites was all or mostly dead by late August, and α was less than 0.3, indicating evapotranspiration was strongly controlled by surface aridity.

The increase of α at each site during the rainy spell of early September likely was caused by wetting of the near-surface soils and the vegetation and vegetation residues (figs. 6 to 8). Most of the plants that were alive during early to mid-September were senesced and likely acquired and transpired little of the newly added soil water, as can be seen in the return of a strongly water-limited evapotranspiration regime ($\alpha < 0.5$) at each site by mid-September. Measured soil water content at the 0.05-m depth at each site during mid-September was larger than it had been at any time prior to the early September rainy spell (figs. 6 to 8). Had the sites been occupied by actively transpiring vegetation that had access to the ample soil water, α during mid-September likely would have approached or surpassed its maximum observed value for each site. Instead, evaporative losses during and after the early September rainy spell likely were dominated by direct evaporation from the soil surface and by evaporation from surfaces of wetted vegetation and vegetation residues. When the soil, vegetation, and vegetation-residue surfaces dried out, evapotranspiration became strongly water limited.

Additional evidence for the role of the vegetation in mediating evapotranspiration can been seen in the ratio of evapotranspiration rate to the reference evapotranspiration rate (E/E_0) and α. Both E/E_0 and α were positively correlated with percentage of site coverage by vegetation that was determined by the objective vegetation surveys at the lot C1B and lot 6 stubble sites (fig. 9). Assuming that E_0 and λE_{EQ} each either is a measure of evaporative demand or is correlated with evaporative demand, the strong positive correlations of E/E_0 and α with percentage of site coverage by vegetation is consistent with the vegetation exerting control on evaporative loss from the lot C1B and lot 6 stubble sites. A similar correlation analysis was not made for the lot 6 cover crop site because percentage of site coverage was estimated from cursory observations, rather than by the objective survey technique, and the estimated site coverage at that site was not considered to be accurate enough to warrant statistical analysis and interpretation.

The role of vegetation residues in controlling evaporative loss at the study sites is less certain than the role of the vegetation. Vegetation residues can reduce evaporation from an underlying moist soil surface by altering the microclimate at the soil surface to reduce evaporative demand, such as by shielding the surface from solar radiation (Hillel, 1980, p. 141). In fact, percentage of coverage by vegetation residues at the lot C1B and lot 6 stubble sites was strongly and negatively correlated with E/E_0 ($r = -0.98$; $n = 6$) and α ($r = -0.99$; $n = 6$). However, most of the area of each of the study sites at any time was covered either by vegetation or by vegetation residues (table 2), and increases or decreases of percentage of coverage by the residues were largely accounted for by opposing changes in percentage of coverage by vegetation.

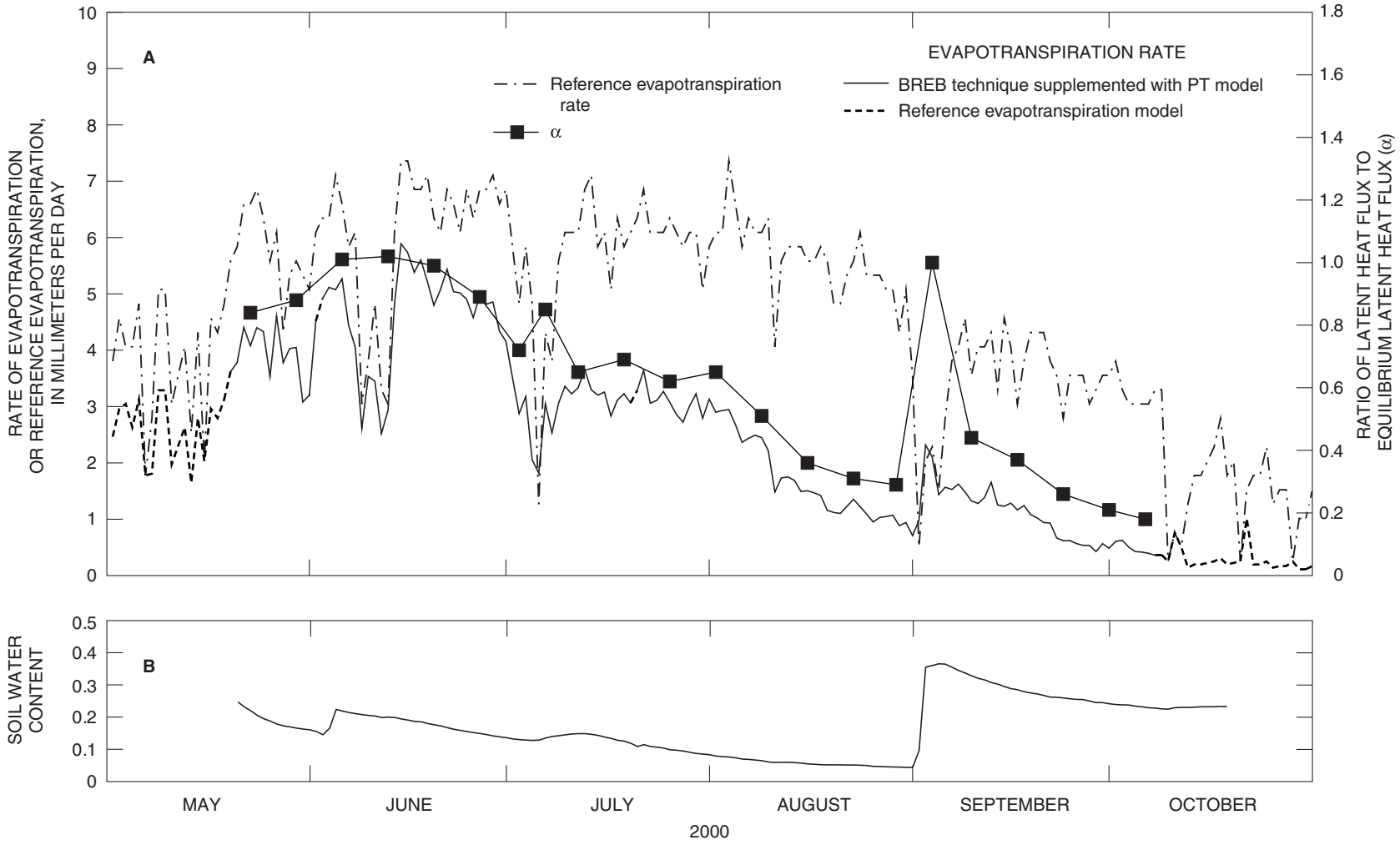

Figure 6. Daily reference evapotranspiration rate at the Intermountain Research and Extension Center during May to October 2000, and at the lot C1B evapotranspiration measurement site, daily evapotranspiration rate computed by the Bowen ratio energy balance (BREB) technique that was supplemented with evapotranspiration rate modeled by the Priestley-Taylor (PT) technique, daily evapotranspiration rate modeled by the reference evapotranspiration technique, and ratio of latent heat flux to equilibrium latent heat flux (α) averaged for 3 to 7 days; (B) daily average volumetric soil water content at a depth of 0.025 or 0.05 meter, averaged among three locations at the lot C1B evapotranspiration measurement site.

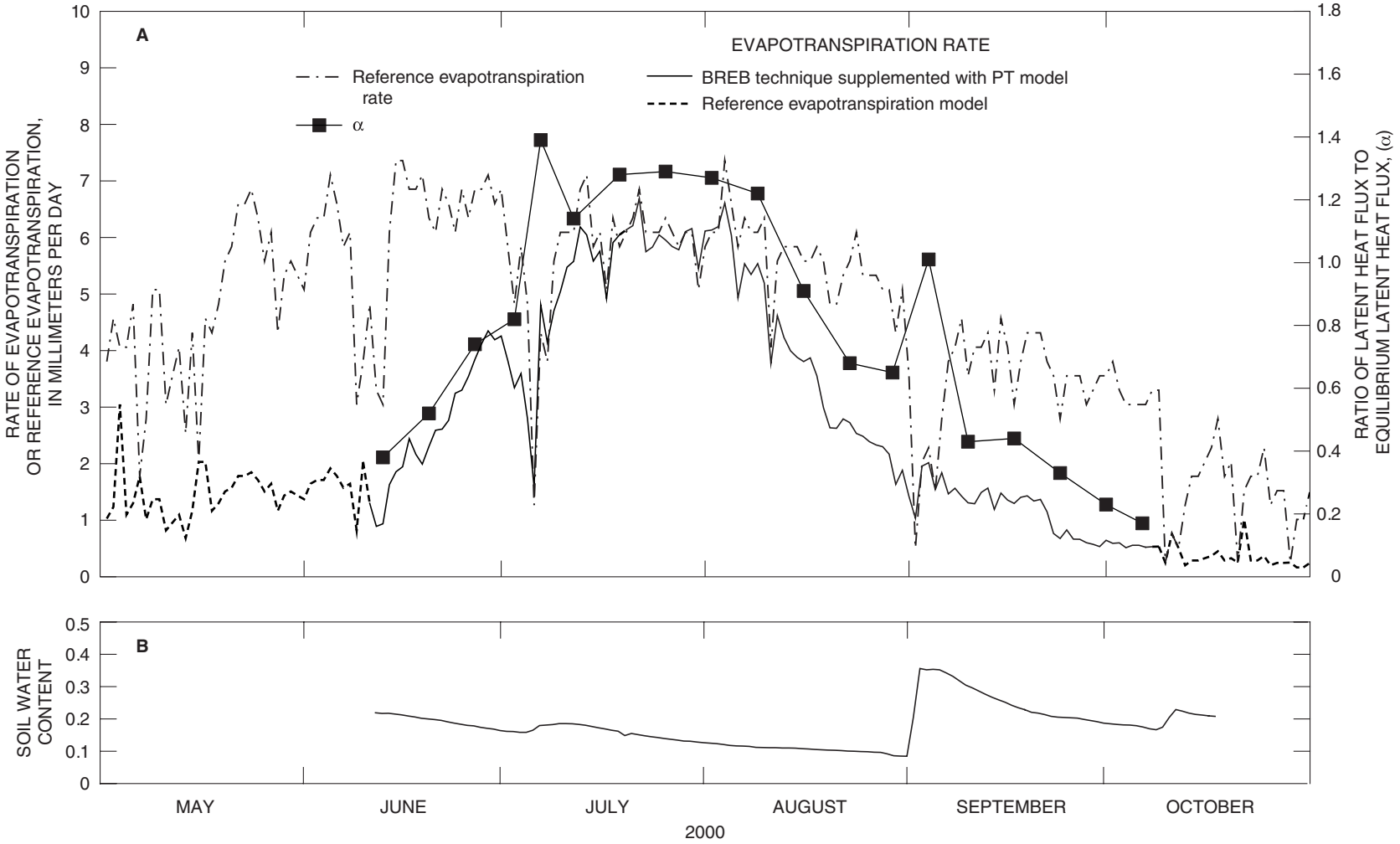

Figure 7. (A) Daily reference evapotranspiration rate at the Intermountain Research and Extension Center during May to October 2000, and at the lot 6 stubble evapotranspiration measurement site, daily evapotranspiration rate computed by the Bowen ratio energy balance (BREB) technique that was supplemented with evapotranspiration rate modeled by the Priestley-Taylor (PT) technique, daily evapotranspiration rate modeled by the reference evapotranspiration technique, and ratio of latent heat flux to equilibrium latent heat flux (α) averaged for 3 to 7 days; (B) daily average volumetric soil water content at a depth of 0.05 meter, averaged among three locations at the lot 6 stubble evapotranspiration measurement site.

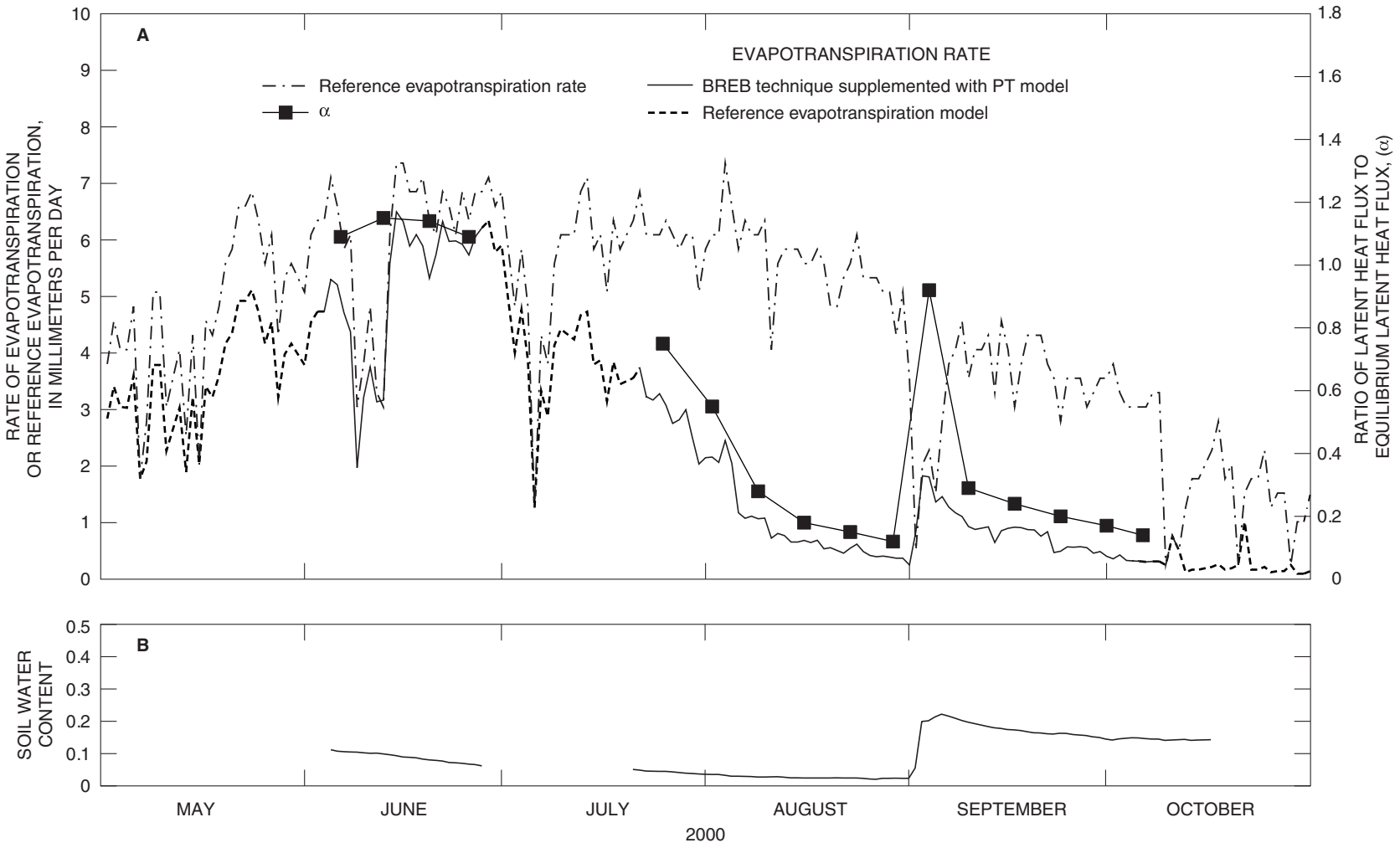

Figure 8. (A) Daily reference evapotranspiration rate at the Intermountain Research and Extension Center during May to October 2000, and at the lot 6 cover crop evapotranspiration measurement site, daily evapotranspiration rate computed by the Bowen ratio energy balance (BREB) technique that was supplemented with evapotranspiration rate modeled by the Priestley-Taylor (PT) technique, daily evapotranspiration rate modeled by the reference evapotranspiration technique, and ratio of latent heat flux to equilibrium latent heat flux (α) averaged for 4 to 8 days; (B) daily average volumetric soil water content at a depth of 0.05 meter, averaged among three locations at the lot 6 cover crop site.

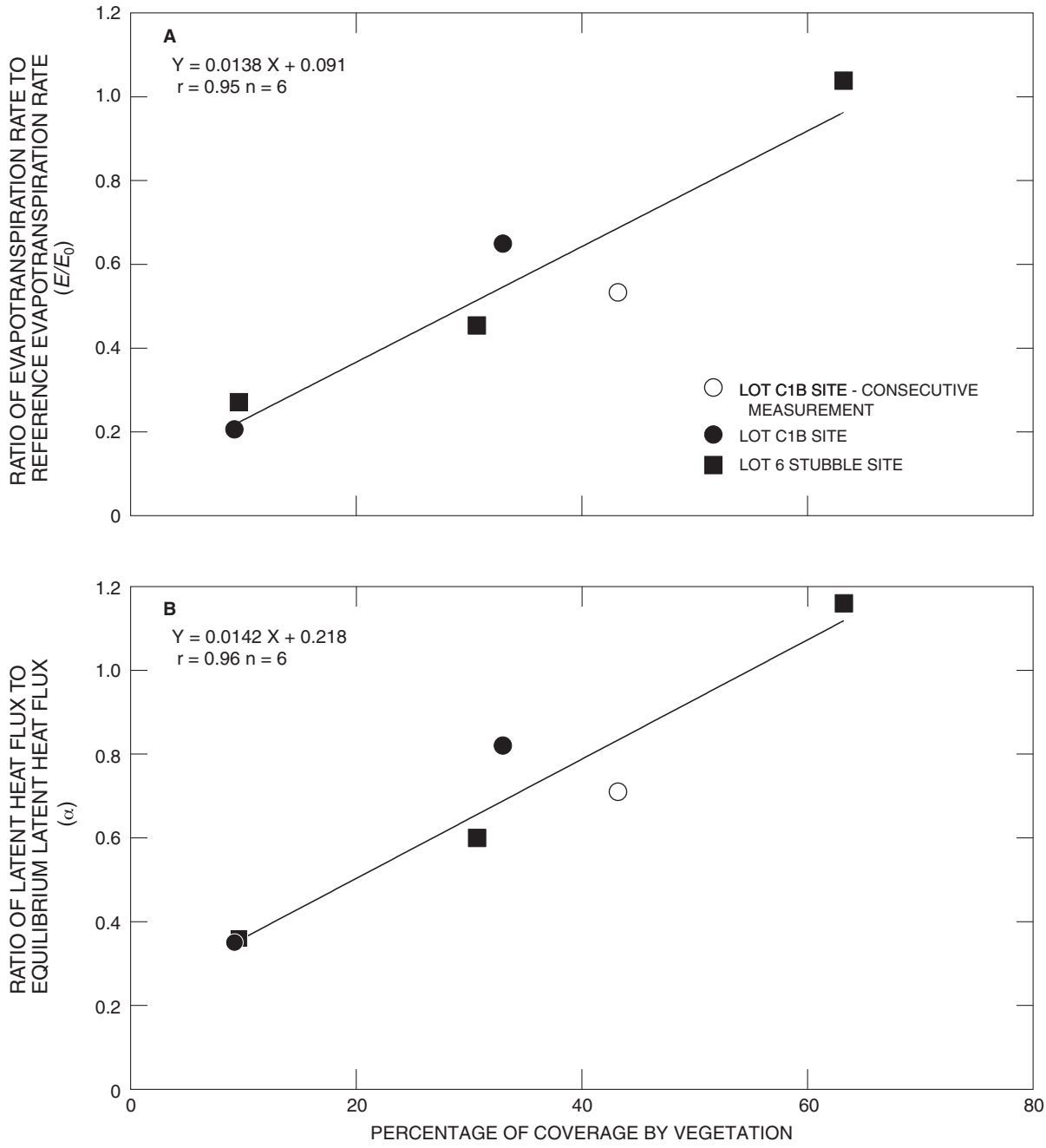

Figure 9. Relation between percentage of site cover by vegetation and (A) the ratio of evapotranspiration rate to reference evapotranspiration rate (E/E_0); and (B) the ratio of latent heat flux to equilibrium latent heat flux (α), all at the lot C1B and lot 6 stubble evapotranspiration measurement sites.
Both members of each abscissa-and-ordinate data pair were determined from data collected on the same day, except the pairs indicated with open symbols, for which E/E_0 and α were computed using data collected one day after percentage of site coverage was measured. Each plotted line represents the indicated equation.

Thus, although E/E_0 and α were statistically related to percentage of coverage by vegetation residues, they likely responded to variations of transpiration from vegetation that either replaced or was replaced by the vegetation residues. Evidence for the role of the residues in controlling evaporative loss could be developed in the future by comparing losses from residue-covered and bare fields where living vegetation is eliminated. Finally, the vegetation residues might have indirectly affected evapotranspiration rates and seasonal timing of evapotranspiration at the lot C1B and lot 6 stubble sites by slowing spring warming of the soils and thereby slowing germination, growth, and development of the vegetation at those sites. Additional study of vegetation residues as they relate to soil temperature and vegetation germination, growth, and development would be required to ascertain this possible indirect effect of vegetation residues on evapotranspiration rates.

Although the observed range of variation of depth to the water table was truncated beginning in late July, when some of the piezometers became dry, the overall trend of increasing depth to the water table at lot C1B and lot 6 with time mirrored the overall trend of decreasing soil water content at the two lots (fig. 10). The overall trend of increasing depth to the water table at the two lots was broken by decreases in depth around the times of the previously discussed rainy spells of early July and early September. These decreases of depth to the water table were partly caused by recharge from precipitation to the shallow ground-water systems and to the overlying unsaturated soils at lot C1B and at lot 6.

During May to mid-July and before piezometers began to go dry, depth to the water table did not vary substantially within each lot at any given time. Depth to the water table at lot C1B during that period varied by less than 0.3 m among the piezometers that were measured, except piezometer $P_{1,3}$, where depth to the water table varied by 0.35 m (fig. 10). Overall, depth to the water table at lot C1B ranged from 0.67 m in early July to greater than 1.39 m in late August. Depth to the water table at lot 6 varied by less than 0.3 m among the measurement locations during May to mid-July and before piezometers in that lot began to go dry. Overall, depth to the water table at lot 6 ranged from 0.77 m in late May to greater than 1.40 m in late August.

Depth to the water table also did not vary substantially between lot C1B and lot 6. On June 27, depth to the water table at $P_{1,1}$, the piezometer closest to the BREB station at the lot C1B evapotranspiration measurement site (fig. 2, lot C1B), was 0.07 m less than depth to the water table at $P_{3,1}$, the piezometer closest to the BREB station at the lot 6 cover crop evapotranspiration measurement site (fig. 2, lot 6). Depth to the water table at $P_{1,1}$ averaged 0.13 m less than depth to the water table at $P_{3,1}$ during July (n=3). Piezometer $P_{3,1}$ was dry on August 4, indicating depth to the water table was greater than 1.30 m; whereas, depth to the water table at $P_{1,1}$ was 1.11 m on that date. Depth to the water table at $P_{1,1}$ increased to 1.30 m by August 18, and the piezometer became dry by August 25, indicating depth to the water table was greater than 1.39 m at that time. During September, depth to the water table at $P_{1,1}$ averaged 0.18 m less than depth to the water table at $P_{3,1}$ (n=3).

Whether or not depth to the water table affected the evapotranspiration rate at any of the sites is generally not known. Soil physics theory indicates that the steady-state evaporation rate from a bare soil surface above a shallow water table, where water flows upward from the water table in response to a soil water-potential gradient, is controlled by evaporative demand as long as the soil profile can transmit water from the water table to the soil surface at rates sufficient to replace water lost by evaporation (Hillel, 1980, p. 114-119). Ability of the soil profile to transmit water at sufficient rates to meet a given evaporative demand decreases with increasing depth to the water table and is generally greater for medium-textured soils (for example, a silt loam) than for coarse-textured soils (for example, a sandy loam). As the water table recedes, a water-table depth can be reached at which the soil cannot transmit water at rates sufficient to meet evaporative demand, the soil begins to dry, and the evaporation rate falls below the rate that is specified by the evaporative demand. Prediction of maximum soil-water transmission rates in the field is almost always complicated by uncertainties concerning soil hydraulic properties.

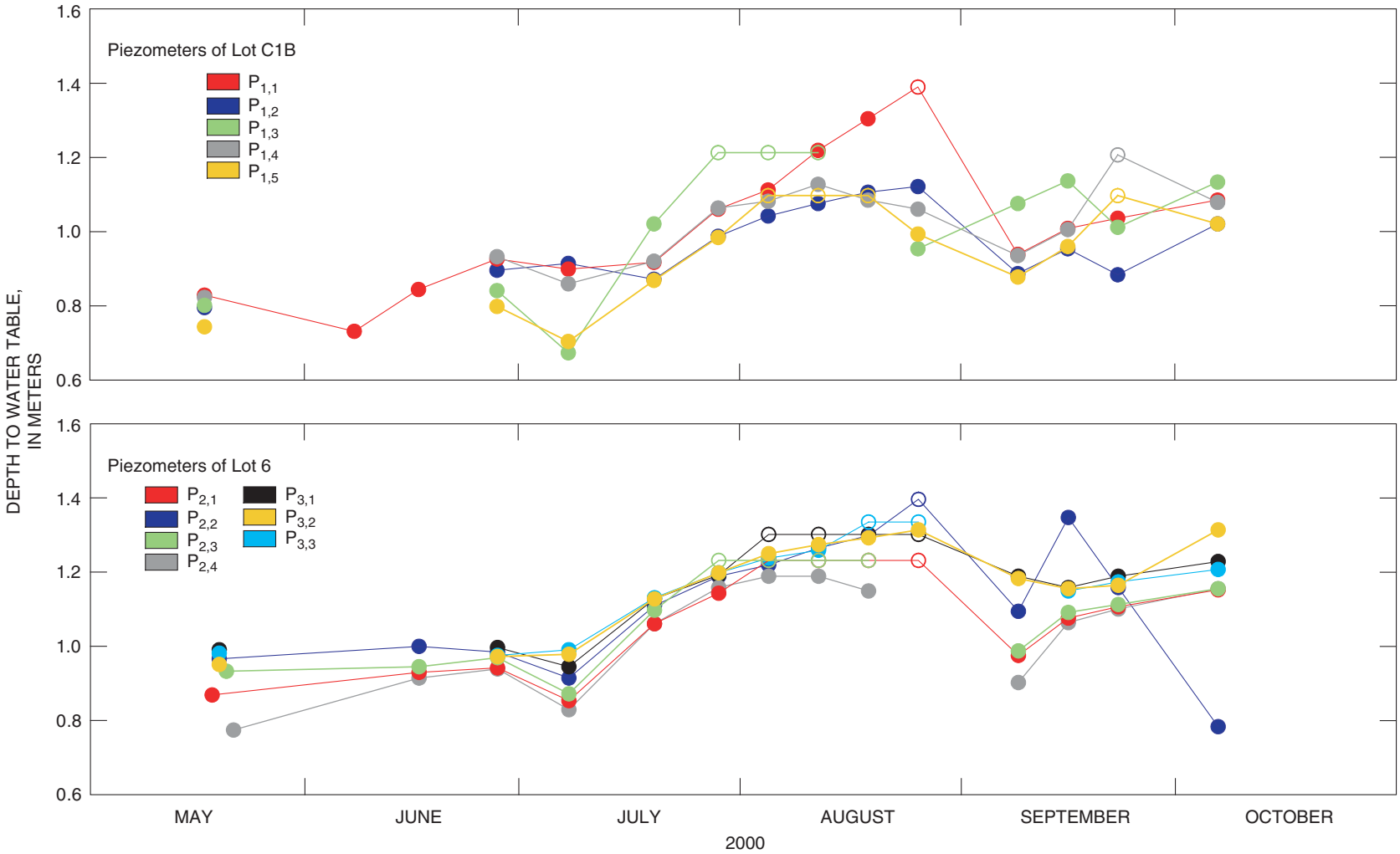

Figure 10. Depth to the water table below the land surface at lot C1B and at lot 6 during May to October 2000, as estimated from water level in shallow piezometers.
Open symbol indicates piezometer was dry, thus, depth to the water table was greater than plotted. Water levels in piezometers $P_{2,2}$ and $P_{2,3}$ for July 28 were estimated.

Evaluation of evaporative demand at the soil surface is often made difficult by the presence of vegetation residues, which can reduce evaporative demand at the soil surface as was described previously. Soil physics theory nonetheless provides a framework for understanding evaporative losses from a soil without plants that lies above a shallow water table.

Assessing possible effects of depth to the water table on evaporative losses from vegetated sites is much more difficult than for sites without plants. Actively transpiring, rooted plants can take up and transpire soil water from throughout their depth of rooting and thereby enhance total evaporative loss as compared to a soil without plants. The magnitude of vegetation enhancement of total evaporative loss from a site with a shallow water table is controlled in part by complex biological and biophysical processes, including growth, development and senescence of plants, biophysical processes of plant water relations and gas exchange, and the physical processes of soil water flow and uptake by plant roots. The detailed treatment of these processes that would be needed to predict effects of depth to the water table on evaporative loss from vegetated sites, although possible, was beyond the scope of this study. However, the available data do show how vegetation can confound the role of water-table depth in controlling evaporative loss. For example, the average evapotranspiration rate at the lot 6 cover crop site during June was roughly twice as great as it was at the nearby lot 6 stubble site (table 5), although measured depth to the water table at lot 6 varied by less than 0.2 m during that month (fig. 10). A likely qualitative explanation for the observed evapotranspiration difference is that the dense, actively growing vegetation at the cover crop site during June was taking up and transpiring soil water at much greater area-average rates than was the initially sparse and developing vegetation at the lot 6 stubble site. In fact, evapotranspiration at the latter site during mid-June might have been dominated by evaporation from the soil surface, rather than by transpiration by the vegetation, although additional study would be needed to ascertain this.

Finally, growing-season evapotranspiration from each study site was greater than the precipitation, indicating that water other than precipitation that fell during the growing season was entrained in the evaporative fluxes. Estimated growing season precipitation accounted for 16 percent of the growing-season evapotranspiration at the lot C1B site and 17 percent of the growing-season evapotranspiration at the lot 6 stubble and cover crop sites. The remaining water that composed the evaporative losses from each site was water from precipitation or irrigation that occurred before the start of the 2000 growing season and was stored in the soils or the shallow ground-water systems at the sites, or water from ground-water inflows to the shallow ground-water systems at the sites.

SUMMARY AND CONCLUSIONS

A study of evapotranspiration, vegetation composition, and depth to the water table below the land surface was made at three sites in two fallowed agricultural lots on the 15,800-ha Tule Lake National Wildlife Refuge in northern California during the 2000 May-to-October growing season. The study area receives approximately 288 mm of precipitation annually. The lot C1B evapotranspiration measurement site was near the center of a 41-ha lot that had been farmed during 1999. The lot 6 stubble and lot 6 cover crop evapotranspiration measurement sites were in a 39-ha lot that had been farmed in 1999. The lot 6 stubble site was in an area of the lot that had been left untreated following harvesting operations of the previous year, and the lot 6 cover crop site was in an area of the lot that had been planted to a cover crop of cereal rye during February 2000. The soil at both lots was Tulebasin mucky silty clay loam.

Evapotranspiration and components of the surface energy balance were measured or computed using the Bowen ratio energy balance (BREB) technique. Evapotranspiration also was computed by using locally calibrated evapotranspiration models that were based either on the Priestley-Taylor equation or on the reference evapotranspiration rate. Modeled evapotranspiration was used to estimate evapotranspiration when it could not be reliably computed by the BREB technique.

Application of the BREB technique involved directly measuring net radiation (R_n) with a net radiometer, and making measurements to compute the Bowen ratio (β) and soil heat flux at the soil surface (G). The Bowen ratio was computed from the difference of air temperature and water-vapor pressure measured with temperature and relative humidity sensors at two heights above the surface of each site. Soil heat flux at the soil surface was computed from the energy balance of the soil to a depth of 0.05 m or 0.1 m. The soil energy balance was evaluated from the calorically computed rate of change of energy storage in the soil layer and the heat flux at the bottom of the layer that was measured with soil heat flux plates. Measured specific heat of dry soil from a sample of Tulebasin mucky silty clay loam from lot C1B averaged 1,170 (J/kg)/ ºC. Soil thermal conductivity was measured to allow for corrections to heat flux that were needed due to the mismatch between the thermal conductivities of the soil and material composing the soil heat flux plates. Thermal conductivity of soil samples packed to bulk densities that ranged from 582 to 614 kg/m^3 varied from 0.08 to 0.41 (W/m)/ ºC for a range of soil volumetric water content of oven dry to 0.39.

Fetch at the two lot 6 evapotranspiration measurement sites was smaller than what would have been ideal for the BREB technique. The BREB stations at those sites were placed to maximize the amount of fetch during westerly winds (azimuth equal to or greater than 180 degrees and less than 360 degrees), which were more common than easterly winds (azimuth equal to or greater than 0 degrees and less than 180 degrees). Latent heat flux and selected environmental variables that were measured during westerly winds were used to calibrate site-specific evapotranspiration models that were used to estimate latent heat flux when winds were not westerly. Minimum fetch during westerly winds was approximately 120 m at the lot 6 stubble site and approximately 115 m at the lot 6 cover crop site.

Vegetation was described by using cursory observations of general vegetation condition, by estimates of vegetation height, and systematically by an objective survey technique. Composition of vegetation and timing of vegetation growth and development varied among the three evapotranspiration measurement sites. Vegetation at the lot C1B evapotranspiration measurement site consisted chiefly of mustard plants, prickly lettuce, and small grain plants. Percentage of site coverage by vegetation varied from 33.0 percent on May 20, to 43.2 percent on July 20, to 9.2 percent on August 29. Vegetation at the lot 6 stubble site included wild oat, small grain plants, and prickly lettuce. Percentage of coverage by vegetation varied from 9.6 percent on June 11, to 63.2 percent on July 18, and to 30.7 percent on August 27. The cereal rye of the lot 6 cover crop site was planted during February 2000. Percentage of site coverage by the plants was estimated to be greater than 80 percent on June 3 and greater than 90 percent by July 20. By July 20, vegetation at the lot C1B and lot 6 cover crop sites had begun to senesce. Vegetation senescence was first noted at the lot 6 stubble site on August 27. All vegetation appeared to be dead by late August at the lot 6 cover crop site and by mid-October at the lot C1B site. The only living vegetation remaining at the lot 6 stubble site by mid-October were scattered, small grass plants that were probably small grain plants.

Partitioning of available energy (R_n - G) to λE and sensible heat flux (H) varied among the three evapotranspiration measurement sites and with time. Average midday (1100 to 1500, Pacific Standard Time) β during westerly winds at the lot C1B site ranged from 0.39 during July 5 to 7 to 7.89 during October 4 to 7. At the lot 6 stubble site, average midday β during westerly winds ranged from 0.19 during July 29 to August 4 to 7.30 during October 4 to 7. Average midday β during westerly winds at the lot 6 cover crop site ranged from 0.40 during June 23 to 27 to 9.69 during October 4 to 7.

An airstream equilibration theory was used to examine possible errors in measured latent heat flux that might have been caused by the influence of the surface that was upwind of the lot 6 stubble and cover crop sites. The upwind “contaminating” surface was thought to cause errors in measured λE at each of the lot 6 sites because the fetch-to-instrument-height ratio at those sites often was smaller than the ideal minimum of 100. Midday, minimum fetch-to-instrument-height ratios for westerly winds during the days selected for analysis with the theory were as small as 60 at the lot 6 stubble site and as small as 64 at the lot 6 cover crop site. The theory predicted that actual midday λE at the stubble site would have been overestimated by as much as 60 percent during mid-June and that actual midday λE at the cover crop site would have been overestimated by as much as 84 percent during mid-August.

Predicted errors in midday λE ranged from -25 to 29 W/m^2 at the lot 6 stubble site and from -15 to 47 W/m^2 at the lot 6 cover crop site. Because of uncertainties in key data needed to apply the theory and because the theory did not account for the increased degree of airstream equilibration that likely occurred due to atmospheric instability, the predicted errors in λE were not considered to be accurate in an absolute sense. Instead, the theory identified periods of time when fetch-related errors likely were most significant.

Sensible heat flux, one of the energy balance components computed by the BREB technique, was cross-checked against sensible heat flux that was computed by the eddy covariance technique. Eddy covariance measurements were made for 24 hours or more at each evapotranspiration measurement site. Sensible heat flux computed by the eddy covariance technique at the lot C1B site during October 18 and 19 averaged 5 percent smaller than sensible heat flux that was computed by the BREB technique. Sensible heat flux computed by the eddy covariance technique at the lot 6 stubble site during August 29 and 30 averaged 12 percent smaller than sensible heat flux that was computed by the BREB technique. Sensible heat flux computed by the eddy covariance technique at the lot 6 cover crop site during August 28 and 29 averaged 23 percent smaller than sensible heat flux computed by the BREB technique.

Total evapotranspiration during May to October varied little among the three evapotranspiration measurement sites, although the timing of evapotranspiration losses did vary among the sites. Total evapotranspiration from the lot C1B site was 426 mm, total evapotranspiration from the lot 6 stubble site was 444 mm, and total evapotranspiration from the lot 6 cover crop site was 435 mm. The months of May to July accounted for approximately 78 percent of the total evapotranspiration from the lot C1B site, approximately 63 percent of the total evapotranspiration from the lot 6 stubble site, and approximately 86 percent of the total evapotranspiration from the lot 6 cover crop site. Estimated growing season precipitation accounted for 16 percent of the growing-season evapotranspiration at the lot C1B site and 17 percent of the growing-season evapotranspiration at the lot 6 stubble and cover crop sites.

Variations of evapotranspiration rate among the sites and with time at each site were linked to quantity and condition of the vegetation, indicating that evapotranspiration was mediated by the vegetation. The ratio of latent heat flux to equilibrium latent heat flux (α) tended to be larger than 1.0 at each site when the site was densely occupied by actively growing vegetation, and α was less than 1.0 when the site was sparsely occupied or occupied by vegetation that appeared to have senesced. Furthermore, the ratio of evapotranspiration rate to the reference evapotranspiration rate and α were each statistically correlated with the percentage of site coverage by vegetation.

Depth to the water table below the land surface was estimated from water-level measurements that were made in shallow piezometers. Measured depth to the water table at any given time prior to late July, when some piezometers in each field became dry, varied by 0.35 or less within each lot and between the lots. Depth to the water table at lot C1B ranged from 0.67 m in early July to greater than 1.39 m in late August. Depth to the water table at lot 6 ranged from 0.77 m in late May to greater than 1.40 m in late August. Depth to the water table was not unambiguously related to evapotranspiration rate, and it is concluded that any effect that depth to the water table had on evapotranspiration rate was obscured by variations of soil water uptake and transpiration by vegetation that was associated with growth, development, and senescence of the vegetation.

REFERENCES CITED

Adams, R.S., Black, T.A., and Fleming, R.L., 1991, Evapotranspiration and surface conductance in a high elevation, grass-covered forest clearcut: Agricultural and Forest Meteorology, v. 56, p. 173-193.

Barton, I.J., 1979, A parameterization of the evaporation from nonsaturated surfaces: Journal of Applied Meteorology, v. 18, p. 43-47.

Bidlake, W.R., Campbell, G.S., Papendick, R.I., and Cullum, R.F., 1992, Seed-zone temperature and moisture conditions under conventional and no-tillage in Alaska: Soil Science Society of America, v. 56, p. 1904-1910.

Bowen, I.S., 1926, The ratio of heat losses by conduction and by evaporation from any water surface: Physical Review, v. 27, p. 779-787.

Brutsaert, W., 1982, Evaporation into the atmosphere: Boston, Mass., D. Reidel, 299 p. [Reprinted with corrections 1984; reprinted 1988].

Campbell, G.S., 1977, An introduction to environmental biophysics: New York, Springer-Verlag, 159 p.

———1985, Soil physics with BASIC: New York, Elsevier, 150 p.

Campbell, G.S., Calissendorff, C., and Williams, J.H., 1991, Probe for measuring soil specific heat using a heat-pulse method: Soil Science Society of America Journal, v. 59, p. 291-293.

Campbell Scientific, Inc., 1997, CR10X measurement and control system operator's manual: Logan, Utah, Campbell Scientific, Inc., revision 5/97, [100 p.].

De Bruin, H.A.R., 1983, A model for the Priestley-Taylor parameter α: Journal of Climate and Applied Meteorology, v. 23, p. 572-578.

Doorenbos, J., and Pruitt, W.O., 1977, Guidelines for predicting crop water requirements: Rome, Italy, Food and Agricultural Organization of the United Nations, FAO Irrigation and Drainage Paper 24, (2d ed.), 156 p.

Duell, L.F.W., Jr., 1990, Estimates of evapotranspiration in alkaline scrub and meadow communities of Owens Valley, California, using the Bowen-ratio, eddy-correlation, and Penman-combination methods: U.S. Geological Survey Water-Supply Paper 2370-E, 39 p.

Flint, A.L., and Childs, S.W., 1991, Use of the Priestley-Taylor evaporation equation for soil water limited conditions in a small forest clearcut: Agricultural and Forest Meteorology, v. 56, p. 247-260.

Fritschen, L.J., Gay, L.W., and Simpson, J.R., 1983, The effect of a moisture step change and advective conditions on the energy balance components of irrigated alfalfa, *in* Conference on Agriculture and Forest Meteorology, 16th, Fort Collins, Colo., 1983, Collection of papers: Boston, Mass., American Meteorological Society, p. 83-86.

Gardner, W.H., 1986, Water content, *in* Klute, A. ed., Methods of soil analysis part 1, physical and mineralogical methods (2d ed.), Agronomy Monograph No. 9: Madison, Wisc., American Society of Agronomy, Inc., and Soil Science Society of America, Inc., p. 493-561.

Harr, R.D., and Price, K.R., 1972, Evapotranspiration from a greasewood-cheatgrass community: Water Resources Research, v. 8, p. 1199-1203.

Heilman, J.L., Brittin, C.L., and Neale, C.M.U., 1989, Fetch requirements for Bowen ratio measurements of latent and sensible heat fluxes: Agricultural and Forest Meteorology, v. 44, p. 261-273.

Hillel, D., 1980, Applications of soil physics: San Diego, Calif., Academic Press, 385 p.

Interagency Technical Team, 1996, Sampling vegetation attributes: Denver, Colo., Bureau of Land Management – National Business Center, Technical Reference 1734-4, 163 p.

Jackson, R.D., and Taylor, S.A., 1986, Thermal conductivity and diffusivity, *in* Klute, A. ed., Methods of soil analysis part 1, physical and mineralogical methods (2d ed.), Agronomy Monograph No. 9: Madison, Wisc., American Society of Agronomy, Inc., and Soil Science Society of America, Inc., p. 945-956.

Jahnke, J.J., 1994, Soil survey of Butte Valley-Tule Lake Area, California, parts of Siskiyou and Modoc Counties: Washington, D.C., U.S. Department of Agriculture, Soil Conservation Service, 284 p., 25 sheets.

Jensen, M.E., Burman, R.D., and Allen, R.G., eds., 1990, Evapotranspiration and irrigation water requirements: New York, American Society of Civil Engineers, 322 p.

Jury, W.A., and Tanner, C.B., 1975, Advection modification of the Priestley and Taylor evapotranspiration formula: Agronomy Journal, v. 67, p. 840-842.

Lafleur, P.M., and Rouse, W.R., 1988, The influence of surface cover and climate on energy partitioning and evaporation in a subarctic wetland: Boundary-Layer Meteorology, v. 44, p. 327-247.

Lowe, P.R., 1977, An approximating polynomial for the computation of saturation vapor pressure: Journal of Applied Meteorology, v. 16, p. 100-103.

Monteith, J.L., 1965, Evaporation and environment, *in* The state and movement of water in living organisms, symposium of the Society for Experimental Biology: San Diego, Calif., Academic Press, v. 19, p. 205-234.

Monteith, J.L., and Unsworth, M.H., 1990, Principles of environmental physics: New York, Edward Arnold, 291 p.

Ohmura, A., 1982, Objective criteria for rejecting data for Bowen ratio flux calculations: Journal of Applied Meteorology, v. 21, p. 595-598.

Priestley, C.H.B. and Taylor, R.J., 1972, On the assessment of surface heat flux and evaporation using large-scale parameters: Monthly Weather Review, v. 100, p. 81-92.

Philip, J.R., 1961, The theory of heat flux meters: Journal of Geophysical Research, v. 66, p. 571-579.

Snyder, R.L., Lanini, B.J., Shaw, D.A., and Pruitt, W.O., 1987, Using reference evapotranspiration (ETo) and crop coefficients to estimate crop evapotranspiration (ETc) for agronomic crops, grasses, and vegetable crops: Davis, Calif., Cooperative Extension, University of California, Division of Agricultural and Natural Resources Leaflet 21427, 11 p., [revised 1989].

Soil Survey Staff, 1975, Soil taxonomy: Washington, D.C., U.S. Department of Agriculture Handbook No. 436, 754 p.

Souch, C., Wolfe, C.P., and Grimmond, S.B., 1996, Wetland evaporation and energy partitioning- Indiana Dunes National Lakeshore: Journal of Hydrology, v. 84, p. 189-208.

Stannard, D.I., 1993, Comparison of Penman-Monteith, Shuttleworth-Wallace, and modified Priestley-Taylor evapotranspiration models for wildland vegetation in semiarid rangeland: Water Resources Research, v. 29, p. 1379-1392.

Stannard, D.I., 1997, A theoretically based determination of Bowen-ratio fetch requirements: Boundary-Layer Meteorology, v. 83, p. 375-406.

Steiner, J.L., Howell, T.A., and Schneider, A.D., 1991, Lysimetric evaluation of daily potential evapotranspiration models for grain sorghum: Agronomy Journal, v. 83, p. 240-247.

Stull, R.B., 1988, An introduction to boundary layer meteorology: Boston, Mass., Kluwer Academic Publishers, 666 p.

Tanner, C.B., 1960, Energy balance approach to evapotranspiration from crops: Soil Science Society of America Proceedings, v. 24, p. 1-9.

Tomlinson, S.A., 1996, Evaluating evapotranspiration for six sites in Benton, Spokane, and Yakima Counties, Washington, May 1990 to September 1992: U.S. Geological Survey Water-Resources Investigations Report 96-4002, 84 p.

University of California, 2000, Formatted daily weather data report, TULELK2.A: Davis, Calif., University of California, California Weather Databases, data accessed November 2000 at URL http://www.ipm.ucdavis.edu/WEATHER/wxretrieve.html.

U.S. Fish and Wildlife Service, 2001, Klamath Basin National Wildlife Refuges Complex, Oregon-California: Tulelake, Calif., information accessed January 2001 at URL http://www.klamathnwr.org.

Weeks, E.P., Weaver, H.L., Campbell, G.S., and Tanner, B.D., 1987, Water use by saltcedar and by replacement vegetation in the Pecos River Floodplain between Acme and Artesia, New Mexico: U.S. Geological Survey Professional Paper 491-G, 33 p.

Western Regional Climate Center, 2001, Climate data summaries for Tulelake, California, National Climatic Data Center Cooperative Station 049053: Reno, Nev., Desert Research Institute, data accessed October 2001 at URL http://wrcc.sage.dri.edu.

Williams, R.J., Broersma, K., and van Ryswyk, A.L., 1978, Equilibrium and actual evapotranspiration from a very dry vegetated surface: Journal of Applied Meteorology, v. 17, p. 1827-1832.

Tables 6, 7, and 8

Table 6. Average of 30-minute-average available energy, latent heat flux, Bowen ratio, and ratio of latent heat flux to equilibrium latent heat flux, by wind direction, time of day, and selected periods of days, and computed for the lot C1B evapotranspiration measurement site

[R_n-G, available energy, in watts per square meter; λE, latent heat flux, in watts per square meter. Because of rounding, tabulated λE might not equal (R_n-G)/(1+β), as indicated by equation 2. β, Bowen ratio, dimensionless; α, ratio of latent heat flux to equilibrium latent heat flux, dimensionless; Hours, number of hours of summarized data; –, no data. LE, absolute value less than 0.5 watts per square meter; <, less than; >, greater than]

	Easterly winds					Westerly winds					Mixed wind directions				
	R_n-G	λE	β	α	Hours	R_n-G	λE	β	α	Hours	R_n-G	λE	β	α	Hours
May 19 to May 25, 2000															
Nighttime	-11	-4	1.77	0.65	10.0	-41	3	-14.34	-0.11	41.5	-17	-3	4.43	0.30	9.0
Sunrise to 1100	104	63	0.64	0.94	13.0	315	187	0.69	0.87	14.0	169	106	0.59	0.92	4.0
1100 to 1500	–-	–-	–-	–-	–-	595	314	0.90	0.71	25.0	602	364	0.65	0.84	0.5
1500 to sunset	–-	–-	–-	–-	–-	280	177	0.58	0.84	34.0	–-	–-	–-	–-	–-
May 26 to June 1, 2000															
Nighttime	-10	-1	10.03	0.17	8.0	-37	LE	<-100	0.00	38.5	-18	-3	5.44	0.29	3.5
Sunrise to 1100	141	152	-0.07	1.59	4.0	235	117	1.01	0.83	22.0	97	43	1.27	0.73	4.0
1100 to 1500	–-	–-	–-	–-	–-	593	317	0.87	0.80	24.0	–-	–-	–-	–-	–-
1500 to sunset	–-	–-	–-	–-	–-	288	172	0.68	0.87	26.5	–-	–-	–-	–-	–-
June 2 to June 8, 2000															
Nighttime	-10	-2	5.61	0.27	10.5	-30	3	-12.06	-0.14	35.5	-19	1	-19.88	-0.09	7.0
Sunrise to 1100	144	94	0.52	1.03	8.5	226	154	0.46	1.00	14.5	269	165	0.62	0.92	5.5
1100 to 1500	–-	–-	–-	–-	–-	541	339	0.60	0.85	24.5	537	333	0.61	0.83	1.5
1500 to sunset	–-	–-	–-	–-	–-	250	210	0.19	1.15	31.5	–-	–-	–-	–-	–-
June 9 to June 15, 2000															
Nighttime	-10	-3	2.33	0.56	9.5	-31	LE	>100	0.02	36.0	-16	-2	5.45	0.27	6.5
Sunrise to 1100	190	105	0.80	0.92	8.0	243	153	0.58	0.97	18.5	268	157	0.71	0.91	3.5
1100 to 1500	314	190	0.65	0.95	1.0	489	316	0.55	0.91	25.5	399	223	0.79	0.90	1.5
1500 to sunset	185	136	0.36	1.09	0.5	239	196	0.22	1.13	34.0	–-	–-	–-	–-	–-
June 16 to June 22, 2000															
Nighttime	-16	-3	3.87	0.36	12.5	-39	2	-17.51	-0.09	40.0	-19	-2	7.21	0.20	10.0
Sunrise to 1100	153	105	0.45	1.03	14.5	351	227	0.55	0.93	15.0	230	149	0.55	0.97	5.0
1100 to 1500	622	406	0.53	0.88	5.0	613	384	0.60	0.83	19.5	618	392	0.58	0.85	3.5
1500 to sunset	304	254	0.20	1.11	5.5	282	234	0.21	1.08	28.0	490	372	0.32	0.95	1.0
June 23 to June 29, 2000															
Nighttime	-8	-3	1.88	0.59	22.0	-39	8	-6.05	-0.28	29.5	-16	LE	>100	0.00	7.0
Sunrise to 1100	152	102	0.49	0.99	13.5	368	219	0.68	0.83	12.5	307	197	0.56	0.89	6.0
1100 to 1500	589	347	0.70	0.75	5.0	591	332	0.78	0.73	16.5	600	349	0.72	0.74	6.0
1500 to sunset	414	278	0.49	0.84	5.0	243	208	0.17	1.08	24.5	376	265	0.42	0.88	3.5

Table 6. Average of 30-minute-average available energy, latent heat flux, Bowen ratio, and ratio of latent heat flux to equilibrium latent heat flux, by wind direction, time of day, and selected periods of days, and computed for the lot C1B evapotranspiration measurement site—*Continued*

	Easterly winds					Westerly winds					Mixed wind directions				
	R_n-G	λE	β	α	Hours	R_n-G	λE	β	α	Hours	R_n-G	λE	β	α	Hours
June 30 to July 4, 2000															
Nighttime	-8	-2	2.83	0.48	9.0	-28	3	-9.23	-0.20	30.0	-12	-3	3.50	0.40	4.0
Sunrise to 1100	207	101	1.04	0.74	8.5	280	122	1.30	0.68	10.0	271	141	0.93	0.76	4.0
1100 to 1500	559	269	1.08	0.66	1.5	534	230	1.32	0.60	16.0	551	249	1.21	0.62	2.5
1500 to sunset	–-	–-	–-	–-	–-	232	141	0.64	0.84	23.0	–-	–-	–-	–-	–-
July 5 to July 7, 2000															
Nighttime	-8	-3	1.62	0.72	3.5	-17	LE	<-100	-0.01	9.5	-10	-2	3.30	0.42	3.5
Sunrise to 1100	196	91	1.15	0.76	9.0	227	140	0.62	1.04	1.5	312	177	0.76	0.93	1.5
1100 to 1500	461	218	1.12	0.68	3.0	139	100	0.39	1.07	3.5	279	153	0.82	0.80	4.5
1500 to sunset	–-	–-	–-	–-	–-	145	97	0.49	0.98	14.5	465	200	1.33	0.58	1.0
July 8 to July 14, 2000															
Nighttime	-7	-1	4.23	0.31	15.0	-28	LE	73.45	0.02	32.5	-14	-2	6.51	0.21	8.0
Sunrise to 1100	190	94	1.01	0.74	17.0	378	162	1.33	0.61	8.5	289	123	1.36	0.61	5.0
1100 to 1500	578	260	1.22	0.58	5.0	562	240	1.34	0.56	16.0	570	247	1.31	0.58	7.0
1500 to sunset	191	131	0.46	0.89	2.5	271	152	0.79	0.72	29.5	329	171	0.93	0.67	3.0
July 15 to July 21, 2000															
Nighttime	-6	-1	2.91	0.43	15.5	-29	2	-18.15	-0.08	39.0	-8	-2	3.95	0.32	4.0
Sunrise to 1100	182	89	1.04	0.70	18.0	350	145	1.41	0.57	6.0	249	108	1.32	0.61	6.5
1100 to 1500	521	231	1.26	0.58	5.0	541	242	1.24	0.58	16.5	562	265	1.12	0.60	4.0
1500 to sunset	196	141	0.39	0.92	6.5	250	157	0.59	0.80	21.0	369	197	0.87	0.68	5.5
July 22 to July 28, 2000															
Nighttime	-5	-2	1.38	0.73	14.0	-36	2	-18.57	-0.08	39.0	-19	-4	3.68	0.33	3.5
Sunrise to 1100	168	66	1.54	0.58	16.0	348	134	1.59	0.54	10.0	281	110	1.56	0.55	3.5
1100 to 1500	560	258	1.17	0.58	2.5	544	220	1.48	0.53	21.5	574	245	1.35	0.55	2.5
1500 to sunset	255	156	0.63	0.77	5.0	283	154	0.84	0.69	23.5	296	166	0.78	0.71	5.0
July 29 to August 4, 2000															
Nighttime	-8	-3	1.77	0.58	20.5	-30	5	-7.53	-0.21	35.0	-11	-1	8.48	0.15	10.0
Sunrise to 1100	152	72	1.11	0.64	20.5	318	129	1.46	0.54	9.5	165	76	1.17	0.63	3.0
1100 to 1500	436	208	1.09	0.60	2.0	498	214	1.32	0.54	22.0	456	227	1.01	0.62	4.0
1500 to sunset	191	150	0.27	0.96	6.0	288	160	0.80	0.68	22.0	225	155	0.45	0.85	3.5

Table 6. Average of 30-minute-average available energy, latent heat flux, Bowen ratio, and ratio of latent heat flux to equilibrium latent heat flux, by wind direction, time of day, and selected periods of days, and computed for the lot C1B evapotranspiration measurement site—*Continued*

	Easterly winds					Westerly winds					Mixed wind directions				
	R_n-G	λE	β	α	Hours	R_n-G	λE	β	α	Hours	R_n-G	λE	β	α	Hours
August 5 to August 11, 2000															
Nighttime	-9	-2	2.92	0.42	18.0	-34	3	-13.27	-0.12	34.5	-14	-2	5.62	0.23	10.0
Sunrise to 1100	154	61	1.51	0.57	17.5	358	115	2.12	0.43	7.5	194	76	1.56	0.54	4.0
1100 to 1500	–-	–-	–-	–-	–-	501	165	2.04	0.42	26.5	502	191	1.63	0.48	1.5
1500 to sunset	–-	–-	–-	–-	–-	233	109	1.14	0.59	26.5	279	142	0.96	0.63	2.5
August 12 to August 18, 2000															
Nighttime	-6	-2	1.75	0.67	18.0	-39	-1	46.12	0.03	39.0	-11	-2	4.26	0.31	8.5
Sunrise to 1100	118	36	2.27	0.49	9.0	334	77	3.32	0.33	13.5	182	51	2.60	0.41	3.5
1100 to 1500	500	109	3.61	0.28	0.5	494	119	3.17	0.32	24.5	489	111	3.40	0.30	3.0
1500 to sunset	–-	–-	–-	–-	–-	258	79	2.27	0.39	27.5	251	78	2.23	0.40	2.5
August 19 to August 25, 2000															
Nighttime	-7	-2	2.61	0.49	17.5	-34	-1	23.16	0.06	34.0	-11	-3	3.19	0.41	16.0
Sunrise to 1100	98	24	3.07	0.40	10.0	305	63	3.85	0.30	14.0	161	26	5.30	0.23	3.0
1100 to 1500	431	128	2.38	0.36	0.5	468	93	4.02	0.26	23.0	496	96	4.16	0.26	3.0
1500 to sunset	326	73	3.50	0.30	0.5	213	60	2.53	0.36	28.5	227	35	5.59	0.19	0.5
August 26 to August 31, 2000															
Nighttime	-6	-2	2.06	0.57	19.5	-33	-1	44.66	0.03	30.5	-15	-3	3.18	0.38	6.5
Sunrise to 1100	142	34	3.19	0.36	13.0	312	59	4.29	0.27	6.5	165	30	4.44	0.27	2.5
1100 to 1500	392	74	4.30	0.24	1.5	422	80	4.27	0.25	20.0	477	95	4.01	0.26	1.0
1500 to sunset	–-	–-	–-	–-	–-	186	43	3.31	0.30	21.5	293	67	3.39	0.29	2.5
September 1 to September 5, 2000															
Nighttime	-3	-1	1.33	0.83	2.0	-12	-1	14.41	0.12	14.0	-7	1	-14.66	-0.13	3.5
Sunrise to 1100	101	61	0.67	1.09	7.0	149	93	0.60	1.09	8.0	168	138	0.22	1.46	1.5
1100 to 1500	221	154	0.44	1.19	5.5	269	139	0.93	0.85	13.0	273	116	1.36	0.68	1.5
1500 to sunset	110	97	0.13	1.49	5.5	133	69	0.93	0.82	11.5	33	29	0.12	1.55	1.0
September 6 to September 12, 2000															
Nighttime	-4	-1	2.12	0.56	6.5	-14	LE	-77.71	-0.02	20.0	-10	-1	8.18	0.18	4.5
Sunrise to 1100	172	71	1.42	0.69	10.0	286	91	2.14	0.51	7.0	273	86	2.17	0.48	4.0
1100 to 1500	374	109	2.42	0.40	0.5	426	114	2.74	0.37	24.5	342	98	2.49	0.41	2.0
1500 to sunset	122	80	0.53	0.89	3.0	241	73	2.29	0.41	19.0	261	88	1.98	0.45	3.0

Table 6. Average of 30-minute-average available energy, latent heat flux, Bowen ratio, and ratio of latent heat flux to equilibrium latent heat flux, by wind direction, time of day, and selected periods of days, and computed for the lot C1B evapotranspiration measurement site—*Continued*

	Easterly winds					Westerly winds					Mixed wind directions				
	R_n-G	λE	β	α	Hours	R_n-G	λE	β	α	Hours	R_n-G	λE	β	α	Hours
September 13 to September 19, 2000															
Nighttime	-7	-3	1.63	0.62	6.5	-16	-2	5.52	0.23	21.0	-11	-2	4.56	0.27	8.5
Sunrise to 1100	141	66	1.15	0.73	9.0	255	80	2.19	0.45	9.0	195	75	1.59	0.56	2.5
1100 to 1500	441	124	2.56	0.39	1.0	393	93	3.25	0.31	26.5	126	53	1.39	0.60	0.5
1500 to sunset	99	57	0.73	0.78	1.0	196	51	2.82	0.34	21.0	39	32	0.19	1.20	1.0
September 20 to September 26, 2000															
Nighttime	-15	-1	9.65	0.18	13.0	-24	LE	-53.83	-0.03	16.0	-19	-1	14.62	0.12	6.0
Sunrise to 1100	123	42	1.91	0.64	6.0	247	48	4.19	0.32	11.5	149	44	2.36	0.49	3.5
1100 to 1500	370	53	6.05	0.20	4.0	375	59	5.34	0.23	21.0	366	58	5.34	0.25	3.0
1500 to sunset	254	28	8.07	0.15	3.5	170	30	4.63	0.25	18.5	240	30	7.13	0.17	1.0
September 27 to October 3, 2000															
Nighttime	-3	-1	1.79	0.68	4.0	-24	-2	10.56	0.13	27.5	-10	-2	3.29	0.39	4.5
Sunrise to 1100	118	40	1.96	0.58	9.0	250	46	4.45	0.28	7.0	184	42	3.39	0.36	4.5
1100 to 1500	320	21	14.03	0.09	0.5	353	47	6.57	0.19	26.5	361	44	7.28	0.17	1.0
1500 to sunset	–-	–-	–-	–-	–-	185	18	9.13	0.13	19.5	–-	–-	–-	–-	–-
October 4 to October 7, 2000															
Nighttime	-1	LE	2.18	0.65	1.5	-33	LE	<-100	0.00	4.0	–-	–-	–-	–-	–-
Sunrise to 1100	114	29	2.98	0.44	5.0	227	34	5.58	0.25	4.0	149	32	3.64	0.37	3.0
1100 to 1500	–-	–-	–-	–-	–-	328	37	7.89	0.16	15.5	280	27	9.23	0.14	0.5
1500 to sunset	–-	–-	–-	–-	–-	152	10	14.64	0.09	11.5	–-	–-	–-	–-	–-
October 18 to October 19, 2000															
Nighttime	-4	-2	1.68	0.75	3.0	-17	-2	6.95	0.20	1.5	-7	-2	2.21	0.59	3.5
Sunrise to 1100	159	47	2.37	0.51	2.5	175	38	3.65	0.37	0.5	207	42	3.89	0.34	0.5
1100 to 1500	234	38	5.15	0.26	1.0	205	33	5.23	0.24	3.5	146	28	4.29	0.28	0.5
1500 to sunset	-4	LE	17.00	0.08	0.5	82	20	3.00	0.37	1.5	55	18	2.09	0.47	1.0

Table 7. Average of 30-minute-average available energy, latent heat flux, Bowen ratio, and ratio of latent heat flux to equilibrium latent heat flux, by wind direction, time of day, and selected periods of days, and computed for the lot 6 stubble evapotranspiration measurement site

[R_n-G, available energy, in watts per square meter; λE, latent heat flux, in watts per square meter. Because of rounding, tabulated λE might not equal $(R_n\text{-}G)/(1+\beta)$, as indicated by equation 2. β, Bowen ratio, dimensionless; α, ratio of latent heat flux to equilibrium latent heat flux, dimensionless; Hours, number of hours of summarized data; –, no data. LE, absolute value less than 0.5 watts per square meter; <, less than; >, greater than]

	Easterly winds					Westerly winds					Mixed wind directions				
	R_n-G	λE	β	α	Hours	R_n-G	λE	β	α	Hours	R_n-G	λE	β	α	Hours
June 11 to June 15, 2000															
Nighttime	-13	-6	1.28	0.81	9.5	-26	-4	5.68	0.23	27.0	-17	-6	1.81	-13	-6
Sunrise to 1100	205	74	1.76	0.56	9.5	237	71	2.35	0.43	9.0	172	63	1.72	205	74
1100 to 1500	317	62	4.09	0.31	0.5	395	99	2.97	0.34	17.0	429	100	3.29	317	62
1500 to sunset	230	48	3.75	0.31	1.0	210	61	2.42	0.39	26.5	253	49	4.15	230	48
June 16 to June 22, 2000															
Nighttime	-19	-3	4.65	0.31	16.5	-32	-3	8.36	0.16	38.0	-20	-5	3.27	0.39	8.0
Sunrise to 1100	162	66	1.45	0.62	16.5	288	106	1.71	0.53	13.5	256	95	1.69	0.54	5.5
1100 to 1500	526	158	2.34	0.40	7.5	523	172	2.03	0.44	16.0	514	190	1.70	0.48	4.5
1500 to sunset	240	88	1.71	0.49	5.5	246	107	1.31	0.56	30.0	486	195	1.49	0.50	1.0
June 23 to June 29, 2000															
Nighttime	-12	-5	1.29	0.75	24.0	-29	LE	74.43	0.02	29.0	-16	-4	3.05	0.40	9.5
Sunrise to 1100	125	78	0.59	0.94	13.5	372	190	0.96	0.71	12.5	235	130	0.81	0.78	8.0
1100 to 1500	546	308	0.77	0.72	3.5	547	263	1.08	0.62	20.0	556	270	1.06	0.63	4.5
1500 to sunset	476	278	0.71	0.73	1.0	235	160	0.47	0.86	30.0	419	255	0.65	0.76	4.0
June 30 to July 4, 2000															
Nighttime	-15	-6	1.37	0.75	11.5	-30	-1	40.22	0.04	27.0	-21	-5	3.21	0.42	5.5
Sunrise to 1100	201	117	0.72	0.88	9.0	253	129	0.96	0.79	9.5	278	148	0.88	0.82	5.5
1100 to 1500	532	283	0.88	0.73	4.0	571	289	0.97	0.70	13.0	434	206	1.11	0.69	3.0
1500 to sunset	–	–	–	–	–	240	155	0.55	0.89	24.0	–	–	–	–	–
July 5 to July 7, 2000															
Nighttime	-12	-5	1.41	0.76	9.5	-20	LE	-58.23	-0.03	8.0	-15	-4	2.73	0.47	3.0
Sunrise to 1100	168	111	0.51	1.08	12.5	324	154	1.11	0.81	0.5	322	212	0.52	1.05	1.5
1100 to 1500	414	267	0.55	0.94	7.0	105	87	0.20	1.38	1.5	220	161	0.37	1.07	3.5
1500 to sunset	224	161	0.39	1.01	2.0	137	122	0.12	1.31	11.5	216	170	0.28	1.11	2.0
July 8 to July 14, 2000															
Nighttime	-17	-8	1.22	0.80	22.5	-36	LE	>100	0.01	28.0	-27	-4	6.25	0.22	9.5
Sunrise to 1100	236	166	0.42	1.04	21.5	347	238	0.46	0.98	4.0	337	216	0.56	0.94	5.5
1100 to 1500	605	416	0.46	0.92	11.5	595	411	0.45	0.92	9.5	587	391	0.50	0.90	6.5
1500 to sunset	298	265	0.13	1.14	1.5	270	246	0.10	1.19	30.0	379	310	0.22	1.06	4.0

Table 7. Average of 30-minute-average available energy, latent heat flux, Bowen ratio, and ratio of latent heat flux to equilibrium latent heat flux, by wind direction, time of day, and selected periods of days, and computed for the lot 6 stubble evapotranspiration measurement site—*Continued*

	Easterly winds					Westerly winds					Mixed wind directions				
	R_n-G	λE	β	α	Hours	R_n-G	λE	β	α	Hours	R_n-G	λE	β	α	Hours
July 15 to July 21, 2000															
Nighttime	-14	-5	1.62	0.64	25.0	-37	4	-10.95	-0.14	32.5	-16	-4	2.59	0.44	7.0
Sunrise to 1100	208	148	0.40	1.02	24.0	297	217	0.37	1.05	5.0	220	159	0.38	1.02	5.5
1100 to 1500	581	420	0.38	0.95	9.5	589	445	0.33	0.99	9.5	605	446	0.36	0.96	8.5
1500 to sunset	300	287	0.05	1.23	5.0	271	286	-0.05	1.36	20.0	294	284	0.03	1.25	5.5
July 22 to July 28, 2000															
Nighttime	-15	-6	1.53	0.68	21.5	-36	2	-19.57	-0.08	38.0	-24	-3	6.61	0.20	6.0
Sunrise to 1100	223	150	0.49	0.99	26.0	365	246	0.48	0.96	2.0	358	244	0.47	0.97	4.5
1100 to 1500	596	436	0.37	0.96	13.5	599	433	0.38	0.96	9.0	575	395	0.46	0.93	5.5
1500 to sunset	406	377	0.08	1.18	5.5	286	295	-0.03	1.34	22.5	396	356	0.12	1.15	4.0
July 29 to August 4, 2000															
Nighttime	-15	-4	3.23	0.38	24.5	-34	15	-3.31	-0.59	30.5	-19	1	-21.49	-0.07	11.0
Sunrise to 1100	221	166	0.33	1.03	25.5	320	237	0.35	1.01	4.0	247	176	0.40	0.96	2.5
1100 to 1500	498	406	0.23	1.04	7.5	552	462	0.19	1.05	17.5	485	391	0.24	1.04	3.0
1500 to sunset	343	345	-0.01	1.25	10.5	253	292	-0.13	1.44	15.5	262	282	-0.07	1.34	5.5
August 5 to August 11, 2000															
Nighttime	-15	-2	5.88	0.24	26.5	-34	11	-4.10	-0.46	26.0	-15	LE	-56.24	-0.03	14.0
Sunrise to 1100	233	161	0.44	0.99	19.0	392	273	0.43	0.95	2.5	272	174	0.57	0.92	7.5
1100 to 1500	556	374	0.49	0.87	9.5	536	375	0.43	0.90	9.5	544	396	0.37	0.94	8.5
1500 to sunset	320	244	0.31	0.97	1.5	256	262	-0.02	1.30	23.5	284	272	0.04	1.20	2.5
August 12 to August 18, 2000															
Nighttime	-12	-4	1.73	0.67	24.0	-38	5	-8.27	-0.21	36.0	-15	-4	2.66	0.47	8.5
Sunrise to 1100	201	107	0.88	0.81	18.0	359	170	1.12	0.69	3.5	339	170	1.00	0.73	6.0
1100 to 1500	516	292	0.77	0.75	4.5	522	282	0.85	0.72	18.0	517	281	0.84	0.72	5.5
1500 to sunset	494	332	0.49	0.85	0.5	283	222	0.28	1.02	20.5	352	258	0.37	0.94	6.0
August 19 to August 25, 2000															
Nighttime	-9	-2	3.76	0.38	27.5	-33	2	-16.10	-0.10	32.0	-12	-2	6.47	0.22	11.0
Sunrise to 1100	124	57	1.17	0.74	16.5	338	128	1.64	0.55	8.0	293	108	1.70	0.54	4.5
1100 to 1500	481	177	1.72	0.50	2.0	475	199	1.39	0.55	20.5	476	187	1.54	0.52	5.0
1500 to sunset	338	160	1.12	0.60	0.5	227	146	0.56	0.83	21.5	349	185	0.89	0.69	5.0
August 26 to August 31, 2000															
Nighttime	-13	-4	2.49	0.50	28.5	-29	LE	<-100	-0.01	26.5	-16	-2	5.44	0.25	8.0
Sunrise to 1100	155	59	1.63	0.58	15.5	313	103	2.04	0.47	4.0	256	81	2.17	0.46	3.0
1100 to 1500	438	136	2.22	0.41	8.5	425	149	1.86	0.46	7.5	387	132	1.94	0.45	7.0
1500 to sunset	290	132	1.20	0.58	2.5	127	79	0.60	0.81	18.5	331	144	1.29	0.56	5.5

Table 7. Average of 30-minute-average available energy, latent heat flux, Bowen ratio, and ratio of latent heat flux to equilibrium latent heat flux, by wind direction, time of day, and selected periods of days, and computed for the lot 6 stubble evapotranspiration measurement site—*Continued*

	Easterly winds					Westerly winds					Mixed wind directions				
	R_n-G	λE	β	α	Hours	R_n-G	λE	β	α	Hours	R_n-G	λE	β	α	Hours
September 1 to September 5, 2000															
Nighttime	-8	-2	2.84	0.50	2.5	-9	-1	8.41	0.20	18.5	-5	-1	5.47	0.29	4.5
Sunrise to 1100	132	78	0.70	1.07	6.5	134	83	0.62	1.07	8.5	134	97	0.38	1.31	1.5
1100 to 1500	228	143	0.59	1.06	6.5	246	137	0.80	0.93	10.5	306	167	0.83	0.89	3.0
1500 to sunset	82	83	-0.01	1.77	4.5	124	79	0.58	1.02	11.5	172	91	0.90	0.84	4.0
September 6 to September 12, 2000															
Nighttime	-7	-2	2.99	0.45	24.5	-18	-1	18.61	0.08	19.5	-10	-2	5.12	0.29	12.0
Sunrise to 1100	141	74	0.91	0.90	8.5	304	94	2.24	0.47	7.0	286	93	2.06	0.52	4.5
1100 to 1500	409	101	3.06	0.37	1.0	417	118	2.53	0.39	23.0	401	114	2.52	0.39	4.0
1500 to sunset	128	58	1.19	0.62	9.5	231	85	1.72	0.49	13.0	262	101	1.60	0.51	5.0
September 13 to September 19, 2000															
Nighttime	-11	-3	2.86	0.42	24.5	-21	-4	4.21	0.29	23.0	-14	-3	3.21	0.38	11.5
Sunrise to 1100	162	74	1.19	0.69	9.5	248	93	1.66	0.55	7.0	167	76	1.20	0.67	7.5
1100 to 1500	418	118	2.53	0.39	2.0	392	117	2.36	0.39	23.0	395	112	2.54	0.39	2.5
1500 to sunset	62	61	0.02	1.28	6.0	215	79	1.71	0.48	17.0	109	59	0.83	0.73	1.5
September 20 to September 26, 2000															
Nighttime	-14	-1	16.14	0.11	32.5	-27	-2	12.96	0.12	20.0	-16	-1	10.40	0.17	16.5
Sunrise to 1100	142	48	1.93	0.62	9.5	249	68	2.67	0.44	8.0	208	58	2.60	0.46	4.5
1100 to 1500	373	60	5.22	0.24	6.5	393	76	4.16	0.28	19.5	414	86	3.83	0.32	2.0
1500 to sunset	127	23	4.60	0.24	2.5	181	47	2.85	0.36	17.5	121	36	2.31	0.40	4.0
September 27 to October 3, 2000															
Nighttime	-6	-2	2.11	0.61	28.5	-27	-4	6.71	0.20	24.0	-7	-2	2.40	0.50	8.0
Sunrise to 1100	136	52	1.61	0.67	7.5	225	55	3.12	0.37	9.5	180	56	2.24	0.49	4.5
1100 to 1500	353	57	5.23	0.23	2.5	359	49	6.38	0.19	19.5	361	55	5.57	0.21	6.0
1500 to sunset	294	38	6.72	0.17	0.5	131	23	4.57	0.24	21.5	178	32	4.56	0.25	1.0
October 4 to October 7, 2000															
Nighttime	-4	-1	3.22	0.49	14.5	-12	-1	8.24	0.18	6.0	-12	-1	8.96	0.17	5.5
Sunrise to 1100	142	40	2.56	0.49	7.0	163	46	2.56	0.51	0.5	232	41	4.68	0.29	4.5
1100 to 1500	339	40	7.40	0.16	2.0	337	41	7.30	0.17	11.0	344	48	6.18	0.20	2.5
1500 to sunset	217	21	9.44	0.12	0.5	128	15	7.76	0.15	9.0	147	20	6.23	0.19	2.5

Table 8. Average of 30-minute-average available energy, latent heat flux, Bowen ratio, and ratio of latent heat flux to equilibrium latent heat flux, by wind direction, time of day, and selected periods of days, and computed for the lot 6 cover crop evapotranspiration measurement site

[R_n-G, available energy, in watts per square meter; λE, latent heat flux, in watts per square meter. Because of rounding, tabulated λE might not equal (R_n-G)/(1+β), as indicated by equation 2. β, Bowen ratio, dimensionless; α, ratio of latent heat flux to equilibrium latent heat flux, dimensionless; Hours, number of hours of summarized data; –, no data. LE, absolute value less than 0.5 watts per square meter; <, less than; >, greater than]

	Easterly winds					Westerly winds					Mixed wind directions				
	R_n-G	λE	β	α	Hours	R_n-G	λE	β	α	Hours	R_n-G	λE	β	α	Hours
June 3 to June 8, 2000															
Nighttime	-19	-5	2.56	0.52	11.0	-35	4	-9.09	-0.20	30.0	-28	LE	-69.82	-0.02	7.5
Sunrise to 1100	176	130	0.36	1.11	6.5	231	161	0.44	1.04	15.0	160	116	0.38	1.13	2.5
1100 to 1500	532	404	0.32	0.98	0.5	490	332	0.48	0.93	21.0	586	402	0.46	0.92	2.5
1500 to sunset	300	274	0.10	1.17	2.0	198	177	0.12	1.23	26.5	256	239	0.07	1.20	1.5
June 9 to June 15, 2000															
Nighttime	-16	-7	1.35	0.79	11.5	-31	2	-18.54	-0.09	35.0	-20	-6	2.36	0.52	9.5
Sunrise to 1100	197	119	0.66	0.98	10.5	237	169	0.41	1.09	15.0	296	190	0.55	0.98	5.0
1100 to 1500	378	227	0.67	0.96	0.5	462	328	0.41	0.99	23.5	491	317	0.55	0.97	4.0
1500 to sunset	256	194	0.32	1.11	1.0	224	206	0.09	1.25	31.5	--	--	--	--	--
June 16 to June 22, 2000															
Nighttime	-24	-5	3.50	0.39	16.0	-43	1	-34.27	-0.05	37.0	-30	-7	3.60	0.37	8.0
Sunrise to 1100	173	128	0.35	1.12	13.0	332	238	0.39	1.03	15.0	334	242	0.38	1.06	6.0
1100 to 1500	612	392	0.56	0.86	6.5	610	434	0.41	0.95	18.5	607	460	0.32	0.99	3.0
1500 to sunset	281	218	0.28	1.03	5.0	273	263	0.04	1.25	30.5	--	--	--	--	--
June 23 to June 27, 2000															
Nighttime	-16	-7	1.26	0.78	13.0	-40	3	-12.47	-0.13	19.0	-24	-5	4.14	0.32	6.0
Sunrise to 1100	157	110	0.42	1.06	6.5	377	268	0.41	1.00	11.0	304	212	0.43	0.99	4.0
1100 to 1500	587	448	0.31	0.99	1.5	608	434	0.40	0.93	17.0	625	434	0.44	0.92	1.0
1500 to sunset	--	--	--	--	--	264	263	0.00	1.27	24.5	546	440	0.24	1.02	1.0
July 21 to July 28, 2000															
Nighttime	-14	-6	1.42	0.71	17.5	-40	3	-13.51	-0.12	42.5	-24	-4	4.71	0.27	5.0
Sunrise to 1100	212	91	1.33	0.63	18.5	381	150	1.54	0.55	6.5	392	157	1.50	0.57	3.5
1100 to 1500	546	244	1.23	0.58	8.5	544	238	1.29	0.57	13.0	530	222	1.38	0.55	9.5
1500 to sunset	347	199	0.74	0.72	4.0	226	143	0.58	0.81	32.5	329	158	1.08	0.61	3.0
July 29 to August 4, 2000															
Nighttime	-14	-4	2.14	0.51	21.5	-38	5	-8.04	-0.19	31.5	-20	-1	20.06	0.07	12.5
Sunrise to 1100	181	75	1.42	0.57	23.0	318	108	1.95	0.46	6.0	194	78	1.48	0.55	2.5
1100 to 1500	392	157	1.50	0.51	5.0	477	172	1.78	0.45	21.0	367	142	1.60	0.49	2.0
1500 to sunset	299	123	1.43	0.50	5.5	181	90	1.00	0.62	23.5	203	97	1.10	0.59	5.5

Table 8. Average of 30-minute-average available energy, latent heat flux, Bowen ratio, and ratio of latent heat flux to equilibrium latent heat flux, by wind direction, time of day, and selected periods of days, and computed for the lot 6 cover crop evapotranspiration measurement site—Continued

	Easterly winds					Westerly winds					Mixed wind directions				
	R_n-G	λE	β	α	Hours	R_n-G	λE	β	α	Hours	R_n-G	λE	β	α	Hours
August 5 to August 11, 2000															
Nighttime	-15	-3	4.07	0.32	24.0	-38	LE	<-100	-0.01	26.0	-19	-2	8.22	0.16	15.5
Sunrise to 1100	170	51	2.34	0.43	17.0	321	56	4.69	0.24	5.5	234	49	3.76	0.29	4.5
1100 to 1500	471	94	4.00	0.26	4.5	463	83	4.60	0.23	18.0	464	89	4.23	0.25	5.5
1500 to sunset	213	42	4.05	0.25	1.0	172	43	2.99	0.31	28.5	374	51	6.28	0.17	1.5
August 12 to August 18, 2000															
Nighttime	-12	-4	1.74	0.66	19.5	-44	-4	10.62	0.13	36.5	-15	-5	2.28	0.52	8.5
Sunrise to 1100	126	33	2.87	0.41	12.5	327	43	6.59	0.19	9.0	295	40	6.35	0.20	4.5
1100 to 1500	432	50	7.64	0.15	0.5	463	62	6.49	0.18	21.5	448	55	7.17	0.16	6.0
1500 to sunset	402	67	4.97	0.21	0.5	184	24	6.56	0.17	30.5	358	46	6.78	0.16	1.5
August 19 to August 25, 2000															
Nighttime	-9	-2	3.13	0.42	27.0	-38	-4	7.57	0.17	33.0	-14	-3	4.10	0.32	9.5
Sunrise to 1100	111	27	3.10	0.39	10.5	310	38	7.25	0.18	9.5	188	24	6.73	0.19	6.0
1100 to 1500	451	62	6.33	0.17	0.5	433	50	7.73	0.15	22.0	447	58	6.72	0.17	5.5
1500 to sunset	--	--	--	--	--	181	20	8.13	0.14	27.0	292	13	20.78	0.06	2.0
August 26 to August 31, 2000															
Nighttime	-12	-4	1.73	0.64	26.5	-32	-5	6.19	0.21	27.0	-14	-4	2.80	0.42	9.5
Sunrise to 1100	132	24	4.53	0.28	11.0	297	36	7.15	0.17	6.0	149	23	5.58	0.22	4.0
1100 to 1500	399	41	8.75	0.13	4.5	386	41	8.31	0.14	12.0	411	47	7.76	0.15	7.5
1500 to sunset	278	22	11.46	0.10	1.5	117	5	23.32	0.05	18.0	296	26	10.33	0.11	5.0
September 1 to September 5, 2000															
Nighttime	-4	-2	1.22	0.88	4.0	-11	-1	16.01	0.11	29.5	-7	1	-9.85	-0.21	3.0
Sunrise to 1100	129	79	0.64	1.11	6.5	129	74	0.73	1.00	8.0	186	137	0.36	1.31	2.0
1100 to 1500	241	158	0.52	1.10	7.0	242	126	0.93	0.87	11.0	323	129	1.51	0.64	2.0
1500 to sunset	71	65	0.10	1.58	4.5	124	62	1.00	0.80	12.0	141	75	0.88	0.86	3.0
September 6 to September 12, 2000															
Nighttime	-10	-2	4.75	0.30	24.0	-21	-1	19.79	0.08	25.0	-11	-2	5.56	0.26	15.0
Sunrise to 1100	195	75	1.60	0.63	10.5	332	92	2.61	0.43	6.0	258	78	2.30	0.48	5.5
1100 to 1500	425	72	4.93	0.24	1.0	438	83	4.27	0.26	24.0	365	62	4.87	0.24	3.0
1500 to sunset	91	37	1.44	0.56	7.5	214	47	3.55	0.29	16.5	286	63	3.54	0.29	3.0
September 13 to September 19, 2000															
Nighttime	-11	-3	2.64	0.44	18.5	-25	-5	3.95	0.31	22.5	-9	-2	3.57	0.34	13.5
Sunrise to 1100	158	64	1.46	0.62	8.5	264	73	2.60	0.40	8.5	196	71	1.78	0.53	6.0
1100 to 1500	462	88	4.26	0.26	1.5	435	68	5.44	0.21	24.0	415	67	5.24	0.22	2.0
1500 to sunset	57	36	0.60	0.83	4.0	226	44	4.11	0.25	19.5	91	32	1.83	0.46	2.0

Table 8. Average of 30-minute-average available energy, latent heat flux, Bowen ratio, and ratio of latent heat flux to equilibrium latent heat flux, by wind direction, time of day, and selected periods of days, and computed for the lot 6 cover crop evapotranspiration measurement site—Continued

	Easterly winds					Westerly winds					Mixed wind directions				
	R_n-G	λE	β	α	Hours	R_n-G	λE	β	α	Hours	R_n-G	λE	β	α	Hours
September 20 to September 26, 2000															
Nighttime	-18	-2	6.71	0.24	14.5	-31	-3	8.96	0.17	22.5	-22	-2	7.72	0.21	7.0
Sunrise to 1100	104	26	3.07	0.43	11.5	273	49	4.62	0.28	10.0	125	42	1.98	0.57	3.0
1100 to 1500	351	42	7.29	0.18	5.0	450	55	7.12	0.17	21.0	388	47	7.32	0.18	2.0
1500 to sunset	319	31	9.29	0.13	1.0	224	37	5.11	0.23	16.0	208	30	5.85	0.19	3.0
September 27 to October 3, 2000															
Nighttime	-10	-4	1.63	0.81	19.0	-31	-5	5.47	0.25	23.0	-15	-5	2.00	0.67	7.5
Sunrise to 1100	64	18	2.54	0.48	6.5	180	33	4.43	0.28	9.0	141	32	3.42	0.36	9.0
1100 to 1500	396	46	7.68	0.16	1.5	365	40	8.10	0.15	21.5	380	48	6.91	0.18	5.0
1500 to sunset	--	--	--	--	--	164	23	6.15	0.19	16.5	217	26	7.42	0.16	1.5
October 4 to October 7, 2000															
Nighttime	-10	-3	1.97	0.76	21.0	-27	-4	5.24	0.27	8.5	-12	-3	3.43	0.45	8.5
Sunrise to 1100	45	10	3.58	0.37	6.0	247	34	6.20	0.22	1.5	135	20	5.66	0.24	5.0
1100 to 1500	328	32	9.29	0.13	1.5	328	31	9.69	0.13	11.0	324	36	8.01	0.16	3.0
1500 to sunset	--	--	--	--	--	129	16	7.13	0.16	11.0	134	21	5.40	0.21	1.0